Aim and Scope

The objective of the *Journal of Residuals Science & Technology* (JRS&T) is to provide a forum for technical research on the management and disposal of residuals from pollution control activities. The Journal publishes papers that examine the characteristics, effects, and management principles of various residuals from such sources as wastewater treatment, water treatment, air pollution control, hazardous waste treatment, solid waste, industrial waste treatment, and other pollution control activities. Papers on health and the environmental effects of residuals production, management, and disposal are also welcome.

Editor-in-Chief

P. Brent Duncan
Department of Biology
University of North Texas
Denton, TX, USA
pduncan@unt.edu

Assistant Editor

James Lee
james.lee3918@gmail.com

Editorial Advisory Board

Muhammad Abu-Orf
AECOM, USA
mohammad.abu-orf@aecom.com

Nafissa M. Bizo
City of Philadelphia Water Department
nafissa.bizo@phila.gov

Richard Dick
Cornell University, USA
rid1@cornell.edu

Eliot Epstein
Epstein Environmental Consultants
epsteinee@comcast.net

Guor-Cheng Fang, Ph.D.
Hungkuang University, Taiwan
gcfang@sunrise.hk.edu.tw

Robert Hale
Virginia Iustitute of Marine Science, USA
hale@vims.edu

Paul F. Hudak
University of North Texas, USA
hudak@unt.edu

Blanca Jimenez Cisneros
Inst. de Ingenieria, UNAM, Mexico
bjc@mumas.iingen.unam.mx

Julia Kopp
Technische Universitat Braunschweig, Germany
j.kopp@tu-bs.de

Uta Krogmann
RutgersUniversity, USA
krogmann@aesop.rutgers.edu

D. J. Lee
National Taiwan University, Taiwan
djlee@ntu.edu.tw

Giuseppe Mininni
Via Reno 1, Italy
mininni@irsa.rm.cnr.it

Lynne H. Moss
CDM Smith
mosslh@cdmsmith.com

John Novak
Virginia Tech, USA
jtnov@vt.edu

Nagaharu Okuno
The University of Shiga Prefecture, Japan
okuno@ses.usp.ac.jp

Jan Oleszkiewicz
University of Manitoba, Canada
oleszkie@ms.umanitoba.ca

Banu Örmeci
Carleton University, Canada
banu_ormeci@carleton.ca

Ian L. Pepper
University of Arizona, USA
ipepper@ag.arizona.edu

Ioana G. Petrisor
Co-Editor-in-Chief
Environmental Forensics Journal, USA
Environmental.Forensics@gmail.com

Bob Reimers
Tulane University, USA
rreimers@tulane.edu

Dilek Sanin
Middle East Technical University, Turkey
dsanin@metu.edu.tr

Heidi Snyman
Golder Associates Africa (Pty) Ltd., South Africa
hsnyman@golder.co.za

Ludovico Spinosa
Consultant at Commissariat for Env. Energ. in Region, Puglia, Italy
ludovico.spinosa@fastwebnet.it

P. Aarne Vesilind
Bucknell University, USA
aarne.vesilind@gmail.com

Doug Williams
California Polytechnic State University, USA
wmsengr@thegrid.net

JOURNAL OF RESIDUALS SCIENCE & TECHNOLOGY—Published quarterly—January, April, July and October by DEStech Publications, Inc., 439 North Duke Street, Lancaster, PA 17602.

Indexed by Chemical Abstracts Service. Indexed/abstracted in Science Citation Index Expanded. Abstracted in Current Contents/Engineering, Computing & Technology. Listed in ISI Master Journal.

Subscriptions: Annual $219 per year. Single copy price $60. Foreign subscriptions add $45 per year for postage.

(ISSN 1544-8053)

DEStech Publications, Inc.
439 North Duke Street, Lancaster, PA 17602-4967, U.S.A.

©Copyright by DEStech Publications, Inc. 2015—All Rights Reserved

CONTENTS

Research

Conditions and Mechanisms in Thiocyanate Biodegradation 113
R.G. COMBARROS, S. COLLADO, A. LACA and M. DÍAZ

Toxic Effects of Chronic Sub-Lethal Cu^{2+}, Pb^{2+} and Cd^{2+} on Antioxidant Enzyme Activities in Various Tissues of the Blood Cockle, *Anadara granosa* 125
CHAO PENG, XINGUO ZHAO, YU HAN, WEI SHI, SAIXI LIU AND GUANGXU LIU

Effects of Fly Ash Content on Properties of Cement Paste Backfilling 133
TINGYE QI, GUORUI FENG, YUJIANG ZHANG, JUN GUO and YUXIA GUO

Hydrothermal Hot-pressing Solidification of Coal Fly Ash and Its Ability of Fixing Heavy Metal 143
FANGBIN XUE, HUIPING SONG, YINGLU JI, LIQIONG CAO and FANGQIN CHENG

Synthesis and Mechanism of a Novel Organosilicone Used as a Selective Plugging Agent 149
BING HOU, QINGYANG LI and YAN LUO

Recovery of Aluminum Residue from Incineration of Cans in Municipal Solid Waste 157
YANJUN HU and M.C.M. BAKKER

Evaluation of Physico-Chemical Pretreatment Methods for Landfill Leachate Prior to Sewer Discharge 165
M. POVEDA, Q. YUAN, S. LOZECZNIK and J. OLESZKIEWICZ

Screening of Bioflocculant and Preliminary Application to Treatment of Tannery Wastewater 177
QINHUAN YANG, HONGMEI MING, XINGXIU ZHAO, JING ZHANG, WEI ZOU, CHANGQING ZHAO and XIUQIONG GUAN

Temperature and Concentration Effects on Biodegradation Kinetics and Surface Properties of Phenol Degrading *Rhodotorula glutinis* 183
AYSUN VATANSEVER BOŞÇA and SELIM L. SANIN

Conditions and Mechanisms in Thiocyanate Biodegradation

R.G. COMBARROS, S. COLLADO, A. LACA and M. DÍAZ*
Department of Chemical Engineering and Environmental Technology, University of Oviedo, Spain

ABSTRACT: Presence of thiocyanate (SCN^-) is a problem of considerable interest in many industrial wastewaters, where this contaminant often appears accompanied by secondary sources of carbon, nitrogen and/or sulphur. In order to understand the effect of these compounds on the biodegradability of SCN^-, this work investigates how the bacterium *Pararacoccus thiocyanatus* utilises the three elements that form the molecule of thiocyanate and compare this behaviour with those obtained in presence of other sources of N, S and C. Result showed that the bacterium was capable of utilizing thiocyanate as the sole substrate, achieving specific biodegradation rates of approximate 1.20 mg SCN^- (mg cell·h)$^{-1}$ and eliminating initial thiocyanate concentrations up to 5,000 mg L^{-1}. Experimental data were successfully fitted to a Teisser model, assuming the existence of substrate inhibition obtaining values of μ_{max} of 0.059 h^{-1}, K_s of 790 mg L^{-1} and K_i of 6,520 mg L^{-1} for free mineral medium. Presence of additional carbon and nitrogen sources implied catabolic repression of the biodegradation of thiocyanate. In this case, only concentrations lower than 3,500 mg L^{-1} could be treated, obtaining specific degradation rates of around 0.70 mg SCN^-·(h·mg cell)$^{-1}$. Tessier model values showed a higher maximum specific growth rate (0.344 h^{-1}), changing also the values for affinity and inhibition constants (1,150 mg L^{-1} and 1,730 mg L^{-1}, respectively).

INTRODUCTION

THIOCYANATE is an inorganic compound generated from a diverse range of natural and industrial sources. Due to some of its rather unique properties, thiocyanate is used in a variety of industrial processes such as photofinishing, plastics, organic chemicals, pharmaceuticals, fertilizer, herbicide and insecticide production, dyeing, acrylic fibre production, manufacturing of thiourea, metal separation and electroplating. Additional uses of thiocyanate include soil sterilization and corrosion inhibition [6,7,13]. Because of such wide use, thiocyanate is found in many industrial wastewaters.

Thiocyanate is stable, non-hydrolysable and non-volatile and it persists in the environment even in acid media [6]. Due to a strong protein-binding tendency and competitive characteristics, thiocyanate is toxic to many higher organisms even at low concentrations (LC50 between 50–100 mg L^{-1}) [1]. It affects the human central nervous system provoking irritability, nervousness, hallucination, psychosis, mania, delirium and convulsions. Besides, it inhibits halide transport to the thyroid glands and affects the stomach enzyme system, cornea and gills [1,6]. Therefore, thiocyanate removal from industrial wastewater and other contaminated sites is of great importance and more effective treatment systems are urgently required.

Several chemical methods, such as electrochemical oxidation, hydrogen peroxide oxidation or ozonation have been proposed for thiocyanate removal and/or detoxification [2,10,28]. However, most of these chemical techniques are either too costly, ineffective or produce a toxic residue, for example, cyanide, and thus are not widely used [10].

Biological processes are an alternative method of treatment without creating or adding new chemicals to the environment [28]. However, it has been reported that substrate inhibition begins to appear at thiocyanate concentrations higher than 20 ppm and complete inhibition occurs at concentrations higher than 1,000 ppm [14]. A number of chemolithotrophic and chemoheterotrophic bacteria isolated from a variety of sources can utilize thiocyanate as a source of energy and nutrients [6,10]. These include *Paracoccus* species which are able to oxidize not only thiocyanate, but also thiosulphate, tetrathionate, sulphide and elemental sulphur [9]. Thiobacilli can also utilize thiocyanate as both a nitrogen and sulphur source. *Arthrobacter* utilizes thiocyanate as a nitrogen source, even in the presence of other nitrogen sources (ammonia or nitrate). *Pseudomonas stutzeri* uses thiocyanate as both a sulphur and

*Author to whom correspondence should be addressed. Tel: 985 10 34 39. Fax: 985103434. E-mail: mariodiaz@uniovi.es

1544-8053/15/03 113-05
© 2015 DEStech Publications, Inc.
doi:10.12783/issn.1544-8053/12/3/1

nitrogen source in absence of ammonium ion [10]. Grigor'eva *et al.* [11] used a co-culture of *Pseudomonas putida* and *Pseudomonas stutzeri* to degrade both cyanide and thiocyanate. Paruchuri *et al.* [20] used a bacterial consortium containing *Pseudomonas* and *Bacillus* species to degrade thiocyanate. None of their single isolates were able to degrade thiocyanate.

In all cases, thiocyanate degradation pathways are sensitive to the thiocyanate concentration, the physicochemical conditions, and the presence of interfering and inhibitory compounds [6]. Thus, in addition to nutrients and carbon and nitrogen sources, other essential conditions for successful biological degradation of cyanide compounds must be taken into account: pH, temperature, oxygen availability, microbial population and nutrient availability being the most important [22].

Paracoccus thiocyanatus is a facultative chemolithotrophic thiocyanate-degrading bacterium which was isolated from activated sludge enriched with thiocyanate. This bacterium has been reported as capable of utilizing thiocyanate as sole energy source [17]. However, the literature describes no investigation into the effect that the presence of other carbon and nitrogen sources have on the degradation process of thiocyanate by this microorganism. Several authors have proposed the following process for the utilization of thiocyanate by *Thiobacillus thiocyanooxidans*. First, thiocyanate is hydrolysed to cyanate (OCN^-) and sulphide, followed by hydrolysis of cyanate to ammonia and bicarbonate, and oxidation of sulphide to sulphate [10,15]. In addition, Kim and Katayama [18] described the hydrolyzation of thiocyanate by *T. thioparus* THI115 to ammonia and carbonyl sulphide, which is subsequently oxidized to sulphate. Although the biological degradation of thiocyanate has been extensively studied, only a limited number of investigations have focused on the effect of the operating conditions and medium composition on the thiocyanate biodegradation kinetics, especially for *Paracoccus thiocyanatus*. In the present work, the effects of medium composition, different stirring speeds and initial inoculum size and growth stage on the degradation potential of the bacterial culture were investigated in order to determine the best conditions for the biodegradation of thiocyanate by *Paracoccus thiocyanatus*.

MATERIALS AND METHODS

Media Composition

Growth Medium (GM): 5 g peptone L^{-1}, 5 g beef extract L^{-1}, 5 g yeast extract L^{-1}, 2.5 g NaCl L^{-1}, 0.1 g K_2HPO_4 L^{-1}, 0.05 g $MgSO_4 \cdot 7H_2O$ L^{-1} [16]. GM-agar medium is composed of GM and 20% of agar.

Mineral Medium (MM): 0.5 g K_2HPO_4 L^{-1}, 0.3 g $(NH_4)_2SO_4$ L^{-1}, 0.05 g $MgSO_4 \cdot 7H_2O$ L^{-1}, 0.01 g $FeCl_3 \cdot 6H_2O$ L^{-1}, 0.01 g $CaCl_2 \cdot 2H_2O$ L^{-1} and 10 mL of trace element solution L^{-1}. The trace element solution was composed of 8 mg $ZnSO_4 \cdot 7H_2O$ L^{-1}, 4 mg H_3BO_3 L^{-1}, 4 mg $Na_2MoO_4 \cdot 2H_2O$ L^{-1}, 4 mg $CuSO_4 \cdot 5H_2O$ L^{-1}, 4 mg $MnCl_2 \cdot 4H_2O$ L^{-1}, 4 mg $CoCl_2 \cdot 6H_2O$ L^{-1} [16]. For the experiments carried out with additional carbon source, glucose (0.1, 0.5, 1, and 3%) and yeast extract (0.5 and 1%) were added to the MM. Sulphur and nitrogen-free medium (FM) was prepared using $MgCl_2$ instead of $MgSO_4$ and without $(NH_4)_2SO_4$. In the trace element solution, $ZnSO_4 \cdot 7H_2O$ and $CuSO_4 \cdot 5H_2O$ were replaced by $ZnCl_2$ and $CuCl_2 \cdot 2H_2O$, respectively. Thiocyanate degradation tests were started by inoculating bacteria into a flask containing MM or FM and 100–10000 mg L^{-1} of thiocyanate. In all cases, KSCN (Panreac, 98% purity) was the source of SCN^- in the medium.

Microbial Strain and Culture Conditions

Paracoccus thiocyanatus (BCCM, Belgian Coordinated Collections of Microorganisms (LMG 24666T)) capable of degrading thiocyanate was used. Bacterial colonies, which had been grown in the GM-agar medium for 4 days at 30°C, were inoculated into 250 ml Erlenmeyer flasks containing 50 mL of GM. After incubation at 28ºC and 250 rpm, an aliquot was taken and used as an inoculum for subsequent experiments. This inoculum was centrifuged at 10,000 g for 10 min and the supernatant was eliminated so that only bacterial cells were added to the MM to avoid introducing compounds from the GM. Inocula were taken at different times of cell growth (12–45 hrs), and different inoculum sizes (5×10^7–3×10^8 cfu mL^{-1}) were also tested.

In order to check the effect of acclimatization to SCN^- before biodegradation, some tests were carried out by supplementing GM with SCN^- (range between 100–300 mg L^{-1}). Moreover, an intermediate medium was used to provide a less abrupt transition in composition between GM and MM, trying to reduce the lag time. The intermediate medium consisted of either a 10% dilution GM or MM with 0.5% glucose or yeast extract with thiocyanate. However, no positive effects were observed, so this acclimatization step was rejected. Additionally, MM was also tried as the growth

medium, but the growth rate was too low to obtain a suitable inoculum for the following experiments.

Biodegradation Experiments

All thiocyanate biodegradation experiments were performed in an incubator (New Brunswick Scientific, Classic Series), with controlled temperature and stirring speed. No attempt was made to maintain a constant pH value. The experiments were performed at bench scale, in 500 mL Erlenmeyer flasks containing 100 ml of medium. Temperature of all experiments was maintained at 28°C and different stirring speeds (150–250 rpm) were tested. Although this temperature can be considered as scarcely high for WWTP, wastewaters containing SCN^- are frequently produced in industrial processes at medium-high temperature such as production of coke, so this temperature, after cooling the stream, appears reasonable in an industrial wastewater treatment. Samples were taken at different times and immediately analysed.

Analytical Methods

The concentration of thiocyanate was determined by a colorimetric process and according to the standard methods. Thiocyanate was estimated using ferric nitrate at acidic pH at 460 nm. This method has a detection limit of 0.1 mg L^{-1} [3]. The equipment employed for the spectrophotometric determinations was a UV/Vis spectrophotometer (Thermo Scientific, Heλiosγ).

Cell concentration in the medium was measured by spread plate counting on GM-agar medium (4 days of incubation time at 30°C) or by measuring the optical density at 660 nm (Shimazdu, UV 1203). Data were converted to cell dry weight (g L^{-1}) using the corresponding calibration curves previously obtained.

All experiments were carried out at least by duplicate and samples were analyzed in triplicate. Standard deviations, SD, obtained in each case are shown in the figures as vertical lines.

RESULTS AND DISCUSSION

Selection of Inoculum Size and Stirring Speed

The inoculum employed for the thiocyanate biodegradation test was taken from a *Paracoccus thiocyanatus* culture grown in GM. The growth curve obtained in this medium showed that the length of lag-phase was around 12 hrs, the stationary phase was reached after 36 hrs with final concentrations of around 8.3×10^9 cfu mL^{-1}, with the endogenous phase beginning after 66 hrs. The inoculum was taken at the end of the exponential phase of growth, after 36 hrs.

Firstly, the influence of the size of the inoculum introduced into the MM containing thiocyanate was studied. With inoculum sizes of 3×10^8, 9×10^7 and 5×10^7 cfu L^{-1}, the thiocyanate was completely removed in 124 hrs, 65 hrs and 60 hrs respectively [Figure 1(a)]. Thus, the higher the inoculum size, the lower was the biodegradation rate. This was due in part to the increase in the induction time (t_i) required for the acclimation of the bacteria. A linear relationship between the induction time and the inoculum size (IS) of the process was obtained ($t_i = 2 \times 10^{-7} \cdot$IS (cfu mL^{-1}), $r^2 = 0.985$).

The inoculum size has been previously described as an important factor in degradative processes, higher inoculum sizes usually leading to an increase in the rate of degradation [12]. However, in this work the behaviour observed was the opposite, and as seen in Figure 1(b), the smallest inoculum size gave the highest specific degradation rates, with a maximum value of 0.29 g SCN^- (g cell·h)$^{-1}$. Zohar *et al.* [29] have already found similar behaviour. These authors reported that different inoculum sizes of *Arthrobacter 4Hβ* produced positive or negative effects on the degradation rate of p-nitrophenol (PNP), depending on the initial concentrations of PNP. So, at concentrations of 50 mg PNP L^{-1}, the increase in inoculum size did not enhance the degradation rate but with 100 mg PNP L^{-1}, a larger inoculum size led to an improvement in the degradation rates. This phenomenon was attributed to substrate limitation at 50 mg PNP L^{-1}. More recently, Salam and Lakshmi [21] investigated the biodegradation of lindane using *Rhodotorula* sp. and checked the effect of the initial inoculum size (10–90 mg dry cell weight L^{-1}) on the contaminant degradation. The yeast showed a maximum biomass production and degradation efficiency with an inoculum of 70 mg dry cell weight L^{-1}. For an inoculum size of 90 mg L^{-1}, these authors did not observe change in the rate of degradation.

Different stirring speeds have been used in previous studies that have focused on the biodegradation of contaminants by *Paracoccus* species. These values range from 120 to 250 rpm [5,25]. In this work, two values of stirring speed were tested to check the effect of agitation on the degradation rate of thiocyanate. The chosen values were 150 and 250 rpm, at the opposite extremes of the usual range. The biodegradation rate of the system was positively influenced by the stirring speed,

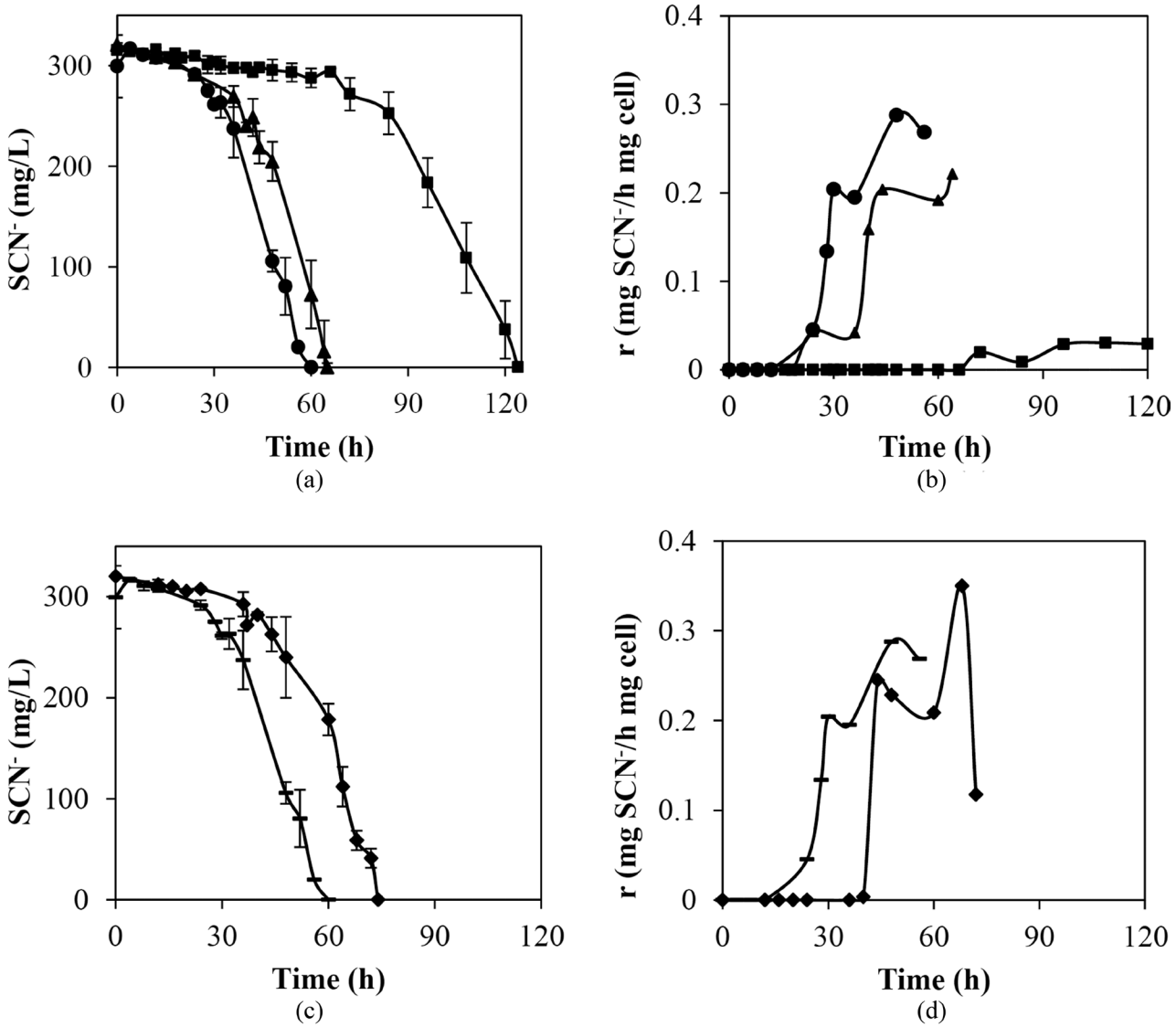

Figure 1. *Thiocyanate degradation (300 mg SCN^- L^{-1}) by Paracoccus thiocyanatus in mineral medium. (a) and (b) Effect of inoculum size at 250 rpm (● 5×10^7 cfu mL^{-1}, ▲ 9×10^7 cfu mL^{-1}, ■ 3×10^8 cfu mL^{-1}) on (a) thiocyanate degradation; and (b) specific degradation rate. (c) and (d) Effect of stirring speed (inoculum size 5×10^7 cfu mL^{-1}) (♦150 rpm, – 250 rpm) on (c) thiocyanate degaradation; and (d) specific degradation rates. In all cases, 28°C and inoculum taken at 36 hours.*

since complete removal of thiocyanate was achieved in 74 hrs at 150 rpm, this being reduced to 60 hrs at 250 rpm [Figure 1(c)]. Higher stirring speed implies higher dissolved oxygen concentration, which benefits the biodegradation of SCN^- by *P. thiocyanatus*, mainly reducing the induction time of the process and not the rate of degradation, as is shown in Figure 1(d).

Consequently, 250 rpm and an initial inoculum size of 5×10^7 cfu mL^{-1} were chosen as optimum conditions for the subsequent experiments. Twenty four hrs of growth in GM culture was selected as the inoculum age, which is a commonly used value reported by several authors because it corresponds to the middle of the exponential phase.

Utilization of Carbon, Nitrogen, and Sulphur

In this section, the way carbon, nitrogen and sulphur from thiocyanate utilized by the bacterial metabolism was studied.

Utilization of Carbon from Thiocyanate

Initially, thiocyanate biodegradation was studied in a MM that contained both nitrogen and sulphur molecules, but not carbon in its composition. The incorporation of carbon into the bacterial metabolism from the thiocyanate molecule was investigated for different thiocyanate concentrations (between 100 and

10,000 mg L^{-1}). Figures 2(a) and 2(b) show the biodegradation of thiocyanate and cell growth. Thiocyanate degradation occurred in two stages, the first where thiocyanate concentration remained almost constant due to the acclimatization of *P. thiocyanatus* to the new conditions and a second stage where the thiocyanate concentration decreased at a constant rate. Complete thiocyanate degradation was achieved after 48, 52, 79, and 107 hrs with initial concentrations of 500, 1,000, 2,500 and 3,500 mg L^{-1} respectively. With initial thiocyanate concentrations of 5,000 and 6,000 mg L^{-1} had not been completely removed at the end of the experiments, 85.5% of the initial amount having been eliminated after 315 hrs and 31% after 336 hrs, respectively. When the initial concentration was 5,000 mg L^{-1}, a constant concentration was observed at the end of the reaction period. This suggests the possibility of a product inhibition mechanism. Considering the pH (6.5) and the possible mechanisms of thiocyanate degradation found in the bibliography, it seems likely that the inhibitory product was NH_4^+. Thus, when the amount of NH_4^+ formed from the degradation of SCN^- is high enough to cause inhibition [4,27], the biodegradation rate decreases and the thiocyanate concentration remains invariable with time. If all the nitrogen metabolized was transformed into NH_4^+, the final concentration of NH_4^+ would be higher than 1,000 mg L^{-1} for an initial thiocyanate concentration of 3,600 mg L^{-1}. According to Vázquez *et al.* [27], the kinetics of SCN^- biodegradation were affected by the presence of ammonium when the concentration of NH_4^+-N increased from 49 mg L^{-1} to 135 mg NH_4^+-N L^{-1}. However, in this work inhibition by product was not observed for initial thiocyanate concentrations of 3,500 mg L^{-1} or lower.

Finally, for initial concentrations of thiocyanate higher than 7,000 mg L^{-1}, removal of thiocyanate was not observed, indicating a mechanism of substrate inhibition.

Figure 2(b) shows the evolution of the cell concentration (X) cfu mL^{-1} in relation to the initial cell concentration (X_0) cfu mL^{-1} for each of the initial thiocyanate concentrations. A continuous increase in biomass concentration was observed during the whole time of the experiment for initial thiocyanate concentrations lower than 2,500 mg SCN^- L^{-1}. With concentrations of 3,500 mg SCN^- L^{-1}, bacterial growth finished after 60 hrs and remained constant at a value of around 3.5 $\times 10^8$ cfu mL^{-1}. For initial concentrations of 5,000 and 6,000 mg SCN^- L^{-1} the maximum concentration of biomass was 4.7×10^8 and 1.4×10^8 cfu mL^{-1} respectively, which then decreased, achieving values below the initial bacterial concentration.

The effect of the initial concentration of thiocyanate on the induction time and kinetics of the process is discussed in more detail in Section 3.2.2.

Utilization of Nitrogen and Sulphur from Thiocyanate

In MM, nitrogen was present in $(NH_4)_2SO_4$ and sulphur in $(NH_4)_2SO_4$, $MgSO_4 \cdot 7H_2O$ and in trace solutions as $ZnSO_4 \cdot 7H_2O$, $CuSO_4 \cdot 5H_2O$. In order to

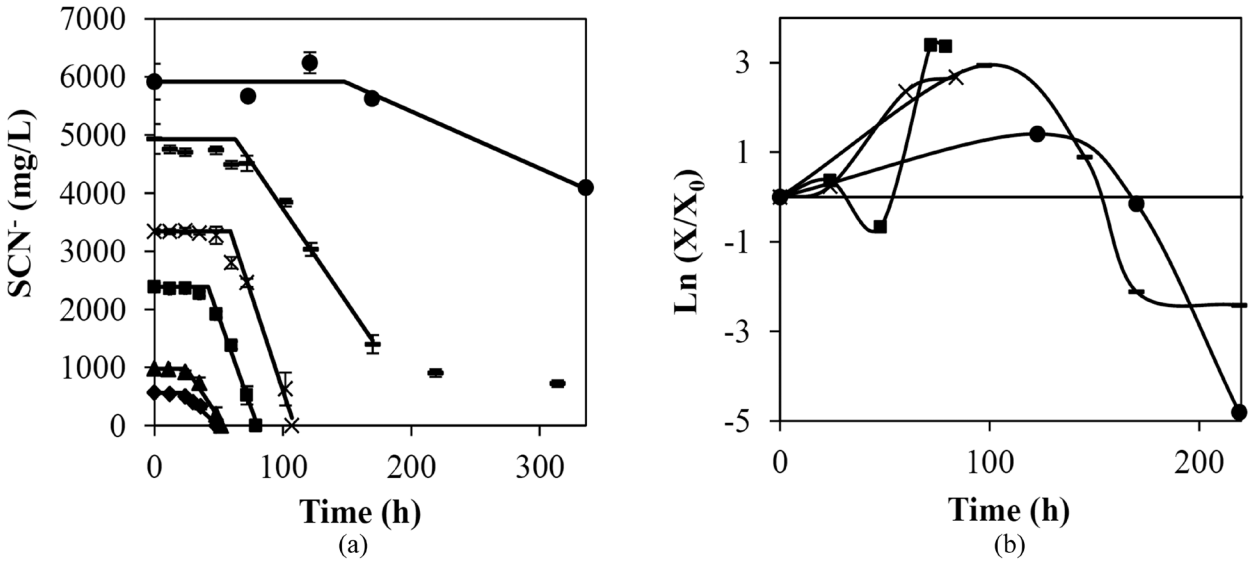

Figure 2. (a) *Thiocyanate biodegradation and (b) growth of Paracoccus thiocyanatus under different initial SCN^- concentrations (♦ 500 mg L^{-1}, ▲1000 mg L^{-1}, ■ 2500 mg L^{-1}, × 3500 mg L^{-1}, – 5000 mg L^{-1}, ● 6000 mg L^{-1}). In all cases: MM, 28ºC, 250 rpm and inoculum size of (2.06 ± 1.26) × 10^7 cfu mL^{-1}. Solid lines in (a) denote fitting of thiocyanate biodegradation to a pseudo zero-order kinetics model.*

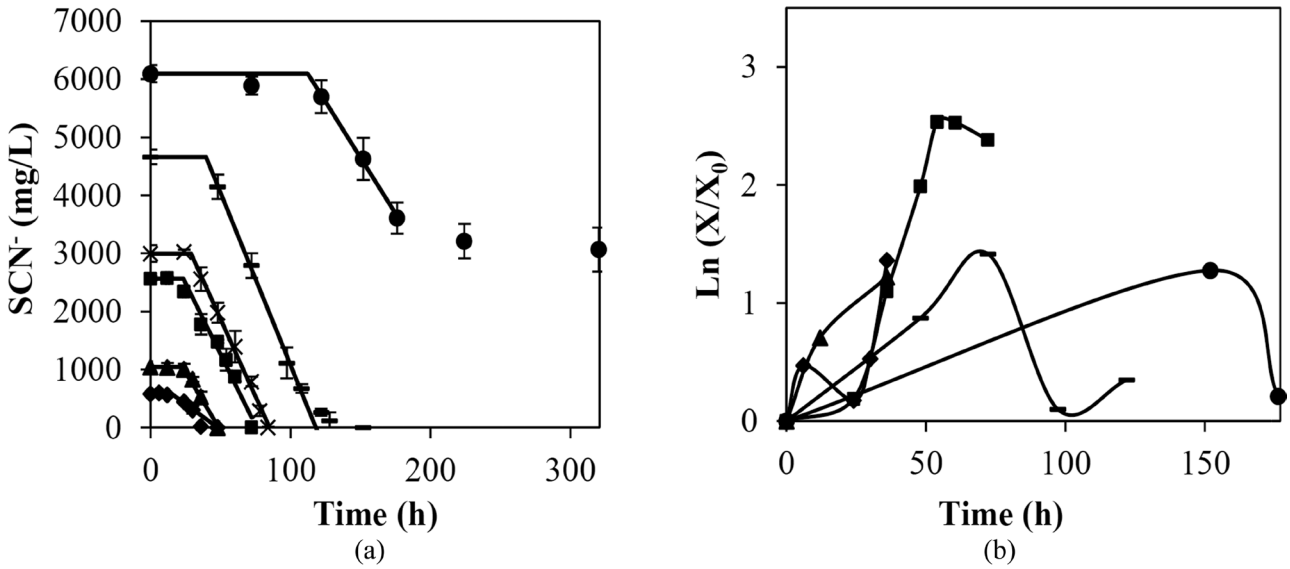

Figure 3. *(a) Thiocyanate biodegradation and (b) growth of Paracoccus thiocyanatus under different initial SCN^- concentrations (♦ 500 mg L^{-1}, ▲1000 mg L^{-1}, ■ 2500 mg L^{-1}, × 3500 mg L^{-1}, – 5000 mg L^{-1}, ● 6000 mg L^{-1}). In all cases: free medium, 28ºC, 250 rpm, inoculum age of 24 hours and inoculum size of (3.74 ± 0.47) × 10^7 cfu mL^{-1}. Solid lines in Figure a denote fitting of thiocyanate biodegradation to a pseudo zero-order kinetics model.*

discover whether the bacterium was capable of using thiocyanate as the sole N and S source, experiments were carried out using a free-mineral medium (FM) that contained these elements only in the thiocyanate molecules.

Again, different initial thiocyanate concentrations between 500 and 6,000 mg L^{-1} were tested (Figure 3). Complete degradation of thiocyanate was achieved after 40, 48, 72, 84, and 132 hrs for initial concentrations of thiocyanate of 500, 1,000, 2,500, 3,500 and 5,000 mg L^{-1}. Comparing these data with the results obtained in MM, the times for complete removal of thiocyanate were reduced when the medium had no additional sources of S and N, at all the thiocyanate concentrations used. Complete biodegradation of thiocyanate was achieved after 132 hrs in FM with an initial thiocyanate concentration of 5,000 mg L^{-1}, whereas after this time only 53% of initial thiocyanate was eliminated in MM. Of the thiocyanate initially present, 47% was removed in FM after 224 hrs when the initial concentration was 6,000 mg L^{-1}, whereas only 18% of the thiocyanate was eliminated during this time when secondary sources of S and N were added.

According to studies that focused on thiocyanate biodegradation, 2,500 mg L^{-1} of thiocyanate were biodegraded in 120 hrs with the co-culture *Klebsiella pneumoniae* and *Ralstonia* sp [6], 3,395 mg SCN^- L^{-1} were removed after 7 days by *Thiobacillus thioparus* THI115 [18] and 970 mg SCN^- L^{-1} were eliminated by *Thioalkalivibrio thiocyanodenitrificans* [24] after 30–40 days. Considering these results, our system is more efficient in terms of the thiocyanate biodegradation rate, especially when the medium is free of C, N and S sources. Kwon *et al.* [19] achieved higher removal rates by employing *Acremonium strictum*: up to 7,400 mg L^{-1} of thiocyanate was degraded in just 85 hrs.

In Figure 3(b), the bacterial growth observed during the biodegradation of thiocyanate in FM is shown. In all cases, bacterial growth exhibited the same behaviour as was observed with MM, since growth tendency and orders of magnitude were similar in both cases. Substrate inhibition of cell growth occurred for initial concentrations of thiocyanate higher than 3,500 mg L^{-1}.

Solid lines in Figures 2(a) and 3(a) denote the theoretical evolution of thiocyanate concentration according to the proposed kinetic model. In all cases, the data were successfully fitted to a zero reaction order model with induction time ($C_{SCN^-} = C_{SCN,0^-} - k(t - t_i)$). The obtained values of induction time (t_i) and the kinetic constant (k) during the fitting of each of the runs are summarized in Figure 4. Figure 4(a) shows the induction period obtained for each initial concentration of thiocyanate (SCN_0^-) and medium (MM or FM). In view of the results, the induction times in FM were always shorter than when biodegradation occurred in MM. It seems that the absence of other sources of N and S accelerate the metabolism of the bacteria in order to utilize thiocyanate as substrate. Figure 4(b) shows the kinetic constants obtained in each case. When us-

ing MM, the kinetic constant was at a maximum when the initial concentration of thiocyanate was 3,500 mg L^{-1} (67 mg $(Lh)^{-1}$). However, the maximum was obtained for an initial concentration of 5,000 mg L^{-1} (59 mg $(Lh)^{-1}$) when the biodegradation occurred in FM. Kinetic constants were higher in MM for the lowest initial concentrations of thiocyanate, whereas the opposite behaviour was observed for concentrations higher than 4,000 mg L^{-1}. Degradation rates between 1 and 87 mg $(Lh)^{-1}$ were reported for the biodegradation of thiocyanate by specific microorganisms [6,18,19,24] similar to the degradation rates obtained in this work. In fact, only *Acremonium strictum* showed higher removal rates [19].

In Figure 5, the comparison of the specific thiocyanate degradation rates in FM and MM for different initial SCN^- concentrations (500–6,000 mg L^{-1}) is shown. It is observed that the specific degradation rates are higher when no secondary sources of S and N are present in the medium. This behaviour is observed in all cases, with the exception of the final hours of the experiments with initial concentrations of thiocyanate higher than 3,500 mg L^{-1}. With initial thiocyanate concentrations of 500 and 1,000 mg L^{-1}, a rising trend of the specific degradation rate was observed. Maximum values of 0.91 and 1.17 mg $SCN^-\cdot(h\cdot mg\ cell)^{-1}$ were obtained with FM, whereas 0.32 and 0.55 mg $SCN^-\cdot(h\cdot mg\ cell)^{-1}$ were obtained with MM. For higher concentrations of thiocyanate, the specific degradation rates reached a maximum and then decreased. In all cases, the maximum value of the specific degradation rates was higher and was reached sooner with FM.

The specific growth rate (μ) was calculated by means of the following equation:

$$r_x = \frac{dX}{dt} = \mu X \tag{1}$$

where r_x is the rate of biomass growth; X is the cell concentration; μ is the specific biomass growth rate and t is time.

The specific growth rates (μ) *versus* thiocyanate initial concentrations obtained from batch tests are shown in Figure 6. As can be seen, μ values achieved a maximum, suggesting that there was inhibition by substrate. A non-competitive model [Equation (2)], a Teisser model [Equation (3)] and an Aiba-Edwards model [Equation (4)] were used for the fitting of substrate-inhibited growth [26].

$$\mu = \frac{\mu_{\max} \cdot S}{(K_S + S)\cdot\left(1 + \frac{S}{K_i}\right)} \tag{2}$$

$$\mu = \mu_{\max} \cdot (e^{-S/K_i} - e^{-S/K_s}) \tag{3}$$

$$\mu = \mu_{\max} \cdot S \cdot e^{\frac{-S/K_i}{(K_s+S)}} \tag{4}$$

where μ_{max} is the maximum specific growth rate; K_s is the substrate-affinity constant; and K_i is the substrate-inhibition constant.

The fitting parameters: maximum specific growth

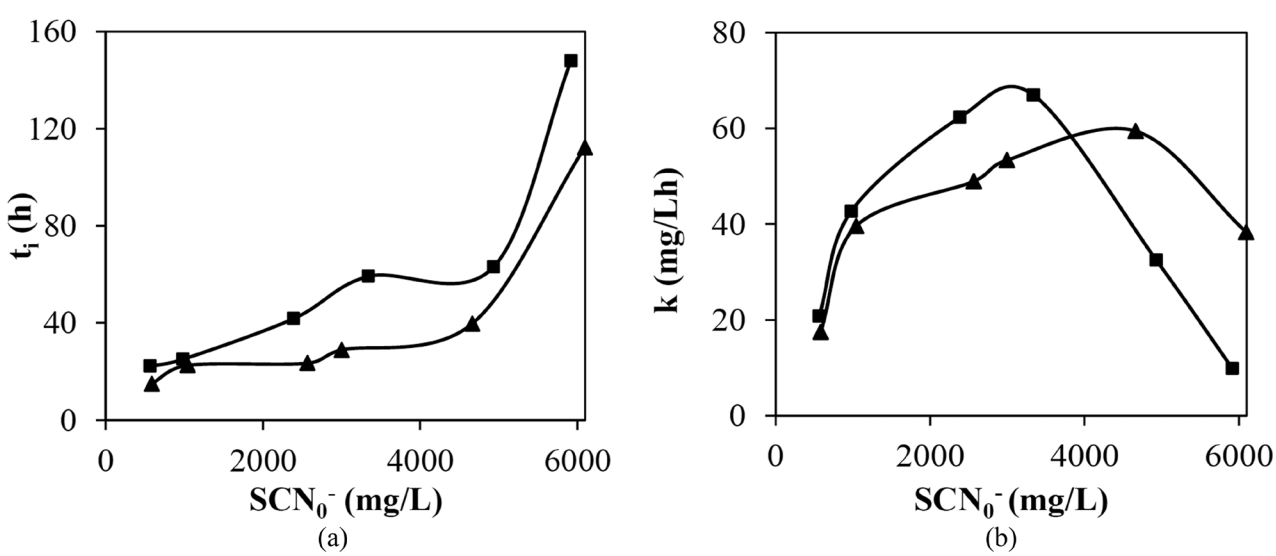

Figure 4. *(a) Induction periods (t_i) and (b) kinetic constants (k) obtained during the fitting of thiocyanate biodegradation data obtained using different initial concentrations in mineral or free media (▲ FM, ■ MM).*

rate (h^{-1}) μ_{max}, substrate-affinity constant, K_s (mg L^{-1}) and substrate-inhibition constant, K_i (mg L^{-1}) were obtained and summarized in Table 1. Experimental results and theoretical data obtained using each of the models are also compared in Figure 6.

These three models were fitted to the μ values obtained in this work and in view of the results (Figure 6) the best fits were obtained using the Teisser and Aiba-Edwards models. These models have generally been used to describe substrate inhibition of the growth of pure mi-

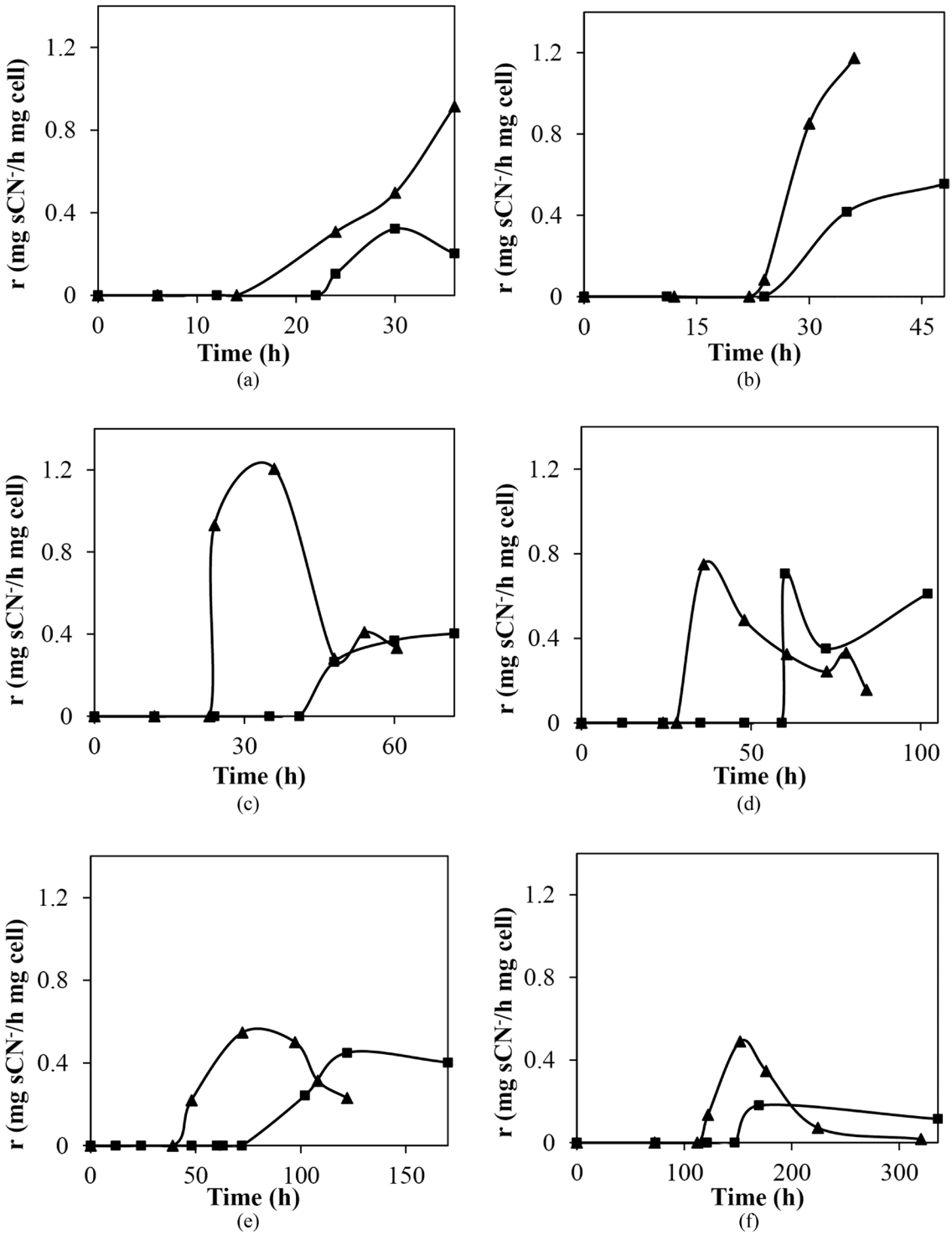

Figure 5. *Specific degradation rate for thiocyanate biodegradation in MM or FM: (a) 500 mg L^{-1}; (b) 1000 mg L^{-1}; (c) 2500 mg L^{-1}; (d) 3500 mg L^{-1}; (e) 5000 mg L^{-1}; (f) 6000 mg L^{-1} (▲FM, ■ MM). In all cases: 28°C, 250 rpm, FM inoculum size of (3.74 ± 0.47) × 10^7 cfu mL^{-1} and MM inoculum size of (2.06 ± 1.26) × 10^7 cfu mL^{-1}.*

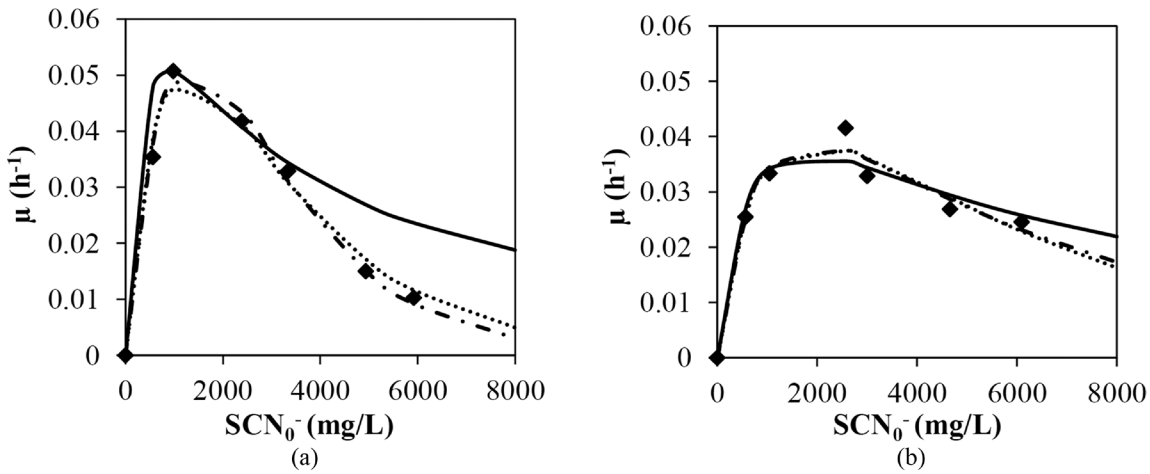

Figure 6. *Specific growth rate of suspended biomass in a thiocyanate solution (500–6000 mg L^{-1}). (♦ Experimental data, — Noncompetitive model, – · – · – · Teisser model, · · · · · Aiba-Edwards model): (a) In MM; (b) In FM. In all cases: 28ºC, 250 rpm, FM inoculum size of (3.74 ± 0.47) × 10^7 cfu mL^{-1} and MM inoculum size of (2.06 ± 1.26) × 10^7 cfu mL^{-1}.*

crobial cultures. The magnitude of K_s values indicates the affinity between substrate and microorganism [26]. For the Teisser and Aiba-Edwards models, K_s in the case of FM was slightly lower than that obtained with MM, indicating that the biomass has a higher affinity for the substrate in the case of mineral medium with no additional sources of N or S. The inhibition constant K_i is the substrate concentration at which μ is reduced to 50% of μ_{max} due to substrate inhibition. The magnitude of this parameter indicates the inhibition tendency and the degree of toxicity of the substrate towards the microorganisms [26]. Comparing the K_i values obtained in MM and FM for the Teisser and Aiba-Edwards models, it can be concluded that the presence of additional sources of N and S increases the inhibitory effect of SCN^- concentration on *Paracoccus thiocyanatus*.

The following data allow comparison with the kinetic parameters obtained for the degradation of thiocyanate with other bacteria such as *Klebsiella* sp [1]. These included μ_{max}, s, Y, K_i, which were evaluated as 0.62 ± 0.05 day^{-1}, 85 ± 8 mg SCN^- L^{-1}, 0.076 ± 0.011 mg dry cell mg^{-1} SCN^-, 131 ± 22 mg SCN^- L^{-1}, respectively, with the fourth order Runge-Kutta approximation. Chaudhari and Kodam [6] obtained values with the Haldane kinetic model of μ_{max} = 0.123 h^{-1}, K_s = 484 mg L^{-1}, K_i = 1.876 mg L^{-1} for degradation of thiocyanate with a co-culture of *Klebsiella pneumoniae* and *Ralstonia* sp. This suggested that the bacterial growth is lower for *Paracoccus thiocyanatus* than for the other species, whereas the substrate affinity was higher. At the same time, *Paracoccus thiocyanatus* shown a higher tolerance to elevated concentrations of thiocyanate than the aforementioned microorganisms.

The yield coefficient Y was estimated as $\Delta SCN^-/\Delta X$ using the experimental data of the exponential growth phase. The yield coefficients for experimental degradation data in MM and FM are listed in Table 2. In all cases, the yield coefficient in FM was lower than in MM. According to Filonov *et al.* [8], preference must be given to microorganisms that produce a lower yield of biomass per unit of the pollutant degraded. A minimum value of Y of 0.060 mg cell mg^{-1} SCN^- in MM for an initial concentration of thiocyanate of 5,920 mg L^{-1} and of 0.45 mg cell mg^{-1} SCN^- with an initial concentration of 6,090 mg L^{-1} in FM was achieved.

Presence of Carbon and Nitrogen that is Easily Assimilable by Bacterium

Influence of additional carbon and nitrogen sources

Table 1. Estimated Values of Parameters for Various Kinetic Models Employed for the Fitting of Experimental Data Obtained during Thiocyanate Biodegradation by Paracoccus Thiocyanatus.

	MM				FM			
	μ_{max} (h^{-1})	K_s (mg L^{-1})	K_i (mg L^{-1})	R^2	μ_{max} (h^{-1})	K_s (mg L^{-1})	K_i (mg L^{-1})	R^2
Noncompetitive	0.178	800	1050	92.9	0.146	1780	1790	99.2
Aiba-Edwards	0.203	1750	2280	99.3	0.094	1300	4980	99.4
Teisser	0.344	1150	1730	99.6	0.059	790	6520	99.4

Table 2. Yield Coefficients for Thiocyanate Biodegradation in MM and FM

MM		FM	
SCN_0^- (mg L^{-1})	*Y* (mg cell mg^{-1} SCN^-)	SCN_0^- (mg L^{-1})	*Y* (mg cell mg^{-1} SCN^-)
560	0.141	580	0.077
980	0.103	1040	0.064
2400	0.122	2560	0.064
3340	0.110	3000	0.108
4930	0.071	4660	0.059
5920	0.060	6090	0.045

in the wastewater during the biodegradation of thiocyanate by *Paracoccus thiocyanatus* was also checked by adding glucose (0.1 and 3%) or yeast extract (0.5 and 1%) to the MM containing thiocyanate. Figure 7 shows the evolution of thiocyanate concentration and specific degradation rate in MM with additional nitrogen and carbon sources. In view of the results (Figure 7a), thiocyanate biodegradation only occurred for the lowest glucose concentrations, 0.1 and 0.5% (61 and 72 hrs). Therefore, the system was adversely affected by the presence of glucose, since the higher the glucose concentrations, the lower was the bacterial growth obtained and the longer the time required for complete degradation of thiocyanate (data not shown). Furthermore, for glucose concentrations above 1%, there was neither bacterial growth nor thiocyanate degradation. It can be concluded that the presence of this substrate has an adverse effect on the biodegradation of thiocyanate by *P. thiocyanatus*. In Figure 7(b) the specific degradation rates of thiocyanate produced in MM containing 0.1 and 0.5% glucose is shown. It can be observed that the lower the proportion of glucose, the higher the degradation rates was.

Yeast extract was also tested as an additional carbon and nitrogen source during the biodegradation of SCN^- by *P. thiocyanatus* [Figure 7(a)]. Using this carbon and nitrogen source, high biomass concentrations were achieved, reaching values higher than 10^9 cfu mL^{-1}. These results suggest that the additional nitrogen source was utilized for biomass metabolism instead of the SCN^-. Similar behaviour was observed by Chaudhari and Kodam [6] with co-culture of *Klebsiella pneumoniae* and *Ralstonia* sp. On the other hand, according to Filonov *et al.* [8], addition of a carbon source as nutrient during naphthalene degradation by *Pseudomonas putida* G7 increases cellular activity, stimulating the growth of microorganisms capable of degrading the target compound. However, this same carbon source can inhibit degradation of some compounds, resulting in diauxic growth. Hence, it is important to add the optimal quantity of nutrients. It is a well-known fact that the addition of nutrients below or above the optimal quantity result in the reduction or cessation of the degradation. In this case, the best results were obtained when SCN^- was the only source of C, S and N.

Physiological State of Bacteria

The influence of physiological stage of the inoculum in the biodegradation process was also analysed.

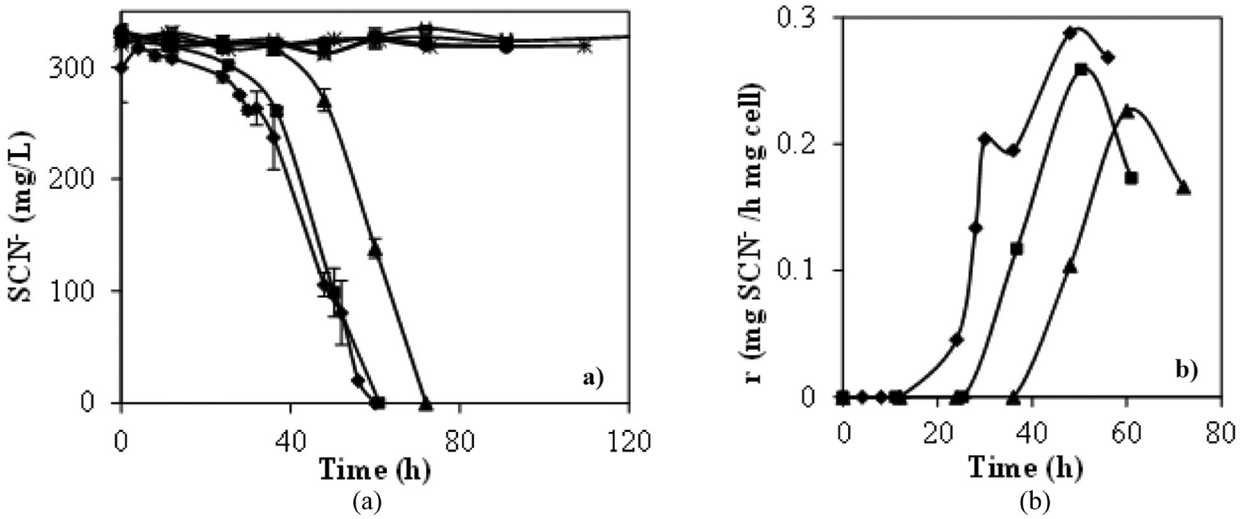

Figure 7. *Effect of addition of glucose or yeast extract in thiocyanate degradation by Paracoccus thiocyanatus. (a) Thiocyanate concentration; and (b) Specific degradation rate. In all cases: mineral medium (300 mg SCN^- L^{-1}), 28ºC, 250 rpm, inoculum size 5×10^7 cfu mL^{-1} and inoculum stage of 36 hours (♦MM, ■ 0.10% glucose, ▲0.5% glucose, ● 1% glucose, ✶ 3% glucose, × 0.5% yeast extract, – 1% yeast extract).*

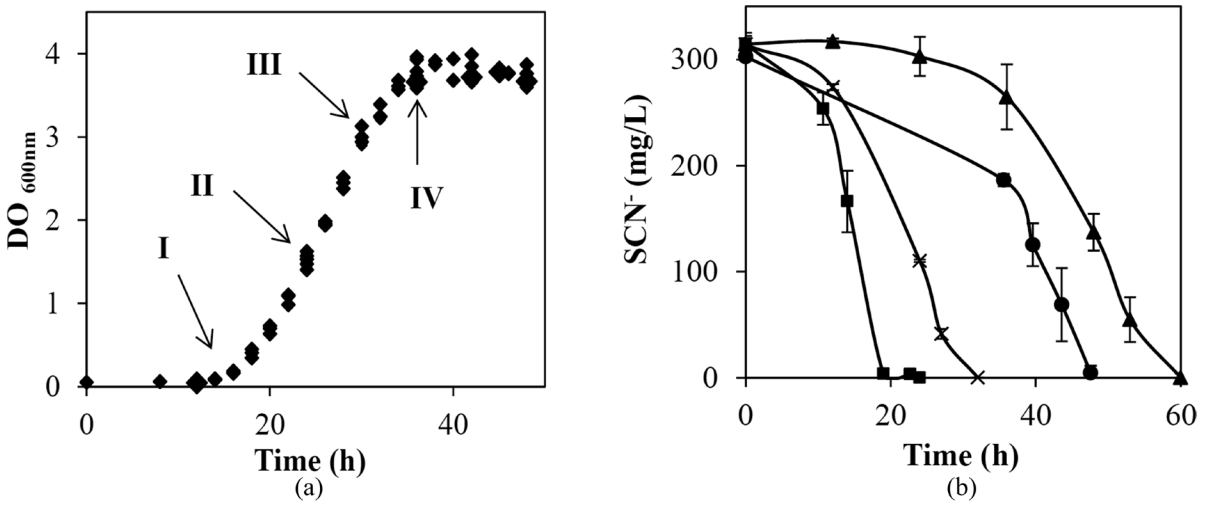

Figure 8. *(a) Growth of Paracoccus thiocyanatus in GM over 2 days. Arrows indicate the time when the inoculum was taken (b) Effect of inoculum stage on thiocyanate degradation by Paracoccus thiocyanatus. Inocula (■ I, × II, ● III and ▲ IV). In all cases: MM (300 mg SCN^- L^{-1}), 28ºC, 250 rpm and inoculum size of 5 × 10^7 cfu mL^{-1}.*

With this aim, bacterial cells taken at different growth times in GM [Figure 8(a)] were used to inoculate MM containing SCN^-, using in all cases the same inoculum size [Figure 8(b)]. When the inoculum was taken earlier, the thiocyanate degradation rate was faster. Therefore, with the inoculum obtained after 16 hrs of growth in GM (beginning of the exponential phase) complete thiocyanate degradation was achieved in just 19 hrs. However, 32 hrs where necessary if the inoculum was taken at 24 hrs of growth (middle of the exponential phase) and 60 hrs if inoculum was taken after the stationary phase of growth was reached. Silva *et al.* [23], tested the effect of the different physiological states of the bacterium *Pseudomonas fluorescens* HK44 in salicylic acid biodegradation. The percentage of salicylic acid degraded was higher (97%) when cells in the exponential phase were used, than when the inoculum corresponded to the stationary state (69%). This can be explained by the fact that cells in the exponential phase are already pre-activated and are capable of degrading their substrates faster than cells in the stationary state. In this work, it seems that cells are more active in the beginning hours of the exponential phase of growth.

CONCLUSIONS

The thiocyanate degradation process was influenced by inoculum size, so that the higher the inoculum size, the lower was the biodegradation rate. In part, this was due to the increase in the induction time required for the acclimation of the bacteria. The degradation time was reduced from 124 to 60 hrs by reducing the inoculum size from 3 × 10^8 to 5 × 10^7 cfu L^{-1}. The physiological stage of the inoculum also influenced the degradation process. In this case, it was found that when the inoculum was taken earlier, the thiocyanate degradation rate was faster. Likewise, the biodegradation rate of the system was positively influenced by the stirring speed, since higher stirring speed implies higher dissolved oxygen concentration that benefits the biodegradation of SCN^- by *P. thiocyanatus*, mainly by reducing the induction time of the process.

The degradation process of thiocyanate was different depending on the composition of the mineral medium. In the complete mineral medium (MM), *P. thiocyanatus* degraded 3,500 mg SCN^- L^{-1} in 107 hrs, whereas at concentrations greater than 5,000 mg L^{-1}, the SCN^- was not completely eliminated. When all sources of N and S were removed from the mineral medium (FM) 3,500 mg SCN^- L^{-1} was eliminated in 84 hrs and 5,000 mg SCN^- L^{-1} was completely degraded in 132 h. There were also significant differences in the specific thiocyanate degradation rates. Thus, the maximum specific degradation rate in FM was 1.21 mg SCN^-·(h·mg cell)$^{-1}$ with an initial thiocyanate concentration of 2,500 mg L^{-1}, whereas in MM the maximum specific degradation rate was 0.71 mg SCN^- ·(h·mg cell)$^{-1}$ with an initial thiocyanate concentration of 3,500 mg L^{-1}. The induction time when biodegradation occurred in FM was always smaller in comparison with the induction time in MM. To improve the degradation process of thiocyanate in real wastewaters, the presence of the other sources of C, N and S that are easily assimilated by the bacteria should be avoided. It was also investigated whether the presence of organic sources of carbon and nitrogen had an adverse effect

on the biodegradation of thiocyanate by *P. thiocyanatus* and it was found that their presence led to a reduction in the degradation rates of the process.

Substrate-inhibited growth models were used for the fitting of the thiocyanate degradation by *P. thiocyanatus* and the best fits were obtained using the Teisser and Aiba-Edwards models. K_s was higher with FM than with MM, indicating that the biomass has a higher affinity for the substrate in the case of mineral medium with no additional sources of N or S. Comparing the K_i values obtained in MM and FM, it can be concluded that the presence of additional sources of N and S increases the inhibitory effect of SCN^- concentration on *Paracoccus thiocyanatus*.

ACKNOWLEGEMENTS

R. G. Combarros wishes to express gratitude for a research grant from the Government of the Principality of Asturias (Severo Ochoa Programme).

REFERENCES

1. Ahn JH, Lee S, Hwang S (2005) Growth kinetic parameter estimation of Klebsiella sp. utilizing thiocyanate. *Process Biochem 40*(3–4). http://dx.doi.org/10.1016/j.procbio.2004.06.004
2. Akcil A, Mudder T (2003) Microbial destruction of cyanide wastes in gold mining: process review. *Biotechnol Lett 25*:445–450. http://dx.doi.org/10.1023/A:1022608213814
3. American Public Health Association APHA (1999) *Standard Methods for the Examination of Water and Wastewater.* 20 th. Ed. Washington.
4. Bryant CW, Cawein CC, King PH (1988) Biological treatability of in situ coal gasification wastewater. *J Environ Eng-ASCE 114*:400–414. http://dx.doi.org/10.1061/(ASCE)0733-9372(1988)114:2(400)
5. Cai S, Li X, Cai T, He J (2013) Degradation of piperazine by Paracoccus sp. TOH isolated from activated sludge. *Bioresource Technol 130*:536–542. http://dx.doi.org/10.1016/j.biortech.2012.12.095
6. Chaudhari AU, Kodam MK (2010) Biodegradation of thiocyanate using co-culture of *Klebsiella pneumoniae* and *Ralstonia* sp. *Appl Microbiol Biotech 85*:1167–1174. http://dx.doi.org/10.1007/s00253-009-2299-7
7. Ebbs S, (2004) Biological degradation of cyanide compounds. *Curr Opin in Biotech 15*:231–236. http://dx.doi.org/10.1016/j.copbio.2004.03.006
8. Filonov AE, Karpov AV, Kosheleva IA, Puntus IF, Balashova NV, Boronin AM (2000) The efficiency of salicylate utilization by *Pseudomonas putida* strains catabolizing naphthalene via different biochemical pathways. *Process Biochem C*: 983–987. http://dx.doi.org/10.1016/S0032-9592(00)00130-8
9. Ghosh W, Roy P (2007) Chemolithoautotrophic oxidation of thiosulphate, tetrathionate and thiocyanate by a novel rhizobacterium belonging to the genus *Paracoccus*. *FEMS Microbiol Lett 270*:124–131. http://dx.doi.org/10.1111/j.1574-6968.2007.00670.x
10. Gould WG, King M, Mohapatra BR, Cameron RA, Kapoor A, Koren DW (2012) A critical review on destruction of thiocyanate in mining effluents. *Miner Eng 34*:38–47. http://dx.doi.org/10.1016/j.mineng.2012.04.009
11. Grigoréva NV, Kondratéva TF, Krasilńikova EN, Karavaiko GI (2006) Mechanism of cyanide and thiocyanate decomposition by an association of *Pseudomonas putida* and *Pseudomonas stutzeri* strains. *Microbiology 75*:266–273. http://dx.doi.org/10.1134/S0026261706030040
12. Guillén-Jiméneza F, Cristiani-Urbinab E, Cancino-Díaz JC, Flores-Morenod JL, Barragán-Huertaa BE (2012) Lindane biodegradation by the *Fusarium verticillioides* AT-100 strain, isolated from *Agave tequilana* leaves: kinetic study and identification of metabolites. *Int Biodeter Biodegr 74*:36–47. http://dx.doi.org/10.1016/j.ibiod.2012.04.020
13. Hong L. Y., Banks M. K., Schwab A. P. (2008). Removal of cyanide contaminants from rhizosphere soil. *Bioremediation Journal, 12*(4):210–215. http://dx.doi.org/10.1080/10889860802491052
14. Hung CH, Pavlostathis SG (1997) Aerobic biodegradation of thiocyanate. *Water Res 31*:2761–2770. http://dx.doi.org/10.1016/S0043-1354(97)00141-3
15. Hung CH, Pavlostathis SG (1999) Kinetics and modeling of autotrophic thiocyanate biodegradation. *Biotechnol Bioeng 62*:1–11. http://dx.doi.org/10.1002/(SICI)1097-0290(19990105)62:1<1::AID-BIT1>3.0.CO;2-Q
16. Katayama Fujimura Y, Kuraishi H (1980) Characterization of thiobacillus novellus and its thiosulfate oxidation. *J. Gen. Appl. Microbiol. 26*:357–367. http://dx.doi.org/10.2323/jgam.26.357
17. Katayama Y, Hiraishi A, Kuraishi H (1995) *Paracoccus thiocyanatus sp*. nov., a new species of thiocyanate-utilizing facultative chemolithotroph, and transfer of *Thiobacillus versutus* to the genus *Paracoccus* as *Paracoccus versutus* comb. nov. with emendation of the genus. *Microbiology 141*:1469–1477. http://dx.doi.org/10.1099/13500872-141-6-1469
18. Kim SJ, Katayama Y (2000) Effect of growth conditions on thiocyanate degradation and emission of carbonyl sulfide by *Thiobacillus thioparus* THI115. *Water Research 34*:2887–2894. http://dx.doi.org/10.1016/S0043-1354(00)00046-4
19. Kwon HK, Woo SH, Park JM (2002) Thiocyanate degradation by Acremonium strictum and inhibition by secondary toxicants. *Biotechnol Lett 24*:1347–1351. http://dx.doi.org/10.1023/A:1019825404825
20. Paruchuri YL, Shivaraman N, Kumaran P (1990) Microbial transformation of thiocyanate. *Environ Pollut 68*:15–28. http://dx.doi.org/10.1016/0269-7491(90)90011-Z
21. Salam JA, Lakshmi V, Das D, Das N (2013) Biodegradation of lindane using a novel yeast strain, *Rhodotorula* sp. VITJzN03 isolated from agricultural soil. *World J Microb Biot 29*(3):475-487. http://dx.doi.org/10.1007/s11274-012-1201-4
22. Sengupta M (1997) *Bioremediation Engineering of Mining & Mineral Processing Wastes*. Northwest Academic Pub, ISBN-10 0965302504.
23. Silva TR, Valdman E, Valdman B, Leite SGF (2007) Salicylic acid degradation from aqueous solutions using *Pseudomonas fluorescens* HK44: Parameters studies and application tools. *Braz J Microbio 38*:39–44. http://dx.doi.org/10.1590/S1517-83822007000100009
24. Sorokin DY, Tourova TP, Antipov A N, Muyzer G, Kuenen JG (2004) Anaerobic growth of the haloalkaliphilic denitrifying sulfuroxidizing bacterium *Thialkalivibrio thiocyanodenitrificans sp*. nov. with thiocyanate. Microbiology 150:2435–2442. http://dx.doi.org/10.1099/mic.0.27015-0
25. Swaroop S, Sughosh P, Ramanathanc G (2009) Biomineralization of N,N-dimethylformamide by *Paracoccus sp*. strain DMF. J Hazard Mater 171:268–272. http://dx.doi.org/10.1016/j.jhazmat.2009.05.138
26. Tazdaït D, Abdi N, Grib H, Lounici H, Pauss A, Mameri N (2013) Comparison of different models of substrate inhibition in aerobic batch biodegradation of malathion. *Turk J Engin Environ Sciences* doi:10.3906/muh-1211-7. http://dx.doi.org/10.3906/muh-1211-7
27. Vázquez I., Rodríguez J., Mara-ón E., Castrillón L., Fernández Y. (2006) Simultaneous removal of phenol, ammonium and thiocyanate from coke wastewater by aerobic biodegradation. *J of Hazard Mater B 137*:1773–1780. http://dx.doi.org/10.1016/j.jhazmat.2006.05.018
28. Vedula R. K., Dalal S., Majumder C. B. (2013). Bioremoval of cyanide and phenol from industrial wastewater: An update. *Bioremediation Journal, 17*(4):278–293. http://dx.doi.org/10.1080/10889868.2013.827615
29. Zohar S, Kviatkovski I, Masaphy S (2013) Increasing tolerance to and degradation of high p-nitrophenol concentrations by inoculum size manipulations of Arthrobacter 4Hβ isolated from agricultural soil. *Int Biodeter Biodegr 84*:80–85. http://dx.doi.org/10.1016/j.ibiod.2012.05.041

Toxic Effects of Chronic Sub-Lethal Cu^{2+}, Pb^{2+} and Cd^{2+} on Antioxidant Enzyme Activities in Various Tissues of the Blood Cockle, *Anadara granosa*

CHAO PENG, XINGUO ZHAO, YU HAN, WEI SHI, SAIXI LIU and GUANGXU LIU*
College of Animal Sciences, Zhejiang University, Hangzhou, China, 310058

ABSTRACT: Blood cockles, *Anadara granosa*, live in coastal mudflats under threaten of low-dose chronic heavy metal exposure. The toxic effects of low dose chronic copper (7.1, 14.2, and 28.4 µg/L), lead (43, 86, and 172 µg/L), and cadmium (55, 110, and 220 µg/L) exposure on the antioxidant enzyme activities in gill, gonad and digestive gland of *A. granosa* were investigated in this study. The activities of superoxide dismutases (SOD), catalase (CAT) and glutathione peroxidase (GPx) fluctuated with increased copper, lead, and cadmium exposure time. The heavy metal exposure concentration and duration (7, 14, 21, and 28 days) showed significant effects on the antioxidant enzyme activities in tested tissues. Moreover, the activities of tested antioxidant enzymes not only varied among different tissues, but also were dependent on metal species, suggesting the reactive oxygen species (ROS) may be produced through different mechanisms for different metals in various tissues. Our results indicate that the application of antioxidant enzyme activities as endpoints in toxicology bioassays for chronic sub-lethal metals must be done with caution due to their complicated produce mechanisms.

INTRODUCTION

OVER the last few decades, large amounts of anthropogenic heavy metals have been released into marine and estuarine environments in China, which pose a great threat to near-shore aquaculture industry [1,2]. Blood cockle, also known as blood clam, *Anadara granosa*, is a traditional aquaculture species that is widely distributed throughout the Indo-Pacific region from the eastern coast of South Africa northwards and eastwards to Southeast Asia, Australian and up to northern Japan [3]. A series of toxic effects of acute heavy metal exposure on *A. granosa* have been reported [4,5]. It has been shown that acute heavy metal exposure can lead to histopathological alterations and subsequent mortality in *A. granosa*.

In reality, organisms are often under long-term sub-lethal heavy metal exposure, in which heavy metals often do not lead to mortality, but show various sub-lethal toxic effects [6,7]. Previous study showed that chronic low dose heavy metal exposure can lead to reductions in both filtration rate and gonad development of *A. granosa* [8]. Furthermore, compared to that of control, a significantly increased sex ratios (the number of male individuals/total number of individuals) of blood cockle was found under chronic sub-lethal heavy metal exposure [8]. Though, heavy metals are theoretically considered to induce the production of reactive oxygen species (ROS) and may result in significant damage to cellular constituents and subsequently affect the activity of antioxidant enzymes such as superoxide dismutases (SOD), catalase (CAT) and glutathione peroxidase (GPx) [9,10]. To our knowledge, there remains no study on the chronic toxic effects of heavy metals on antioxidant enzymes in *A. granosa*.

In this study, the effects of chronic sub-lethal copper, lead, and cadmium exposure on the antioxidant enzyme activities in gill, gonad, and digestive glands of *A. granosa* were investigated to determine the toxic effects of heavy metals on bioactive molecules. The results will contribute to a better understanding of heavy metal toxicity in mudflat marine bivalves.

MATERIALS AND METHODS

Blood Cockles and Metal Solutions

Adult blood cockles (shell length, 41.2 ± 6.43 mm) were collected from Yueqing, Wenzhou, China in April

*Author to whom correspondence should be addressed.
E-mail: guangxu_liu@zju.edu.cn

1544-8053/15/03 125-07
© 2015 DEStech Publications, Inc.
doi:10.12783/issn.1544-8053/12/3/2

2010 for antioxidant enzyme bioassay. The blood cockles were acclimatized for 7 days in 26 ± 3°C flowing seawater and fed with microalgae *Platymonas subcordiformis* before the experiment.

Experiments were performed using the following analytical grade salts: $Cu(NO_3)2\cdot 3H_2O$, $Pb(NO_3)_2$ and $Cd(NO_3)_2\cdot 4H_2O$. Stock solutions were prepared in deionized water at concentration (1 M), which was high enough to prevent weighing errors and salinity change [11]. Nominal experimental concentrations were chosen on the basis of preliminary trials [4], 7.1, 14.2, and 28.4 μg/L were used as experimental concentration for Cu^{2+}, 43, 86, and 172 μg/L were used as experimental concentration for Pb^{2+}, and 55, 110, and 220 μg/L were used as experimental concentration for Cd^{2+}, respectively.

Antioxidant Enzyme Activity Bioassays

Forty blood cockles were placed in each plastic tank with total seawater volume of 40 liters. For each tested metal, four tanks were set up to simulate various exposal doses. Three replicates were used for each experimental concentration and control tests. During the experiment, the blood cockles were fed with microalgae *P. subcordiformis* daily before the change of seawater and re-adding of corresponding tested metals. No dead animals were detected during the whole experiment. After adult blood cockles were exposed to various heavy metals for 7, 14, 21, and 28 days, six live individuals from each tank were dissected on ice and the gills, gonads, and digestive glands were peeled off and weighed separately. Twenty milligrams of each tissue type were homogenated with ice-cold 0.154 M KCl-50 mM Tris·HCl solution (pH 7.4) using a standard Teflon tissue homogenizer. After centrifuging at 10,000 g for 5 minutes, the tissue supernatants were used for antioxidant enzyme activity analysis. All procedures were conducted at 0–4°C.

Total protein concentrations were determined according to Bradford [12]. Estimations of anti-oxidant enzyme activities were conducted following the method of Wang [13]. SOD activity was measured through the inhibition of nitroblue tetrazolium reduction using spectrophotometer at 550 nm. One SOD activity unit was defined as the enzyme amount causing 50% inhibition in 1 mL reaction solution / mg tissue protein. CAT activity was measured using a spectrophotometric assay of hydrogen peroxide at 405 nm. An enzyme activity unit was defined as the degradation of 1 mol H_2O_2/mg tissue protein/second. GPx was analyzed spectrophotometrically by measuring the decrease of the enzymatic reaction of glutathione at 412 nm. One unit of GPx activity was defined as the decrease in the amount of 1 nmol/L glutathione in the enzymatic reaction system of 1 mg protein/minute. The activities of antioxidant enzymes were measured for three replicates of each trial with kits (Nanjing Jiancheng Bioengineering Institute, Nanjing, China) following the manufacturer's instruction with a spectrophotometer (WFZ UV-2800AH, Unico, Shanghai, China) and expressed in Unit/mg protein.

Statistics

The relative values of antioxidant enzyme activities incubated at different heavy metal concentrations were obtained by dividing their values by that of control tests [11]. Linear models "Relative activities = $a\cdot C + \beta\cdot T + \gamma\cdot C\cdot T$ + residuals" were constructed for the relative antioxidant enzyme activities in gills, gonads, and digestive glands under the stress of different tested metals. In total, 27 linear models were constructed for all combinations of three tissues (gill, gonad, and digestive gland), three tested metals (copper, lead, and cadmium), and three antioxidant enzymes (SOD, CAT and GPx). Two-way ANOVAs were then applied to each linear model to assess the effects of exposure concentration (C), exposure time (T) and their combination on the relative antioxidant enzyme activities for each metal. For all analyses, assumptions of normality and homogeneity of variance were assessed using Levene's tests. For the cases that these assumptions were not satisfied by the raw data, data were log-transformed prior to analysis. All statistics were performed using "R" statistic packages [14]. A p-value < 0.05 was accepted as statistically significant for all tests.

RESULTS

As shown in Figures 1–3 and Table 1, the exposure time had significant influences on the activities of antioxidant enzymes in gills, gonads and digestive glands of blood cockles in all experimental trials. In general, the influences of exposure time on antioxidant enzyme activities fluctuated and did not show a consistent pattern across various tested metals, antioxidant enzymes, and tissues. When comparing toxic effects of low dose cadmium on the activities of SOD among various tissues (Figure 3), it was evident that this effect was tissue specific. For instance, when 110 μg/L Cd showed highest toxicity to gonad at 14 days, it was found to

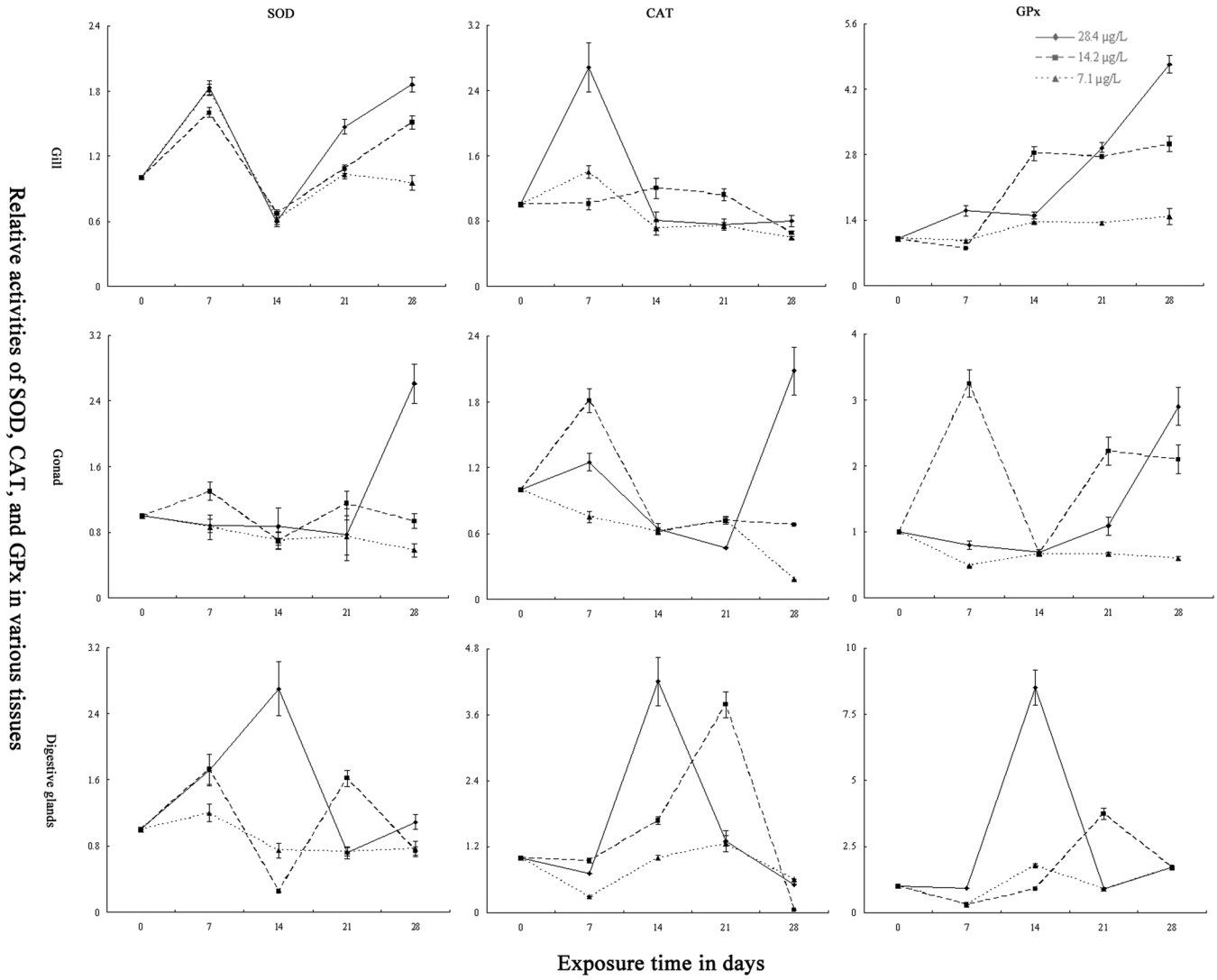

Figure 1. *Relative activities of SOD, CAT, and GPx in gills, gonads, and digestive glands of A. granosa exposed to copper at different exposure concentration (7.1, 14.2, and 28.4 μg/L) for 7, 14, 21, and 28 days.*

Table 3. Two-way ANOVAs on the Effects of Heavy Metal Exposure Concentration (C) and Time (T) on the Relative Activities of Antioxidant Enzymes in Gills, Gonads and Digestive Glands (DG) of A. granosa.

		p-values from Two-way ANOVAs for								
		SOD			CAT			GPx		
Metals	**Factors**	**Gill**	**Gonad**	**DG**	**Gill**	**Gonad**	**DG**	**Gill**	**Gonad**	**DG**
Cu^{2+}	*C*	0.52	< 0.01*	0.02*	0.04*	< 0.01*	0.02*	< 0.01*	< 0.01*	< 0.01*
	T	< 0.01*	< 0.01*	0.04*	< 0.01*	< 0.01*	< 0.01*	< 0.01*	< 0.01*	< 0.01*
	C·T	< 0.01*	< 0.01*	< 0.01*	< 0.01*	< 0.01*	< 0.01*	< 0.01*	< 0.01*	< 0.01*
Pb^{2+}	*C*	0.22	0.17	< 0.01*	< 0.01*	< 0.01*	< 0.01*	< 0.01*	< 0.01*	< 0.01*
	T	< 0.01*	< 0.01*	< 0.01*	< 0.01*	< 0.01*	< 0.01*	< 0.01*	< 0.01*	< 0.01*
	C·T	< 0.01*	< 0.01*	< 0.01*	< 0.01*	< 0.01*	< 0.01*	< 0.01*	< 0.01*	< 0.01*
Cd^{2+}	*C*	0.43	0.27	0.31	< 0.01*	< 0.01*	0.03*	0.36	0.04*	0.03*
	T	0.04*	0.02*	0.04*	< 0.01*	< 0.01*	< 0.01*	< 0.01*	< 0.01*	< 0.01*
	C·T	< 0.01*	< 0.01*	< 0.01*	< 0.01*	< 0.01*	< 0.01*	< 0.01*	< 0.01*	< 0.01*

Note: *indicates significant at $p < 0.05$.

be least toxic to gill and digestive glands. Moreover, it was showed that the effects of chronic sub-lethal metal exposure differed among various antioxidant enzymes. For example, when copper led to an increasing in GPx activities in gill with the increased exposure time, a reversed effect of copper on CAT activities were demonstrated (Figure 1).

The activities of antioxidant enzymes in various tissues were significantly affected by heavy metal concentration in most trials (Table 1). However, an evident non dose-response relationship between metal concentration and antioxidant enzymes activities were found. For instance, when exposed to sub-lethal lead for 28 days, it was shown that lead was more toxic at 86 μg/L than 172 and 43 μg/L for all tested antioxidant enzymes and tissues (Figure 2). Furthermore, few cases showed that the metal concentration had no significant effect on some antioxidant enzymes in specific tissues. For example, the concentration of cadmium had no significant influence on the activities of GPx in gills and digestive glands, or on the SOD activities in all three tested tissues (Figure 3). Both copper and lead concentration did not affect the activities of SOD in gills (Figure 1). Activities of SOD in gonads were also not affected by lead concentration (Figure 2).

DISCUSSIONS

It is well known that both organic and inorganic contaminations can induce oxidative stress by producing ROS such as hydrogen peroxide and superoxide anion. SOD, CAT, and GPx are cytosolic enzymes found in

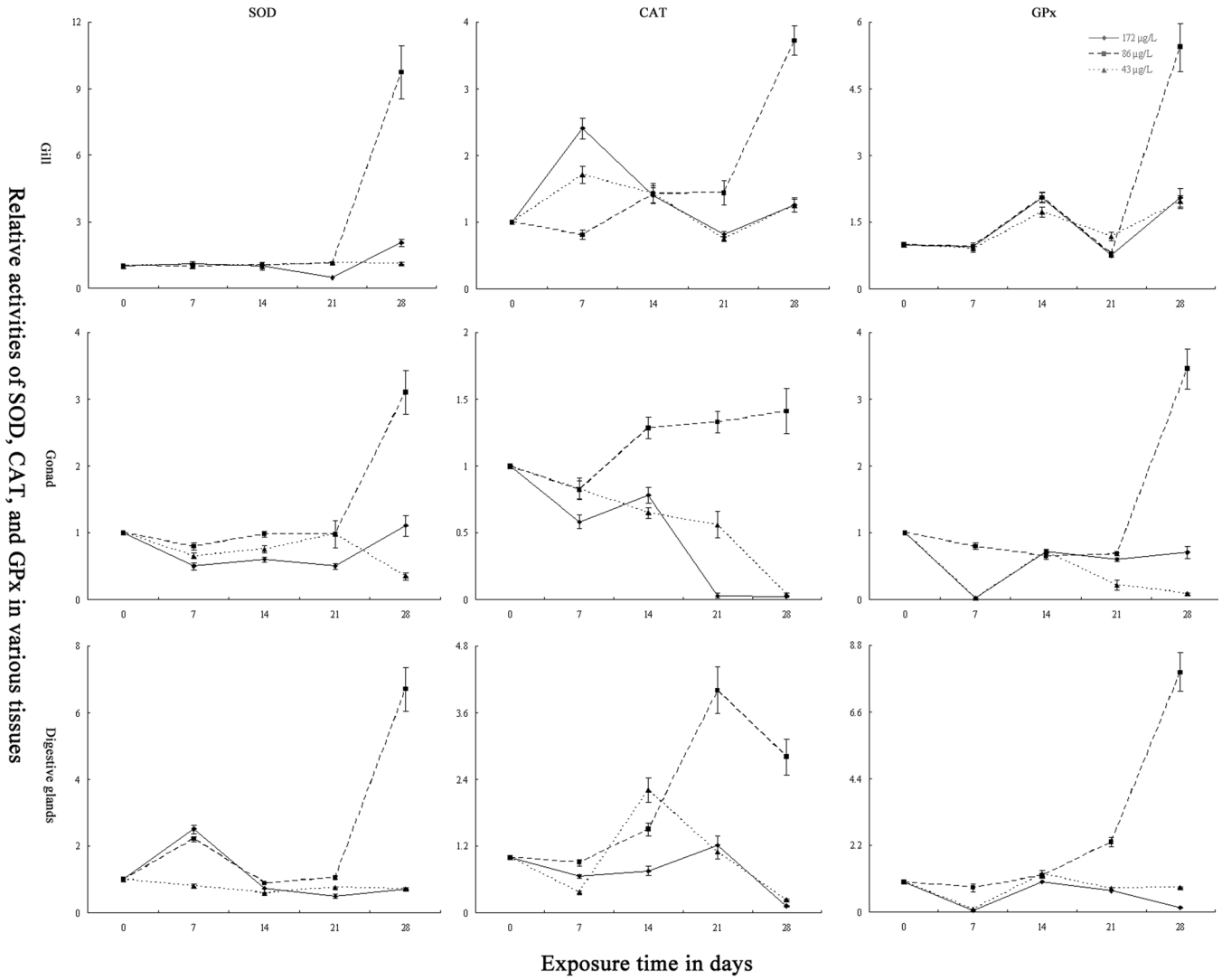

Figure 2. *Relative activities of SOD, CAT, and GPx in gills, gonads, and digestive glands of A. granosa exposed to lead at different exposure concentration (43, 86, and 172 μg/L) for 7, 14, 21, and 28 days.*

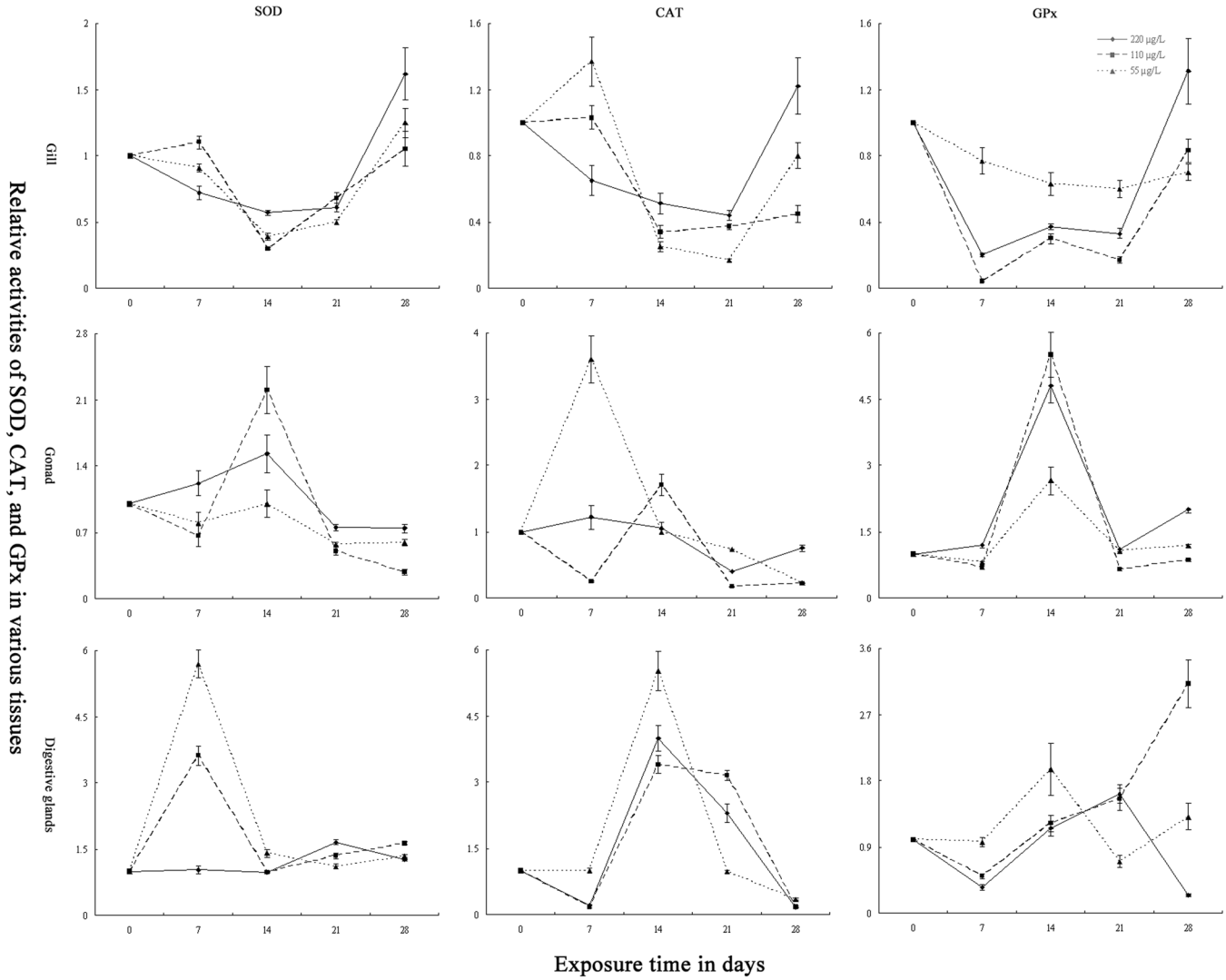

Figure 3. *Relative activities of SOD, CAT, and GPx in gills, gonads, and digestive glands of A. granosa exposed to cadmium at different exposure concentration (55, 110, and 220 μg/L) for 7, 14, 21, and 28 days.*

nearly all living organisms exposed to oxygen, and function to protect the biological system against ROS [15]. SOD catalyzes the dismutation of superoxide into oxygen and hydrogen peroxide; CAT and GPx subsequently catalyze the decomposition of free hydrogen peroxide to water and oxygen. GPx also reduces lipid hydroperoxides to their corresponding alcohols. Therefore, theoretically exposure to environmental contaminations, such as heavy metals, can be evaluated by antioxidant enzyme activities [16–19].

However, as shown in the present study, several factors can influence the effects of copper, lead, and cadmium on the antioxidant enzyme activities and has to be taken into consideration when applying antioxidant enzyme activities as heavy metal contamination bioindicators.

Firstly, the activities of antioxidant enzymes in various tissues responded differently to heavy metal exposure, which suggests different pathways of ROS reproduction for different tissues. This result is in accordance with those from other species. Cantú-Medellín *et al.* [20] found that SOD activity varied among muscle, gonads and digestive glands in the black chocolate clam *Megapitaria squalida*. Similar results showed that activities of SOD, CAT, and GPx differed between gills and digestive glands in *Ruditapes decussates* [21] and between gills and mantle tissue in *Bathymodiolus azoricus* [16]. This difference detected in the present study and reported in previous researches may due to the intrinsic differences among various tissues. For instance, in comparison to gonad and digestive glands, gills are used by filter feeder bivalves for

feeding and breathing, which leads to a direct contact with environmental variations such as metal contaminations and therefore are shown to be different in its antioxidant system response.

Secondly, exposure time had a significant effect on the activities of antioxidant enzymes, which have been overlooked in most heavy metal toxicological studies to date. Due to application of fixed exposure time in most previous researches, only few studies have been able to show the effect of exposure time of heavy metals on antioxidant enzymes activities. It has been shown that the activities of SOD, CAT, and GPx of *R. decussates* exposed to copper (0.5, 2.5 and 25 μg/L) varied with exposure times (1, 3, 7, 14, 21, 28 days) and that the oxygen metabolism imbalance was only induced in the first week of exposure [22]. Similar temporal variations in antioxidant enzyme activities were also found in *B. azoricus* at an even larger seasonal scale [16].

Thirdly, the response of antioxidant enzyme activity was dependent on metal species, which suggests that metal-induced ROS production occurring through different mechanisms. Copper is essential metal, and is necessary for organisms to form many enzymes, such as Cu/Zn-SOD [23]. Therefore, at low concentrations, copper may have a protective effect by forming Cu/Zn-SOD. In contrast, lead and cadmium are non-essential metals with no recognized biological functions and therefore can be extremely toxic even at low concentrations.

Lastly, unlike the acute effects of metals on the mortality, in which the endpoints were normally shown to be dose dependent, the effects of chronic sub-lethal metals on the activities of antioxidant enzymes can not be simply derived from the dose-response relationship. The non-existence of dose-response relationship found in the present study is partially due to the fact that low dose metal exposure may fail to elicit detectable enzyme activity responses in short exposure time. More importantly, the results obtained were combined effects of antioxidant enzyme activity inducing and antioxidant enzyme system damage caused by accumulated metals.

CONCLUSIONS

This study clearly demonstrated that the antioxidant enzyme activities of *A. granosa* are sensitive to chronic sub-lethal heavy metal exposure. However, caution should be exercised when using antioxidant enzyme activity as the endpoint for chronic eco-toxicological bio-assays due to the complicated responses related to tissue types, metal species, and exposure times. Information obtained in the present study contributes to the understanding of heavy metal toxicity in coastal invertebrates.

ACKNOWLEDGEMENTS

This work was financially supported by the Natural Science Foundation of China (31372503), Open fund of Zhejiang Key Laboratory of Aquatic Germplasm Resources (KL2013-1), Major Science and Technology Project of Zhejiang (2012C13005), and Open Fund of Key Laboratory of Exploration and Preservation of Costal Bio-resources of Zhejiang (J2013003, J2015002).

REFERENCES

1. Huang, H., J. Y. Wu, and J. H. Wu, "Heavy metal monitoring using bivalved shellfish from Zhejiang coastal waters, East China Sea". *Environmental Monitoring and Assessment*, Vol. 129, 2007, pp. 315–320. http://dx.doi.org/10.1007/s10661-006-9364-9
2. Meng, W., Y. W. Qin, B. H. Zheng, *et al.*, "Heavy metal pollution in Tianjin Bohai Bay, China". *Journal Environmental Sciences*, Vol. 20, 2008, pp. 814–819. http://dx.doi.org/10.1016/S1001-0742(08)62131-2
3. Wang, R. C. and Z. P. Wang, 2008. *Science of marine shellfish culture* (1st ed, in Chinese). Qingdao: China Ocean University Press.
4. Liu, G. X., X. L. Chai, Y. Q. Shao, *et al.*, "Specific death symptoms and organic lesions of blood clam *Tegillarca granosa* in acute copper, zinc, lead and cadmium exposures". *Advanced Materials Research*, Vol. 518-523, 2012, pp. 490–493.
5. Liu, G. X., X. L. Chai, Y. Q. Shao, *et al.*, "Histological alternation of blood clam *Tegillarca granosa* in acute copper, zinc, lead and cadmium exposures". *Advanced Materials Research*, Vol. 518-523, 2012, pp. 422–425.
6. Meenakumari S., A. P. Showkat, and T. S. Saravanan, "Ambient copper induced alternations in hematology and biochemistry of major carp, *Labeo rohita* (Hamilton)". *International Journal of Integrative Biology*, Vol. 10, No. 2, 2010, pp. 119–123.
7. Posthuma, L. and M. Van Straalen, "Heavy metal adaptation in terrestrial invertebrates: a review of occurrence, genetics, physiology and ecological consequences". *Comparative Biochemistry and Physuology Part C: Pharmacology, Toxicology and Endocrinology*, Vol. 106, No. 1, 1993, pp. 11–36. http://dx.doi.org/10.1016/0742-8413(93)90251-F
8. Liu, G. X., M. A. Shu, X. L. Chai, *et al.*, "Effect of chronic sublethal Cu^{2+}, Zn^{2+}, Pb^{2+} and Cd^{2+} exposure on filtration rate, sex ratio, and gonad development of the blood clam, *Tegillarca granosa*", *Bulletin of Environmental Contamination and Toxicology*, Vol. 92, 2014, pp. 71–74. http://dx.doi.org/10.1007/s00128-013-1138-9
9. Chandran, R., A. A. Sivakumar, S. Mohandass, *et al.*, "Effect of cadmium and zinc on antioxidant enzyme activity in the gastropod, Achatina fulica". *Comparative Biochemistry and Physiology Part C: Toxicolology and Pharmacology,* Vol. 140, 2005, pp. 422–426. http://dx.doi.org/10.1016/j.cca.2005.04.007
10. Drevet, J. R., "The antioxidant glutathione peroxidase family and spermatozoa: A complex story". *Molecular and Cellular Endocrinology,* Vol. 250, 2006, pp. 70–79. http://dx.doi.org/10.1016/j.mce.2005.12.027
11. Liu, G. X., X. L. Chai, Y. Q. Shao, *et al.*, "Toxicity of copper, lead and cadmium on motility of two marine microalgae *Isochrysis galbana* and Tetraselmis chui". *Journal of Environmental Sciences*, Vol. 23, No. 2, 2011, pp. 330–335. http://dx.doi.org/10.1016/S1001-0742(10)60410-X
12. Bradford, M., "A rapid and sensitive method for the quantification of

microgram quantities of protein utilizing the principle of protein-dye binding". *Analytical Biochemistry*, Vol. 72, 1976, pp. 248–254. http://dx.doi.org/10.1016/0003-2697(76)90527-3

13. Wang, Q., X. M. Wang, X. Y. Wang, *et al.*, "Analysis of metallotionein and antioxidant enzyme activities in *Meretrix meretrix* larvae under sublethal cadmium exposure". *Aquatic Toxicology*, Vol. 100, 2010, pp. 321–328. http://dx.doi.org/10.1016/j.aquatox.2010.08.012
14. R Development Core Team, 2012. R: a language and environment for statistical computing. Vienna. Austria.
15. Matozzo, V., L. Ballarin, and M. G. Marin, "Exposure of the clam *Tapes philippinarum* to 4-nonylphenol:Changes in anti-oxidant enzyme activities and re-burrowing capability". *Marine Pollution Bulletin*, Vol. 48, 2004, pp. 563–571. http://dx.doi.org/10.1016/j.marpolbul.2004.01.011
16. Company, R., A. Serafim, R. Cosson, *et al.*, "Temporal variation in the antioxidant defense system and lipid peroxidation in the gills and mantle of hydrothermal vent mussel *Bathymodiolus azoricus*". *Deep-Sea Research*, Vol. 53, 2006, pp. 1101–1116. http://dx.doi.org/10.1016/j.dsr.2006.05.008
17. You, L. P., X. X. Ning, L. L. Chen, *et al.*, "Expression profiles of two heat shock proteins and antioxidant enzyme activity in *Mytilus galloprovincialis* exposed to cadmium at environmentally relevant concentrations". *Chinese Journal of Oceanology and Limnology*, Vol. 32, 2014, pp. 334–343. http://dx.doi.org/10.1007/s00343-014-3111-9
18. Espín, S., E. Martínez-López, M. León-Ortega, *et al.*, "Oxidative stress biomarkers in Eurasian eagle owls (*Bubo bubo*) in three different scenarios of heavy metal exposure". *Environmental Research*, Vol. 131, 2014, pp. 134–144. http://dx.doi.org/10.1016/j.envres.2014.03.015
19. Kanak, E. G., Z. Dogan, A. Eroglu, *et al.*, "Effects of fish size on the response of antioxidant systems of *Oreochromis niloticus* following metal exposures". *Fish Physiology and Biochemistry*, Vol. 40, 2014, pp. 1083–1091. http://dx.doi.org/10.1007/s10695-014-9907-x
20. Cantú-Medellín, N., N. O. Olguín-Monroy, L. C. Méndez-Rodríguez, *et al.*, "Antioxidant enzymes and heavy metal levels in tissues of the black chocolate clam *Megapitaria squalida* in Bahía de La Paz, Mexico". *Archives of Environmental Contamination and Toxicology*, Vol. 56, No. 1, 2009, pp. 60–66. http://dx.doi.org/10.1007/s00244-008-9156-z
21. Geret, F., A. Serafim, and M. J. Bebianno, "Antioxidant enzyme activities, Metallothioneins and lipid peroxidation as biomarks in *Ruditapes decussates*?" *Ecotoxicology*, Vol. 12, No. 5, 2003, pp. 417–426. http://dx.doi.org/10.1023/A:1026108306755
22. Geret, F., A. Serafim, L. Barreira, *et al.*, "Response of antioxidant systems to copper in the gills of the clam *Ruditapes decussates*". *Marine Environmental Research*, Vol. 54, 2002, pp. 413–417. http://dx.doi.org/10.1016/S0141-1136(02)00164-2
23. Roméo, M., N. Bennani, M. Gnassia-Barelli, *et al.*, "Cadmium and copper display different responses towards oxidative stress in the kidney of the sea bass *Dicentrarchus labrax*". *Aquatic toxicology*, Vol. 48, 2000, pp. 185–194. http://dx.doi.org/10.1016/S0166-445X(99)00039-9

Effects of Fly Ash Content on Properties of Cement Paste Backfilling

TINGYE QI, GUORUI FENG*, YUJIANG ZHANG, JUN GUO and YUXIA GUO
College of Mineral Engineering, Taiyuan University of Technology, NO. 79, Yinze Western Street, Taiyuan 030024, Shanxi Province, China

ABSTRACT: Fly ash has been considered as an ideal raw material component of cement paste backfilling (CPB) due to its good pozzolanic activity. In this study, the effects of fly ash content (340–420 kg/m^3) on the compressive strength, resistivity and microscopic characteristics of CPB were investigated. The results indicated that at the early curing age, the resistivity decreased with increasing fly ash content, while the compressive strength did not vary significantly; at the curing times of 7 d, 14 d and 28 d, the compressive strength exhibited an increasing trend because of the higher content of reaction products and the compaction of pore structure, and the resistivity also increased due to the decreased ionic concentrations of pore solution and the greater resistance to transporting current through the pore network system. Apparently, there existed a linear relationship between the compressive strength and the resistivity of CPB samples.

INTRODUCTION

CEMENT PASTE BACKFILLING (CPB) for coal mining backfilling is an engineering mixture of milled gangues, fly ash, hydraulic binder and water. Each component of CPB plays a significant role in its rheological and mechanical performance (i.e., transportation, placement, strength and stability) [1,2]. Cemented paste backfill is a technique to control the overlying hard rock in modern underground mines. Besides, it can also be used to exploit the coal below buildings, railways and water bodies, which achieves the effective extraction of coal resources. From this aspect, CPB can reduce landfill area requirements and prevent environmental pollution [3].

Fly ash is a dust waste discharged from existing coal-fired power plants, and its quantity has reached over 300 million tons per year in China [4]. Fly ash particles can accelerate the cement hydration kinetics by heterogeneous nucleation and surface absorption effects [5,6]. Moreover, fly ash exhibits a pozzolanic activity, and soluble Al_2O_3 and SiO_2 can participate in the pozzolanic reaction to generate calcium silicate hydrate and calcium aluminate hydrate [7]. Hence, fly ash has an intermediate cementitious potential [8]. Furthermore, it is resistant to sulfate attack and can reduce strength deterioration to some extent, which improves the long-term performance of cement based samples [9].

Based on the above properties, fly ash can be mixed with cement as a helpful additive to prepare concrete and CPB [10,11]. Senapati and Mishra [12] found that the addition of bottom ash fractions to fly ash slurry at a given solid concentration had a beneficial effect on reducing the pumping power requirement. Yao and Sun [13] showed the compressive strength attained to a stable level when fly ash content reached a certain value within the range from 20% to 70% at early curing time. Katz and Kovler [14] reported that the increasing mass of water and fly ash content could give rise to a concern of a high bleeding rate for slurry. However, few studies focus on the effects of fly ash content on the micro-characteristics and resistivity of CPB.

Several researchers also pay attention to the relationship between compressive strength and resistivity of concrete. Wei *et al.* [15] made several samples with different cements, and measured their resistivity at 24 h, as well as the compressive strength at 28 d. They found that there existed a linear relationship between the two couple of values and concluded that the compressive strength and resistivity mainly depended on the pore structure and micro-morphology of products, which were influenced by hydration. Lübeck *et al.* [16] used White Portland cement, ground granulated blast-furnace slag and Na_2SO_4 to make different samples with three water-to-binder ratios, and discovered that the resistivity and compressive strength with the same

*Author to whom correspondence should be addressed. E-mail: fguorui@163.com; Tel: +86 0351 6010177; Fax: +86 0351 6018040)

1544-8053/15/03 133-09
© 2015 DEStech Publications, Inc.
doi:10.12783/issn.1544-8053/12/3/3

binder followed a nearly linear relationship owing to the compactness of the structure irrespective of the concrete saturation degree, together with the pore solution conductivity which imposed the influence on the resistivity [17]. Ferreira and Jalali [18] observed a linear relationship between electrical resistivity and compressive strength for the concrete samples prepared by an ordinary Portland cement and a fly ash cement, because the variation of compressive strength and electrical resistivity depended on the pore structure and the sample geometry change caused by cement hydration. Ramezanianpour *et al.* [19] prepared 57 concrete mixtures by Portland cement with some supplementary materials including Tuff, Pumice, rice husk ash, metakaolin and Silica fume. Interestingly, the compressive strength and resistivity of concrete mixtures prepared with different cementitious materials presented no sensible correlation, because the interfacial transition zone (ITZ) only affected the compressive strength but had no obvious influence on the resistivity of concrete, whereas the chemical composition of the pore solution played an important role in resistivity but had little effect on the compressive strength of concrete. Regrettably, there have been few studies so far on the relationship between resistivity and compressive strength of CPB with different fly ash contents.

Fly ash content has a significant effect on the performances of CPB, namely the resistivity of CPB is subjected to the main ionic concentrations of pore solution and the pore structure, and the compressive strength is also influenced by porosity and micro-morphology of products. For these reasons, this paper focuses on the change of microstructure, resistivity and compressive strength associated with the variation of fly ash content, and builds the relationship between compressive strength and resistivity of CPB samples at different curing times.

MATERIALS AND METHODS

Materials

Coal gangue

The coal gangue samples were obtained from Xinyang Colliery, which were discharged during coal mining and washing processes. The samples were mechanically crushed and then categorized into two groups of aggregates based on particle size, i.e., fine gangue (0–5 mm) and coarse gangue (5–15 mm). The fineness modulus μ of the fine gangue (0–5 mm) was 3.02. Table 1 lists the physical properties of the gangue samples. A Thermo Fisher Scientific Thermo ICAP 6300 inductively coupled plasma optical emission spectrometer (ICP-OES) was used to determine the chemical compositions of the gangue samples (Table 1).

Fly Ash

The fly ash samples were obtained from the power plant of Xingyang Colliery. The physical properties of the fly ash samples were analyzed according to the Technical Specification for Fly Ash Used in Concrete and Mortar (JGJ28-86). An ICP-OES was used to analyze the chemical compositions of the fly ash samples (Table 1).

Cement and Water

Ordinary Portland cement (42.5 grade) was used in this study. Table 1 lists the chemical composition and the physical properties of the cement (provided by the manufacturer). The initial and final setting times were 165 min and 231 min, respectively. The compressive strengths were 18.4 MPa (3-d curing time) and 46.4 MPa (28-d curing time), respectively. The water source was tap water.

Sample Preparation and Test Methods

Sample Preparation

The raw materials used in the present study were ordinary Portland cement, coal gangue, fly ash and water. The CPB samples were divided into five groups based

Table 1. Chemical Composition and Physical Properties of the Various Materials.

Major Element	Cement (%)	Fly Ash (%)	Gangue (%)
SiO_2	22.27	52.42	28.46
Al_2O_3	5.59	32.48	16.11
Fe_2O_3	3.47	3.62	10.86
CaO	65.90	3.05	7.15
MgO	0.81	1.01	3.50
TiO_2		1.26	0.80
Specific gravity (g/cm^3)	3.1	2.2	2.0
Specific surface (m^2/kg)	349	415	499
Fineness (> 45 μm)/%	5	42.54	53.78
Moisture content/%	—	0.56	8.0
Lose on ignition/%	2	3.8	—

Notes: SiO_2 was first burned at 800°C to remove organic matter and then measured in a NaOH solution at 650°C. All other oxides were subject to sealed digestion in $HF+HNO_3$ at 185°C.

on different fly ash contents (M1 – M5). In these five groups, the fly ash content in each group was 340 kg/m^3 (M1), 360 kg/m^3 (M2), 380 kg/m^3 (M3), 400 kg/m^3 (M4) and 420 kg/m^3 (M5), respectively. In order to ensure that the mass concentration for each group was the same (80 %), the water content was set as 370 kg/m^3 (M1), 375 kg/m^3 (M2), 380 kg/m^3 (M3), 385 kg/m^3 (M4) and 390 kg/m^3 (M5), respectively.

The raw materials were mixed according to the designed mix proportions and then mechanically stirred. Subsequently, the slurry was transferred into 70 mm × 70 mm × 70 mm testing moulds. After casting, the specimens were cured in a curing room for performance testing (temperature: 20 ± 2°C; humidity: 80%).

Microscopic Test

After curing for 7 d, 14 d and 28 d, the interior of the specimens was removed and immersed in anhydrous ethanol for 24 h. At the next stage, the pastes were oven-dried for 48 h at 40°C in order to avoid microstructure changes caused by intense oven drying at 105°C. The slurry particles were subjected to porosity test using mercury intrusion porosimetry (MIP) by a CE Pascal 140/240 porosimeter. A field emission transmission electron microscopy (FETEM) unit (JSM-7001F) was used for the microscopic observation of the slurry particles cured for 28 d.

Solution pH Value and Ion Concentration Test

After curing for 7 d, 14 d and 28 d, the processed slurry particles were ground into powder, and then immersed in deionised water [20]. The ratio of water to solid mass was 100:1. The solution was stirred using a magnetic stirrer for 10 min. To prevent the reaction between the particles and water, the solution was filtered and the concentrations of major ions in the filtrate were immediately measured using ICP-AES. The pH value was analyzed by a BPH-220 Meter. The testing temperature of the solution was 20 ± 1°C. Although the measured pH of suspension solution was not the true pH value of the pore solution, it was relevant to the true one and could reflect the alkalinity and ionic concentration changes of pore solution. The above procedure was used in all mixtures in the test and the obtained results were compared [21–23].

Resistivity and Compressive Strength

A Wenner dipole array was used to determine the resistivity of the specimens cured for 3 d, 7 d, 14 d and 28 d, respectively. The test voltage was 5 V. To reduce the effect of contact resistance on testing stability , silver papers were used as electrodes, and a piece of cotton cloth that was pre-immersed in a saturated copper sulphate solution was placed between the silver paper and the specimen.

After resistivity test, the compressive strength test was conducted using a computer-controlled mechanical press with a load capacity of 1000 kN and a pressure speed of 6.75 kN per minute according to GB50081. All the experiments were carried out in triplicate.

RESULTS AND DISCUSSION

Effects of Fine Gangue Content on Microstructure of CPB

The pore solution of CPB mainly contains Na^+, K^+, Ca^{2+}, Mg^{2+}, Al^{3+}, Fe^{3+}, Si^{4+}, SO_4^{2-}, $Al(OH)_4^-$, $H_3SiO_4^-$, OH^- and $[FeO_2(OH)]^{2-}$, which originated from the gangue, the dissolution of the fly ash and the hydrolysis between the hydration and the pozzolanic reaction products [24]. The hydration and pozzolanic reactions occur among the minerals in CPB, and the hydration products include portlandite ($Ca(OH)_2$), hydrated calcium silicate (C–S–H) gel, and AFt (ettringite, etc.) or AFm (monosulphate, etc.) phases. Then, active Si^{4+}, Al^{3+} and Fe^{3+} ions in gangue and fly ash react with $Ca(OH)_2$ to produce AFt or AFm phases [25].

Table 2 lists the variations of 7 major ion concentrations and pH value in the pore solution after different curing times. As can be seen, after curing for 7 d and 14 d, the concentrations of Si^{4+}, Fe^{3+}, Al^{3+}, Ca^{2+}, Na^+, K^+ and pH value decrease with increasing fly ash content, due to the hydration and pozzolanic reactions in CPB. Meanwhile, the reaction contact area between $Ca(OH)_2$ and fly ash grain increases, and consumptions of Ca^{2+}, OH^-, Al^{3+}, Si^{4+} and Fe^{3+} ions in the pore solution also increase. At 28 d, Fe^{3+}, K^+, Na^+ and Ca^{2+} decrease while Al^{3+} and Si^{4+} increase, because the pozzolanic reaction levels off and the specific surface separates out more soluble Al^{3+} and Si^{4+} as they dissolve in the pore solution. The variation trend of alkali (Ca^{2+}, Na^+, K^+) ion concentrations is consistent with the measured pH value. It can be calculated that the overall iron concentrations decrease with increasing fly ash content, and that the high Ca^{2+} concentration in the solution is a major influencing factor on the properties of the pore solution.

CPB like concrete is a kind of porous material with

Table 2. Concentrations of Major Ions and pH in the Pore Solution at 7d, 14d and 28d.

	Fly Ash Content (kg/m^3)	Element (mg/L)							pH
		Al	Fe	Si	Ca	Na	K	Mg	
7d	340	5.786	0.529	1.38	86.5	2.17	3.18	0.153	9.45
	360	5.519	0.49	1.46	77.6	2.18	2.41	0.09	9.27
	380	5.475	0.466	1.15	74.3	2.16	2.60	0.194	9.23
	400	5.28	0.447	1.02	72.1	2.05	2.3	0.285	9.25
	420	5.158	0.387	0.955	63.7	1.96	2.29	0.124	9.19
14d	340	6.966	0.518	0.617	82.5	2.25	2.15	0.254	8.92
	360	6.788	0.49	0.56	78.2	2.27	2.41	0.239	8.87
	380	6.495	0.458	0.518	74.1	1.98	3.05	0.175	8.74
	400	6.353	0.465	0.487	72.6	2.06	2.86	0.284	8.71
	420	5.73	0.364	0.257	60.8	2.26	2.47	0.219	8.68
21d	340	7.516	0.447	0.288	72.0	2.46	3.46	0.324	8.35
	360	7.484	0.412	0.369	71.6	2.38	2.87	0.318	8.4
	380	7.813	0.342	0.406	67.6	2.28	2.82	0.349	8.20
	400	8.177	0.438	0.475	64.6	2.34	2.88	0.417	8.23
	420	10.165	0.387	0.502	62.5	2.17	2.68	0.467	8.16

complex pore system. It can be regarded as a mixture of gangue, fly ash particles and products distributed in paste matrix. There are different-size pores including capillary pores, small gel pores and so on in the position of CPB, and four size ranges of pore distribution can be defined as large capillary pores (> 100 nm), middle capillary pores (50–100 nm), meso-pores (4.5–50 nm) and gel micropores (< 4.5 nm) [26]. The pore network systems of CPB may be considered as a network of large spaces (large and middle capillary pores) interconnected by narrow channels (smaller capillary or gel pore) [27]. The MIP results show that the porosity decreases with the increase of fly ash dosage, and that the porosity development closely relates to the reaction degree in CPB [28].

Fly ash plays double roles during the pore structure development and hydration process. The bigger pore space among the gangues is filled with more fly ash, which means a higher reaction degree. Meanwhile, this phenomenon also has a close relation with the packing pattern of hydration products. Figure 1 indicates that increasing fly ash content can result in the change of pore size distribution in CPB. At 7 d, the peak of the pore size distribution curve appears at the pore size of 1,000 nm, and the large capillary pores and large chambers take over a large proportion of space. With the fly ash content increasing from 340 to 400 kg/m^3, the peak value gradually drops [Figure 1(a)]. At 28 d, the peak of the pore size distribution curve appears at the pore sizes of 10–100 nm and 1,000 nm, indicating that the pore structure has changed and that the content of middle capillary pores increases at the later age. Besides, due to the reaction products filling in large pores, the peak value of 1,000 nm pore size also drops with the increase of fly ash dosage.

The critical pore diameter can be described as the most frequent diameter that permits the maximum percolation of pore solution in the interconnected pore network of CPB [29,30]. This parameter controls the transport properties of CPB. Figure 1(b) shows that as fly ash content increases, the critical diameter also increases. For pore size distribution measurement, the MIP results are sensitive to percolation properties of the pore network, which in turn affects flow characteristics of pore solution in the pore network. According to the variations of pore structure and critical diameter, the higher the fly ash dosage is, the weaker the flow characteristics of CPB are.

Figure 2 shows the morphology of hydration and pozzolanic reaction products in the CPB samples at different fly ash dosages after 28 d. The microstructure of the samples confirms the formation of various phases such as C–S–H, AFt and gangue particles, and the continuous structure formed by outgrowth can interconnect the reacted grains. At the fly ash content of 340 kg/m^3 in CPB [Figure 2(a)], typical hydration and pozzolanic reaction products such as C–S–H appear in the sample, together with short acicular and needle like crystals. At the fly ash dosage of 420 kg/m^3 [Figure 2(c)], the microstructure of CPB becomes denser with distinct formation of needle like and floccus like crystals. The densification of microstruc-

ture at 420 kg/m^3 fly ash content indicates the higher degree of pozzolanic reaction, which may be responsible for the significantly increased strength. The higher degree of pozzolanic reaction means more soluble Si^{4+} and Al^{3+} ions release from the fly ash particles, which can continually react with $Ca(OH)_2$ from cement hydration in CPB.

Effects of Fly Ash Content on Compressive Strength and Resistivity of CPB

As shown in Figure 3, at 3 d, the compressive strength of CPB varies between 1 and 2 MPa with increasing fly ash content, and the lower CaO in fly ash and gangue results in a slow reaction rate at early curing times [31,32]. At 7 d, 14 d and 28 d, however, the compressive strength of CPB increases with the increase of fly ash content, and the maximum values are respectively 3.57 MPa, 5.8 MPa and 7.8 MPa at 420 kg/m^3 fly ash content. In contrast, Changir [33] asserted that 0.7 MPa and 1 MPa at 28 d were regarded by mine operators as the threshold for the self-supporting stopes adjacent to ore extraction. The results of MIP and SEM tests show that increasing fly ash content can not only increase the amount of C–S–H gel and AFt phase due to the higher hydration and pozzolanic reaction degree, but also decrease the content of large capillary pores. As a result, the compressive strength of CPB presents an obvious increment.

The resistivity of the gangue is measured to be 1×10^7 Ω·m, which is far greater than that of the measured CPB. Therefore, the solution in the pores of CPB is the primary contributor to the conductivity. In other words, the resistivity of CPB depends on its pore structure, ion

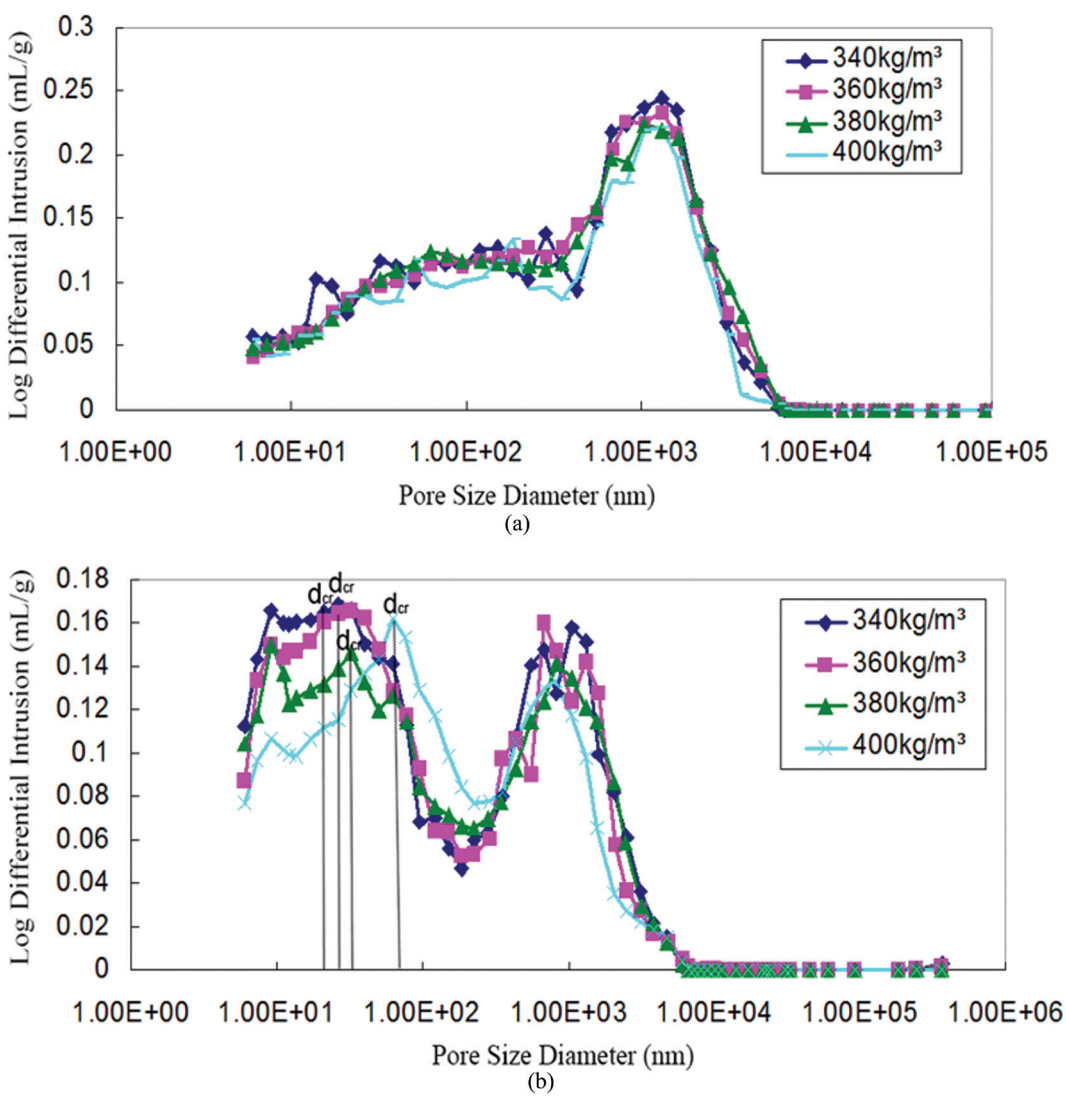

Figure 1. *MIP pore size distribution at 7 d (a) and 28 d (b).*

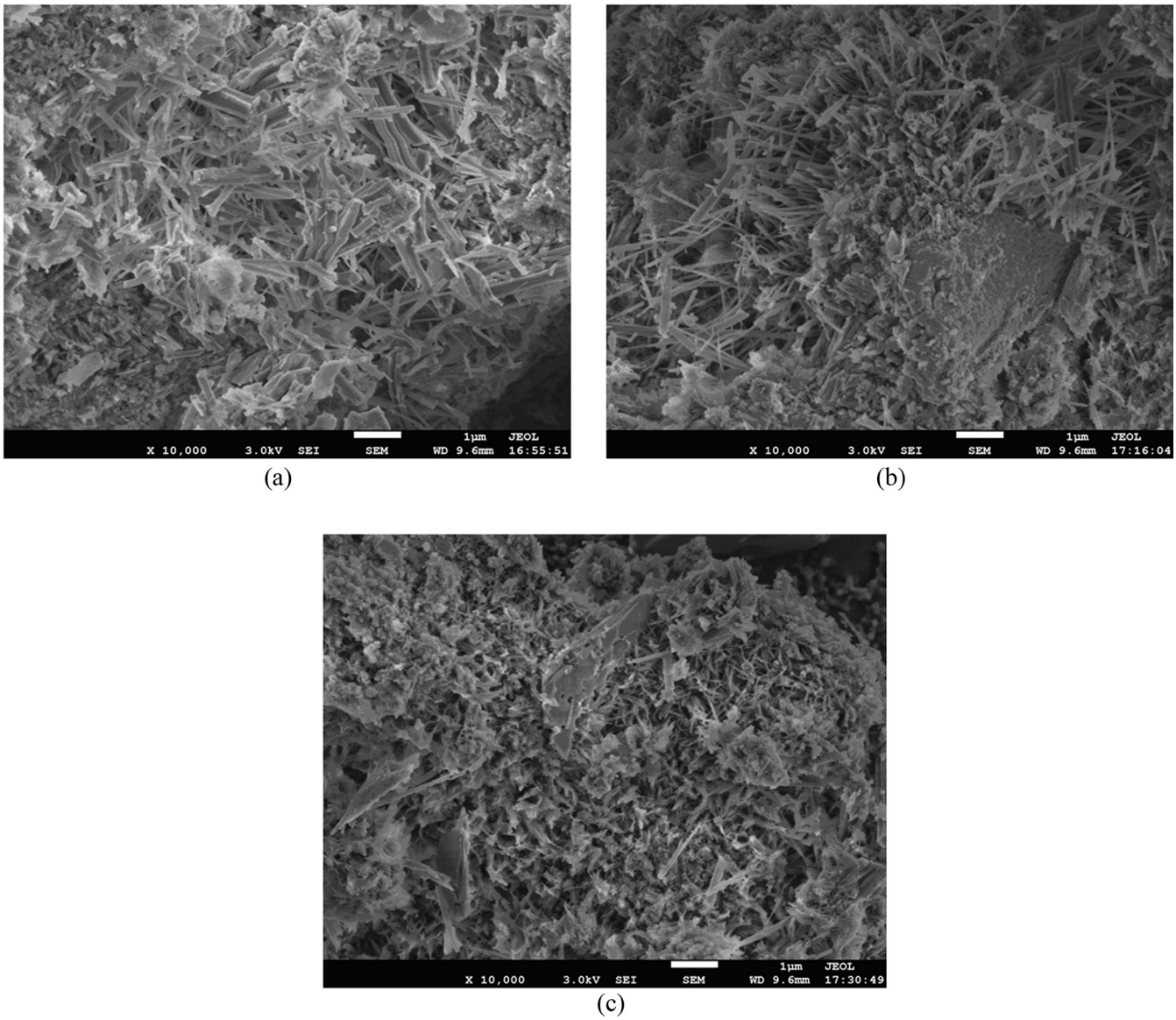

Figure 2. *Morphology of minerals in CPB at: (a) 340 kg/m^3; (b) 380 kg/m^3; and (c) 420 kg/m^3 fly ash content.*

concentration and the mobility of ions in the pore solution [34]. Figure 4 shows a resistivity decrease with increasing fly ash content at 3 d. In this case, the amount of ions dissolved in the pore solution increases, which improves the capacity of transporting current and thus leads to a lower resistivity. It is noted that the influence of pore structure on resistivity at 3 d is negligible. This can be attributed to two reasons: Firstly, the pore network is better connected on account of the lower degree of hydration reaction, so that the connectivity of pore network is less blocked up by hydration products; Secondly, the high degree of saturation of CPB results in the filling of pore structure with conductive pore solution. After curing for 7 d, 14 d and 28 d, the higher fly ash dosage leads to a higher resistivity. This phenomenon can be attributed to the denser microstructure and the lower ionic conductivity of the pore solution. The decrease of total concentration of main irons in the pore solution leads to a lower migration rate and reduces the capability of transporting current. Additionally, an excess of fly ash decreases the porosity of CPB and weakens the flow characteristics of the pore structure in CPB at later ages, which may also be responsible for the decreased resistivity of CPB.

Relationship Between Compressive Strength and Resistivity

Figure 5 shows the relationship between compressive strength and resistivity at 3 d, 7 d, 14 d and 28 d.

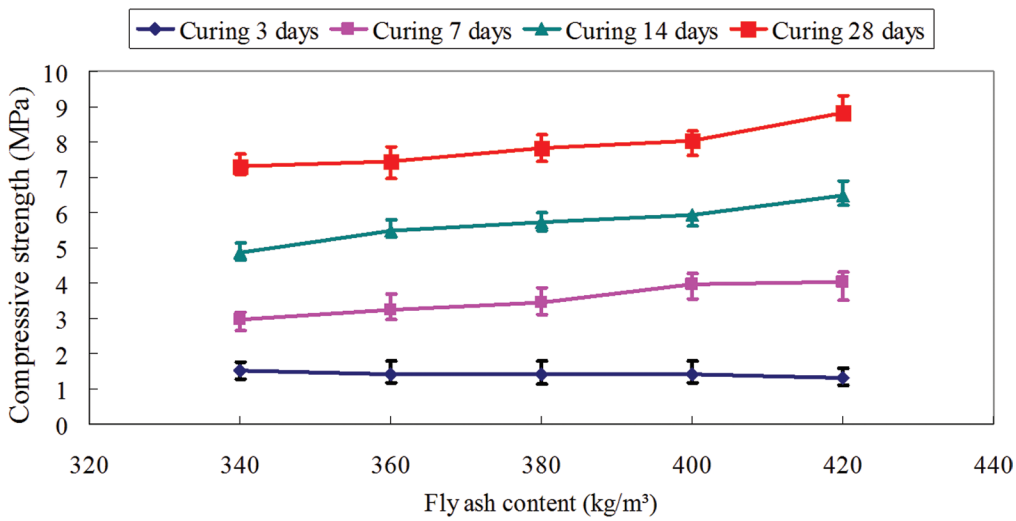

Figure 3. *Compressive strength of CPB at 340-420kg/m³ fly ash content.*

The resistivity increases with increasing compressive strength at 3 d [Equation (1)], 7 d [Equation (2)], 14 d [Eqquation (3)] and 28 d [Equation (4)]. In the current study, the least squares regression method is used to analyze the resistivity and compressive strength results. It is found that there is a linear relationship with a high correlation coefficient between compressive strength and resistivity of the CPB samples in the fly ash dosage range from 340 to 420 kg/m^3 at different curing times. The regression equations at different curing times and the general expression can be given as Equations (1–4) and Equation (5), respectively.

$$Y = 0.0374x - 2.0397 \quad R^2 = 0.8754 \quad \text{(at 3 days)} \tag{1}$$

$$Y = 0.0187x + 1.1691 \quad R^2 = 0.8616 \quad \text{(at 7days)} \tag{2}$$

$$Y = 0.0075x + 3.6468 \quad R^2 = 0.7433 \quad \text{(at 14 days)} \tag{3}$$

$$Y = 0.0075x + 2.8777 \quad R^2 = 0.8118 \quad \text{(at 28 days)} \tag{4}$$

$$Y = ax + b \quad \text{(general expression)} \tag{5}$$

where Y is the standard compressive strength of CPB at different curing times, MPa; x is the electrical resistivity of CPB at different curing times, Ω • m; and a and b are the linear equation parameters, which depend on the contents of cement and fly ash, as well as the curing time. To obtain more practical values for a and b, a wider range of CPB properties should be provided based on more tests in further study. Accordingly, these linear models can be used to estimate the compressive strength of CPB samples using the resistivity data.

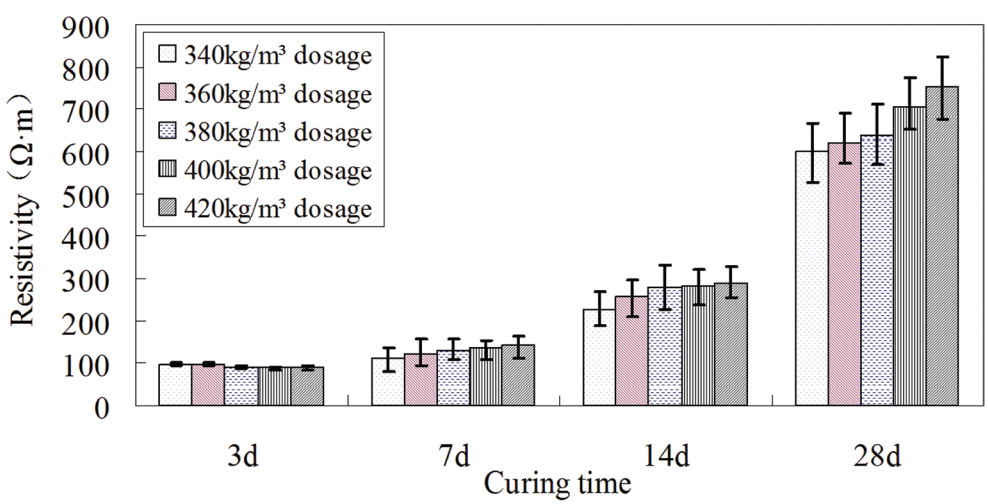

Figure 4. *Resistivity of CPB at 340–420 kg/m³ fly ash content.*

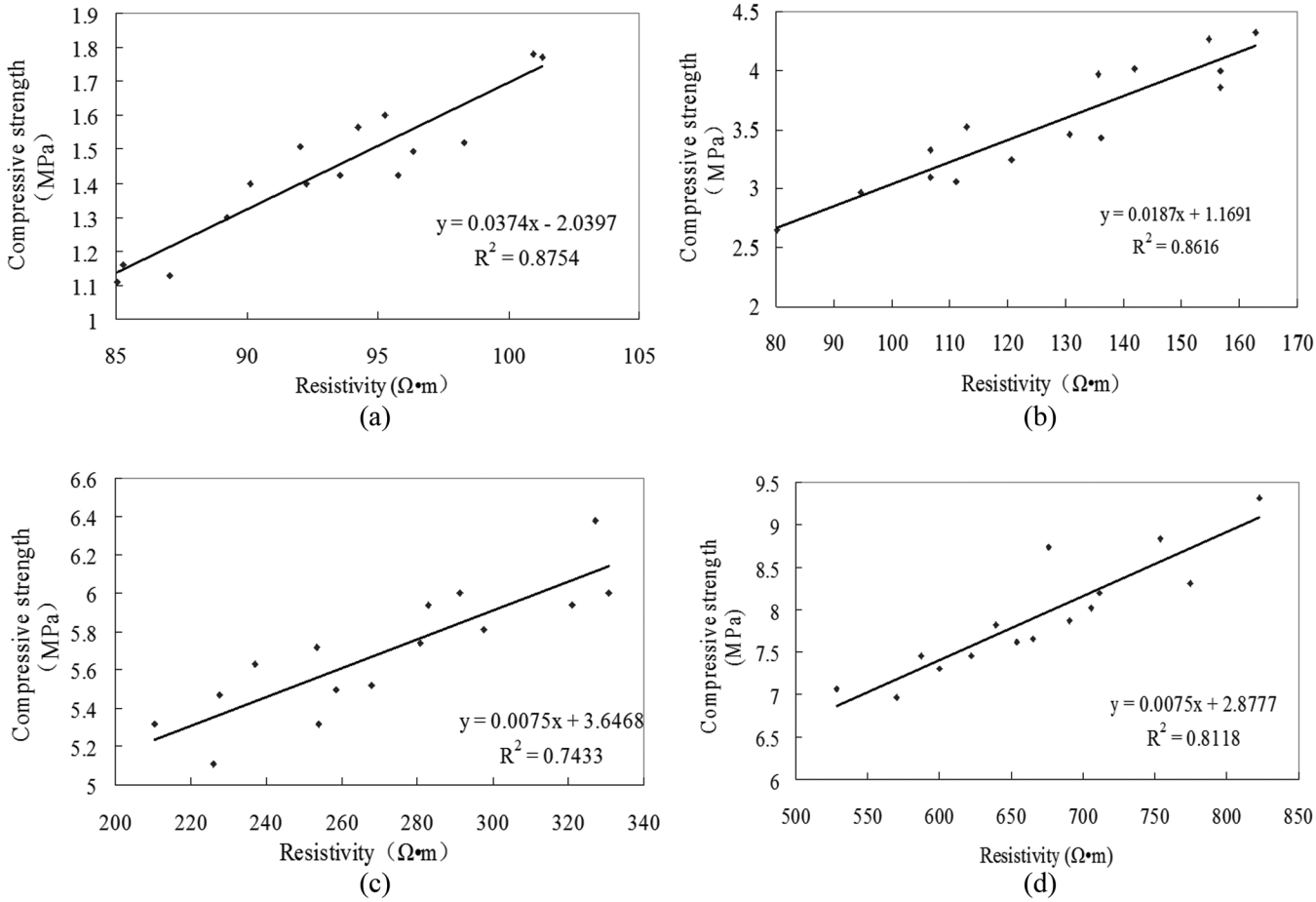

Figure 5. *Relationship between compressive strength and resistivity for CPB samples produced from 340–420 kg/m^3 fly ash dosages at: (a) 3 d; (b) 7 d ; (c) 14 d; and (d) 28 d.*

It is noticed that the relationship between resistivity and compressive strength is approximately linear for the same binder with different fly ash contents at 3 d, 7 d, 14 d and 28 d, since both of them directly depend on the pore structure and the micro-morphology of products. In addition, the resistivity is also influenced by the ionic concentration of the pore solution and the degree of CPB saturation. To sum up, these properties are affected by hydration and pozzolanic reactions.

CONCLUSIONS

Based on the results of current investigation, some conclusions can be drawn as follows:

1. At curing times of 7 d, 14 d and 28 d, the compressive strength of CPB increases with increasing fly ash content, which can be attributed to the higher content of pozzolanic products and the lower content of large pores.
2. At curing times of 7 d, 14 d and 28 d, the resistivity of CPB increases with increasing fly ash content, which can be attributed to the decreased ionic concentrations of the pore solution and the lower transporting current of the pore network system.
3. The compressive strength values are correlated with the resistivity values of CPB samples for different fly ash dosages at a certain curing time, and the linear relationship between compressive strength and resistivity can be established. These findings suggest that resistivity test is a practical and less time-consuming method that can be used to determine the microstructure and compressive strength of CPB samples.

ACKNOWLEDGEMENTS

This work was financially supported from the National Natural Science Foundation of China (51174142, 514224404), Program for New Century Excellent Talents in University of Chinese Ministry of Education (NCET-11-1036) and the Fok Ying Tung Education Foundation

(132023), Science and technology research project of Shanxi Province (20110321015-03), Postgraduate Innovate Project of Shanxi Province (02100489).

REFERENCES

1. Kesimal A., Ercikdi B., Yilmaz E., The effect of desliming by sedimentation on paste backfill performance, *Miner. Eng.*, Vol. 16, No. 10, 2003, pp. 1009–1011. http://dx.doi.org/10.1016/S0892-6875(03)00267-X
2. Yilmaz E.; Kesimal A.; Ercikdi B.: Strength properties in varying cement dosages for paste backfill samples. In: *Proceedings of the 10th International Conference on Tailings and Mine Waste, Balkema, Swets and Zeitlinger*, Lisse12– 15 October, Colorado, USA, 2003, pp. 109–114.
3. Landriault D.: Backfill in underground mining. In *Underground mining methods: engineering fundamentals and international case studies* Hustrulid WA and Bullock RL. Society for Mining Metallurgy & Explorationp, Littleton, USA, 2001, pp. 601–614.
4. Sale L. Y., Chanasyk D. S. and Naeth M. A., Temporal influence of fly ash on selected soil physical properties, *Can. J. Soil Sci.*, Vol. 77, 1997, 677–683. http://dx.doi.org/10.4141/S96-078
5. Xu A., Sakar S. L. and Nilsson L. O., Effect of fly ash on the microstructure of cement mortar, *Mater. Struct.*, Vol. 26, 1993, 414–424. http://dx.doi.org/10.1007/BF02472942
6. Cyr M., Lawrence P. and Ringot E., Efficiency of mineral admixtures in mortars: quantification of the physical and chemical effects of fine admixtures in relation with compressive strength. *Cement Concrete Res.*, Vol. 36, No. 2, 2006, pp. 264–277. http://dx.doi.org/10.1016/j.cemconres.2005.07.001
7. Peyronnard O. and Benzaazoua M., Alternative by-product based binders for cemented mine backfill: Recipes optimisation using Taguchi method. *Miner. Eng.*, Vol. 29, 2012, 28–38. http://dx.doi.org/10.1016/j.mineng.2011.12.010
8. Long G. C., Xie Y. J. and Jiang Z. W., Efficiency of fly ash in cementitious materials, *Adv. Cem. Res.*, Vol. 17, No. 3, 2005, pp. 113–119. http://dx.doi.org/10.1680/adcr.2005.17.3.113
9. Benzaazoua M., Ouellet J., Servant S., Newman P. and Verburg R., Cementitious backfill with high sulfur content Physical, chemical, and mineralogical characterization, *Cement Concrete Res.*, Vol. 29, No. 5, 1999, pp. 719–725. http://dx.doi.org/10.1016/S0008-8846(99)00023-X
10. Mahlaba J. S., Kearsley E. P. and Kruger R. A., Effect of fly ash characteristics on the behaviour of pastes prepared under varied brine conditions, *Miner. Eng.*, Vol. 24, No. 8, 2011, pp. 923–929. http://dx.doi.org/10.1016/j.mineng.2011.04.009
11. Sabet F. A., Libre N. A. and Shekarchi M., Mechanical and durability properties of self consolidating high performance concrete incorporating natural zeolite, silica fume and fly ash, *Constr. Build. Mater.*, Vol. 44, 2013, 175–184. http://dx.doi.org/10.1016/j.conbuildmat.2013.02.069
12. Senapati P. K. and Mishra B. K., Design considerations for hydraulic backfilling with coal combustion products (CCPs) at high solids concentrations, *Powder Technol.*, Vol. 229, 2012, pp. 119–125. http://dx.doi.org/10.1016/j.powtec.2012.06.018
13. Yao Y. and Sun H. H., Characterization of a new silica alumina-based backfill material utilizing large quantities of coal combustion byproducts, *Fuel*, 2012, Vol. 97, pp. 329–336. http://dx.doi.org/10.1016/j.fuel.2012.01.057
14. Katz A. and Kovler K., Utilization of industrial by-products for the production of controlled low strength materials (CLSM), *Waste Manage*., Vol. 24, No. 5, 2004, pp. 501–512. http://dx.doi.org/10.1016/S0956-053X(03)00134-X
15. Wei X. S., Xiao L. Z. and Li Z. J., Prediction of standard compressive strength of cement by the electrical resistivity measurement, *Constr. Build. Mater.*, Vol. 31, 2012, pp. 341–346. http://dx.doi.org/10.1016/j.conbuildmat.2011.12.111
16. Lübeck A., Gastaldini A. L. G., Barin D. S. and Siqueira. H.C., Compressive strength and electrical properties of concrete with white Portland cement and blast-furnace slag, *Cement Concrete Comp.*, Vol. 34, No. 3, 2012, pp. 392–399. http://dx.doi.org/10.1016/j.cemconcomp.2011.11.017
17. Weiss, J., Snyder, K., Bullard, J., and Bentz, D., Using a Saturation Function to Interpret the Electrical Properties of Partially Saturated Concrete, J. Mater. Civil Eng., Vol. 25, No. 8, 2013, pp.1097–1106. http://dx.doi.org/10.1061/(ASCE)MT.1943-5533.0000549
18. Ferreira R. M. and Jalali S., NDT measurements for the prediction of 28-day compressive strength, *NDT&E International*, Vol. 43, No. 2, 2010, pp. 55–61. http://dx.doi.org/10.1016/j.ndteint.2009.09.003
19. Ramezanianpour A. A., Pilvar A., Mahdikhani M. and Moodi F., Practical evaluation of relationship between concrete resistivity, water penetration, rapid chloride penetration and compressive strength, *Constr. Build. Mater.*, Vol. 25, No. 5, 2011, pp. 2472–2479. http://dx.doi.org/10.1016/j.conbuildmat.2010.11.069
20. Gastaldini A. L. G., Isaia G. C., Hoppe T. F., Missau F. and Saciloto A.P., Influence of the use of rice husk ash on the electrical resistivity of concrete: A technical and economic feasibility study, *Constr. Build. Mater.*, Vol. 23, No. 11, 2009, pp. 3411–3419. http://dx.doi.org/10.1016/j.conbuildmat.2009.06.039
21. Xi Y., Siemer D. D. and Scheetz B. E., Strength development, hydration reaction and pore structure of autoclaved slag cement with added silica fume, *Cement Concrete Res.*, Vol. 27, No. 1, 1997, pp. 75–82. http://dx.doi.org/10.1016/S0008-8846(96)00196-2
22. Pu Q., Jiang L. H., Xu J. X., Chu H.Q., Xu Y. and Zhang Y., Evolution of pH and chemical composition of pore solution in carbonated concrete, *Constr. Build. Mater.*, Vol. 28, No. 1, 2012, pp. 519–524. http://dx.doi.org/10.1016/j.conbuildmat.2011.09.006
23. Haque M. N. and Kayyall O. A., Aspect of chloride ion determination in concrete, *ACI Mater. J.*, Vol. 92, No. 5, 1995, pp. 532–541.
24. Reardon E. J., Problems and Approaches to the Prediction of the Chemical Composition in Cement/Water Systems, *Waste Manage.*, Vol. 12, No. 2-3, 1992, pp. 221–239. http://dx.doi.org/10.1016/0956-053X(92)90050-S
25. Konsta-Gdoutos M. S. and Shah S. P., Hydration and properties of novel blended cements based on cement kiln dust and blast furnace slag, *Cement Concrete Res.*, Vol. 33, No. 8, 2003, pp. 1269–1276. http://dx.doi.org/10.1016/S0008-8846(03)00061-9
26. Metha P. K. and Monterio P. J. M., *Concrete, Microstructure, Properties and Materials*, McGraw-Hill, London, UK, 2006.
27. Kaufmann J., Loser R. and Leemann A., Analysis of cement-bonded materials by multi-cycle mercury intrusion and nitrogen sorption, *J. Colloid Interf. Sci.*, Vol. 336, No. 2, 2009, pp. 730–737. http://dx.doi.org/10.1016/j.jcis.2009.05.029
28. Zeng Q., Li K. F., Teddy F. C. and Dangla P., Pore structure characterization of cement pastes blended with high-volume fly-ash. *Cement Concrete Res.*, Vol. 42, No. 1, 2012, 194–204. http://dx.doi.org/10.1016/j.cemconres.2011.09.012
29. Aligizaki K., *Pore structure of cement-based materials*, Taylor & Francis, New York, USA, 2006.
30. Winslow D. N. and Diamond S., A mercury porosimetry study of the evolution of porosity in Portland Cement, *J. Mater.* Vol. 5, No. 3, 1970, pp. 564–585.
31. Helmuth R., *Fly ash in cement and concrete.* Portland Cement Association, 1987, pp 193.
32. Venkatanarayanan H. K. and Rangaraju P. R., Decoupling the effects of chemical composition and fineness of fly ash in mitigating alkali-silica reaction, *Cement Concrete Comp.*, Vol. 43, 2013, pp. 54–68. http://dx.doi.org/10.1016/j.cemconcomp.2013.06.009
33. Cihangir F., Investigation of utilisation of alkali activated blast furnace slag as binder in paste backfill. Ph.D. thesis, Karadeniz Technical University, Trabzon, Turkey, Turkish, 2011.
34. Whittington H. W., The conduction of electricity through concrete, *Mag. Concrete Res.*, Vol. 33, 1981, pp. 114. http://dx.doi.org/10.1680/macr.1981.33.114.48

Hydrothermal Hot-pressing Solidification of Coal Fly Ash and Its Ability of Fixing Heavy Metal

FANGBIN XUE, HUIPING SONG, YINGLU JI, LIQIONG CAO and FANGQIN CHENG*
State Environment Protection Key Laboratory of Efficient Utilization Technology of Coal Waste Resources, Institute of Resources and Environmental Engineering, Shanxi University, Taiyuan 030006, China

ABSTRACT: In this paper, hydrothermal hot-pressing solidification of coal fly ash has been done by mixing with different contents of calcium hydroxide and distilled water for 45 min at the condition of 7 MPa and 200°C. The strength of solidified specimens can reach the highest value of more than 63 MPa with 20% calcium hydroxide and 20% distilled water. During strength development, tobermorite may have a larger effect than CSH, and the immobilization of the solidified specimens for heavy metals can be also attributed to the new phases formed in the solidified bodies with different heavy metals. The results showed that Zn and Cd were to be fixed more readily than Cu and Pb.

INTRODUCTION

HYDROTHERMAL HOT-PRESSING (HHP) is a new technology of synthesizing materials under continued external mechanical forces [1], which has been widely applied in curing solid wastes and synthesizing new functional materials. Since ion product constant of water under hydrothermal conditions is much larger than that under normal pressure and temperature. The reaction rate at hydrothermal conditions would be significantly increased, and the diagenetic process of cumulates can accordingly be accomplished in a short time. Yamasaki *et al.* [2,3] found that the high-level radioactive waste could be successfully fixed by borosilicate glass under hydrothermal conditions. Furthermore, HHP solidified specimens of shell powder with a certain amount of organics usually present beautiful appearance like natural marble and can be used as building decoration materials [4,5].

Coal fly ash (CFA) contains a large amount of amorphous phase and its main components are SiO_2 and Al_2O_3 [6]. In the process of hydrothermal synthesis [7], $Ca(OH)_2$ can react with SiO_2 and Al_2O_3 in coal fly ash to form the hydrated calcium silicate with high strength and water hardness. Meanwhile, hydrothermal synthesis is carried out at low temperatures, so that the energy consumption during this process is only about one sixth of the preparation process of ceramic materials [8]. Therefore, it is reasonable to prepare an eco-friendly material with high strength and water hardness by HHP synthesis using coal fly ash and calcium hydroxide.

In this paper, solidified specimens with high strength and stability made by the low-calcium coal fly ash were investigated by HHP synthesis. Then, the fixing efficiency of HHP material of CFA-$Ca(OH)_2$ for heavy metals was evaluated through toxicity characteristic leaching procedure analysis.

EXPERIMENTAL

Materials

Coal fly ash, obtained from a power plant in Taiyuan (52.5% SiO_2, 31.2% Al_2O_3 and 1.9% CaO), was used as the raw material in this work. The calcium hydroxide, trihydrate copper nitrate, zinc nitrate hexahydrate, cadmium nitrate tetrahydrate, lead nitrate and glacial acetic acid used in this work were all analytical pure reagents.

Hydrothermal Hot-pressing Solidification Method

The coal fly ash and calcium hydroxide were mixed at the different mass ratios. Distilled water at a certain ratio was added into the mixed starting material. Then

*Author to whom correspondence should be addressed.
E-mail: cfangqin@sxu.edu.cn; Tel/Fax: +86-351-7018813; Postal address: No. 92 road, Taiyuan, Shanxi, China, 030006

1544-8053/15/03 143-06
© 2015 DEStech Publications, Inc.
doi:10.12783/issn.1544-8053/12/3/4

it was mixed sufficiently in a mortar. Next the mixture was put into a cylindrical chamber of the autoclave for HHP apparatus (Tohoku University), as shown in our previous work [9]. After that, the specimen was heated at a constant rate up to 200°C, and kept for 45 min at 7 MPa. After solidifying, the solidified samples were dried at 50–80°C for a day.

Methods for Solidification and Leaching of Heavy Metals

Dissolved nitrate solution of heavy metals was added into the distilled water, which generated reaction solution with metal ion concentration of 0.5 mass %. The solid materials were mixed with the solution and then solidified in the HHP apparatus under optimal hydrothermal conditions. The sample was dried at 50–80°C for a day. The contents of heavy metals in the resultant samples were: Sample A (Cu^{2+} 0.5%), Sample B (Zn^{2+} 0.5%), Sample C (Cd^{2+} 0.5%), Sample D (Pb^{2+} 0.5%), Sample E (Cu^{2+} 0.5%, Zn 0.5%, Cd^{2+} 0.5%, Pb^{2+} 0.5%), Sample F (no heavy metal added).

Leaching tests was done in accordance with the US EPA toxicity characteristic leaching procedure (TCLP) [10]. In addition, it should be pointed out that the horizontal shock method was used in TCLP leaching; and in order to maximize the leaching concentration of heavy metals, the horizontal shock method was replaced by the reverse method in this paper. Specimens were pressed and ground into particles, and their diameter were < 9.5 mm. Then, 2g ground particles were put into glacial CH_3COOH at the ratio of 20:1 (liquid: solid). The mixtures were shaken in the homogeneous reactor (JBJX-8, Jianbang, China) at a speed of 30 rpm for 18 h. After settling for 30 min, the leachate was filtered by membrane filter of 0.45 μm. The filtrate was used to determine heavy metal concentration.

Analysis Methods

The dried samples were used to measure the compressive strength by a pressure-measuring instrument (TYA-2000, China). Their characteristics were analyzed by the X-ray powder diffraction instrument (XRD, D2, Bruker, Germany), the fourier transform infrared spectrometer (FTIR, Waltham, MA, USA) and the field emission scanning electron microscope (SEM, S-4800, Hitachi, Japan). The heavy metals leached from the samples A~F were analyzed by the atomic absorption spectrometer (TAS-990, Puxi, China).

RESULTS AND DISCUSSION

Influence of the Water Content on the Compressive Strength of Samples

Dissolution and precipitation are usually considered as the main process in hydrothermal reaction [11]. Water can contribute to full wetting and package of raw materials, which is conductive to solution crystallization of raw material particles [12].

In the content range of 0–25%, the influence of distilled water was investigated. With increase of distilled water content, the compressive strength increased initially and finally reached the highest value, which could be specialized as: 22.1 MPa (5% water), 34.7 MPa (10% water), 51.5 MPa (15% water), 63.8 MPa (20% water) and 64.8 MPa (25% water).

Besides, the alkali environment formed by water and $Ca(OH)_2$ reduced the polymerization of network polymer of Si–O–Al, and promoted the fracture of T–O (T=Al or Si) bonds in fly ash surface. The unsaturated bond could react with $Ca(OH)_2$ to generate CSH gel, which enhanced compressive strength of solidified specimens. It was found that when the distilled water content was more than 25%, the compressive strength increased slightly, and most water bled out in the solidification process. As a result, the distilled water content was set as 20% in the following experiments.

Influence of $Ca(OH)_2$ Addition on Specimen Properties

As the open literatures indicate [13–15], tobermorite and CSH gel have a significant influence on compressive strength development. There is low concentration of Ca in the raw ash, and addition calcium hydroxide may promote the pozzolanic reaction of Ca^{2+} and the active SiO_2/Al_2O_3 in fly ash. Thus, the generated productions were CSH gel and tobermorite with high strength and water hardness.

The influence of $Ca(OH)_2$ addition on the compressive strength was investigated at 200°C and 7 MPa. The compressive strength of samples increased dramatically from 18.5 MPa (no $Ca(OH)_2$) to 63.8 MPa (20% $Ca(OH)_2$), and then decreased to 55.5 MPa (30% $Ca(OH)_2$) and 54.8 MPa (40% $Ca(OH)_2$). This indicated that a large amount of tobermorite or CSH gel formed readily in the coal fly ash mixed with 20% $Ca(OH)_2$.

The mineral transformation was investigated by XRD (Figure 1). The major mineral matters in raw

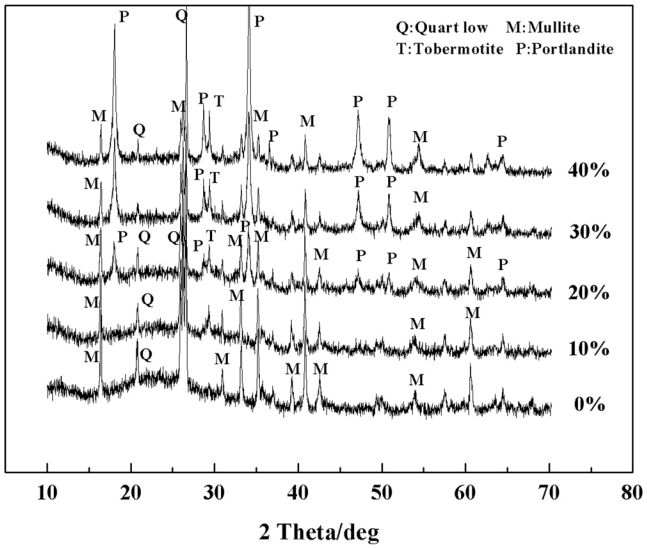

Figure 1. *XRD patterns of solidified specimens with different $Ca(OH)_2$ contents.*

coal ash were identified as mullite and quartz, which transformed to tobermorite gradually during $Ca(OH)_2$ content of 0~40%. When the concentration of $Ca(OH)_2$ was 40%, the content of tobermorite reached the maximum value; however, excessive $Ca(OH)_2$ had an adverse influence on the hydrothermal reaction.

Figure 2 showed FTIR patterns of samples with different $Ca(OH)_2$ contents. The band at about 970 cm^{-1} was consistent with the stretching vibration of Si–O in tetrahedral structure, which was corresponding to the chemical progress that coal fly ash reacted with $Ca(OH)_2$ to generate CSH or tobermorite [16]. The peak at about 3643 cm^{-1} was due to O–H bonds vibration. And the band tended to become more intense with increasing $Ca(OH)_2$ content. In addition, at around 1430, 875 and 713 cm^{-1}, three bands corresponding to CO_3^{2-} anions appeared, which resulted from the presence of $CaCO_3$ [17]. The above results were in good agreement with those obtained from the XRD.

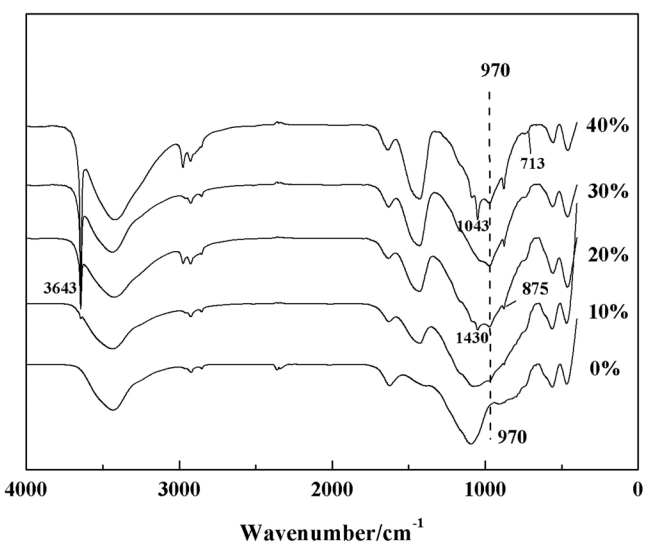

Figure 2. *FTIR patterns of solidified specimens with different $Ca(OH)_2$ contents.*

Figure 3 shows the SEM images for microstructure evolution of the specimens. When the content of Ca(OH)2 was 20 %, there were many close directional micro-fibrous textures [Figure 3(a)]. On the EDS result, the fibrous materials may be tobermorite, which was in accord with the XRD results. The tobermorite with micro-fibrous textures enhanced the strength of samples, because the void between the coal fly ash particles could be filled up and the well-densified matrix genarated [18,19]. However, when the content of $Ca(OH)_2$ was 40 mass% [Figure 3(b)], the fibrous materials aggregated and transformed to laminated materials. Based on the corresponding EDS results, the laminated materials should be CSH gel.

Solidification Efficiency of the Solidified Specimens for Heavy Metals

Samples (A~F) were prepared at 200°C for 45 min with 5 mass% different metals, 20 mass% $Ca(OH)_2$ addition and 20 mass% distilled water. Table 1 showed the effects of different heavy metals on the compressive strength and leaching data of samples A~F. Solidification of heavy metal had a greater impact on the compressive strength of Cu and Zn than those of Cd and Pb. The underlying mechanism was complex and uncertain, and more investigations would be done in the near future.

The fixed efficiency (Y) of metal ion in the solidified bodies was calculated by Equation (1):

$$Y(\%) = \left[1 - \frac{(C_{leaching} - C_{blank}) \times V}{m}\right] \times 100\% \qquad (1)$$

where $C_{leaching}$ is the metal ion concentration leaching from the solidified bodies fixing heavy metal (mg/L); C_{blank} is the metal ion concentration leaching from Sample F (mg/L); V is the leaching solution volume, V = 40 ml = 0.04 L; and m is the weight of all heavy metal in the solidified bodies, m = 2 g × 0.5% × 1000 = 10 mg.

So, the initial concentration of Cu^{2+}, Zn^{2+}, Cd^{2+} and Pb^{2+} in the solidified bodies were about 250 mg L^{-1}. The fixed efficiencies of Cu^{2+}, Zn^{2+}, Cd^{2+} and Pb^{2+} in

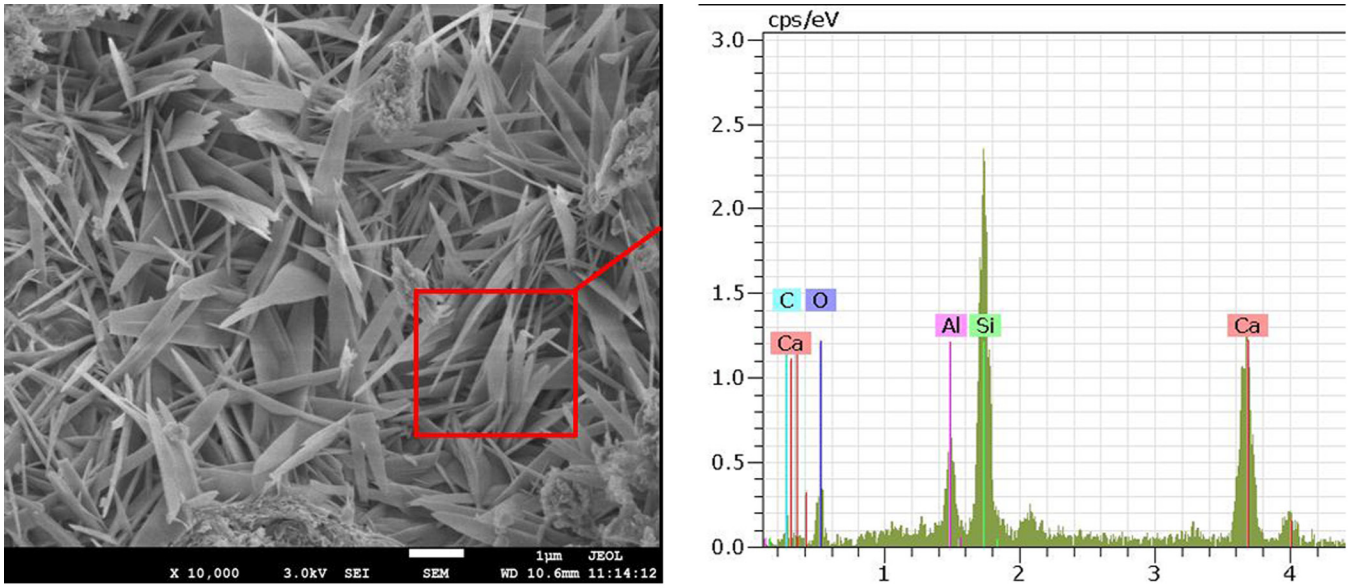

(a)

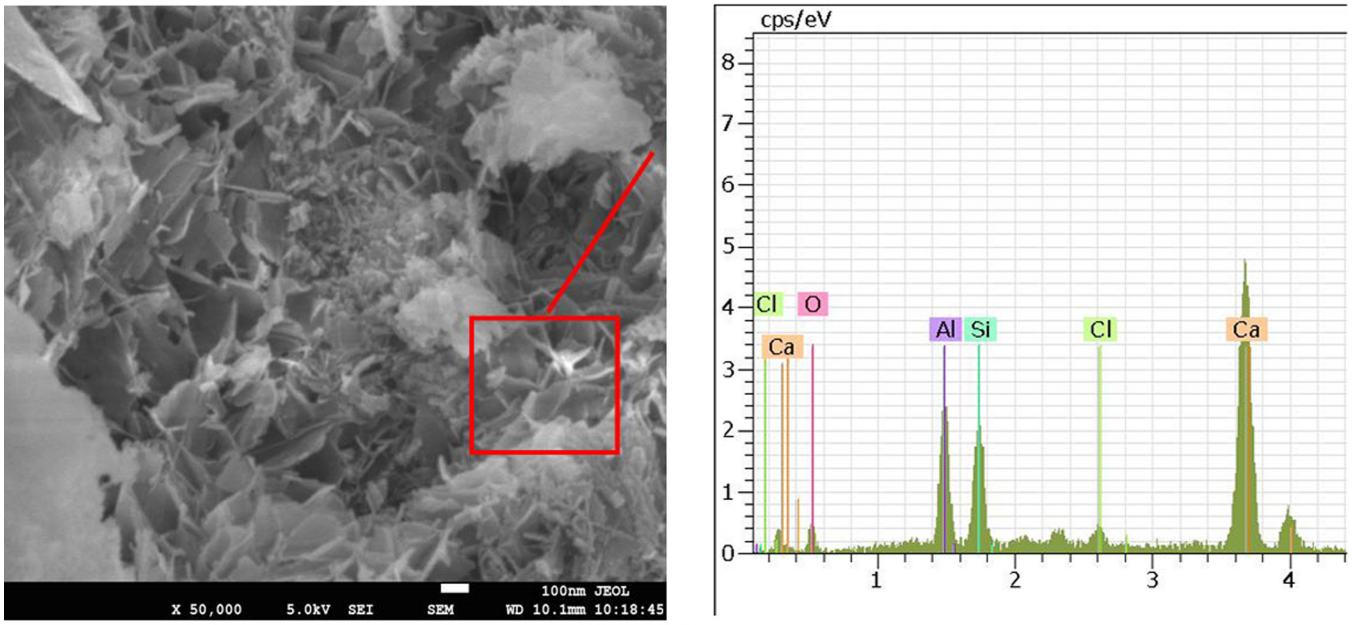

(b)

Figure 3. *SEM and EDS images of solidified specimens with (a) 20% and (b) 40% $Ca(OH)_2$ contents.*

the solidified bodies were calculated as 92.7%, 99.6%, 99.5%, 97.7%, respectively. Zn^{2+} and Cd^{2+} were easier to be immobilized than Cu^{2+} and Pb^{2+}. Leaching concentration of different heavy metals was influenced by the existence of other metals. Moreover, when these heavy metals existed simultaneously, the fixed efficiencies reduced as 80.1%, 72.3%, 96.9%, 67.5%, respectively. The existing of other metal had lowest impact on the fixed efficiency of Cd.

The evolution of the solidified bodies (A~F) was also characterized by FTIR (Figure 4). The bonds of 1010 and 570 cm^{-1} respectively corresponded to the asymmetric stretching vibration of Si–O–Si and the symmetric stretching vibration of Si–O–Al in the dual-ring-structure of tetrahedron [20], which tended to move and change after adding heavy metals. In addition, the peak at around 1400 cm^{-1} tended to appear. The FTIR results showed that the heavy metals were

Table 1. The Properties of Samples from A to F.

Sample	$C_{Leaching}$ (mg L^{-1})				Compressive Strength (MPa)
	Cu^{2+}	Zn^{2+}	Cd^{2+}	Pb^{2+}	
A (Cu^{2+} 0.5%)	**18.3**	0.313	0.031	0.117	43.4
B (Zn^{2+} 0.5%)	0.121	**1.08**	0.033	0.073	37.0
C (Cd^{2+} 0.5%)	0.119	0.148	**2.04**	0.074	51.9
D (Pb^{2+} 0.5%)	0.106	0.037	0.336	**5.85**	59.6
E (each 0.5%)	**50**	**69.2**	**8.40**	**81.4**	53.6
F (blank)	0.115	0.041	0.712	0.170	63.8

fixed to the skeleton structure of solidification body and replaced a part of groups of the polymer chains.

Compared with the XRD pattern of sample F (blank), the intensity of many peaks of samples A~E became higher or lower in Figure 5, and some new peaks appeared at the same time, such as 2 Theta was about 18º, 32°, 34°, 40°, 45~52°. It indicated that some new reaction and the formation of new phases in the solidified bodies with different heavy metals. Fixing heavy metals of the solidified specimens can be mainly attributed to the new phases formed in the solidified bodies with different heavy metals. But the exactly mechanism for fixing the trace heavy metals by HHP method was not very clearly so far.

CONCLUSIONS

Coal fly ash could be solidified by hydrothermal hot-pressing under a constant pressure (7 MPa) at 200°C by addition of calcium hydroxide and water. $Ca(OH)_2$ and water could provide the alkali environment and accelerate the dissolution of Si–O bond and Al–O bond in coal fly ash, which promoted the fly ash to generate CSH gel or tobermorite. And tobermorite promoted the strength development because of the reinforced matrix with its interlocked structure. The highest strength of the solidified specimens had potential for fixing many heavy metals, and the fixing efficiencies of Cu^{2+}, Zn^{2+}, Cd^{2+} and Pb^{2+} in the solidified specimens were all good, especially those of Zn^{2+}, Cd^{2+} (more than 99.5%). Meanwhile, the immobilization of metals was influenced by other metals and the affected level was different for different metals. Therefore, this study provides a method for solidification of CFA by hydrothermal hot-pressing and for fixing heavy metals. This has a high potential for recycling solid wastes and fixing heavy metals under low temperatures and pressures.

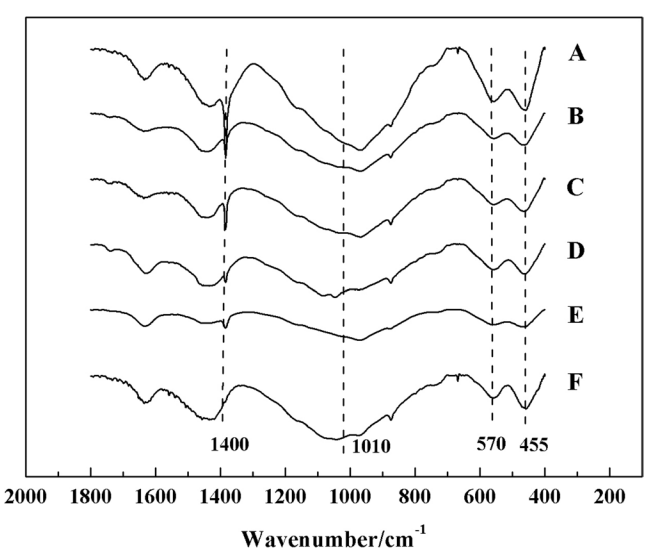

Figure 4. *FTIR patterns of solidified specimens A to F.*

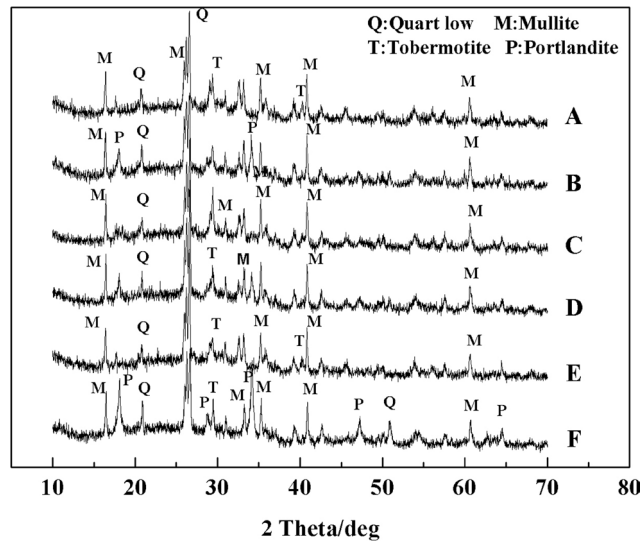

Figure 5. *XRD patterns of solidified specimens A to F.*

ACKNOWLEDGEMENTS

This work was financially supported by the National Key Technology R&D Program (2013BAC14B05) and the Research Projects of Shanxi Province (MC2014-06 and 20131101027). The authors would also like to give special thanks to Prof. Yamasaki and Lan Xiang for their assistance in testing HHP.

REFERENCES

1. Lin, H., Yamasaki, N., Xu, S., "Study on the hydrating process of borosilicate glass by HHP", *Glass Enamel China,* Vol.29, No.5, 2001, pp. 15–20.
2. Yamasaki, N., Yanagisawa, K., Nishioka, M., "A hydrothermal hot-pressing method: apparatus and application", *J. Mater. Sci. Lett.*, Vol.5, No.3, 1986, 355–356. http://dx.doi.org/10.1007/BF01748104
3. Yamasaki, N., Yanagisawa, K., Nishioka, M., "Hydrothermal immo-

bilization of glass powder containing simulated high-level redioactive-waste", *J. Atom. Energ. Soc. Jpn.*, Vol. 28, No. 3, 1986, 266–273. http://dx.doi.org/10.3327/jaesj.28.266

4. Terai, R., "Characterization of borosilicate glasses containing simulated high-level radioactive wastes", *J. Atom. Energ. Soc. Jpn.*, Vol. 21, No. 5, 1979, 423–433.
5. Yanagisawa, K., Nishioka, M., Yamasaki, N., "Immobilization of Radioactive Wastes by Hydrothermal Hot Pressing", *Am. Ceram. Soc. Bull.*, Vol. 64, No .12, 1985, 1563–1567.
6. Luo, Z., Ma, B., Li, X., "Study of fly ash hydrated course in hydrothermal and alkaline environment", *J. China Univ. Min. Tech.*, Vol. 39, No. 2, 2010, 25–30.
7. Zhang, H.B., Wei, L.B., "Screening of surface medication agents and modification mechanism of fly ash", *J. China Univ. Min. Tech.*, Vol. 17, No. 3, 2007, 341–344. http://dx.doi.org/10.1016/S1006-1266(07)60101-1
8. Ishida, E.H., 1999, "To restore potentialities of soil-development of hydrothermally solidified soil: earth ceramics", *Proceedings of the 4th International Conference on Ecomaterials*, 7–10.
9. Ji, Y.L., Song, H.P., Cheng, F.Q., Zhang, P.H., "Preparation of geopolymer material by hydrothermal hot-pressing", *Fly Ash Comprehensive Utilization*, Vol.28, No.5, 2014, 22–25.
10. US EPA. Method 1311 SW2846, 1986, "Test methods for evaluating solid waste: physical chemical methods", Washington DC: Governmental Printing Office.
11. Jing, Z.Z., Fan, X., Zhou, L., "Hydrothermal solidification behavior of municipal solid waste incineration bottom ash without any additives", *Waste Manage*, Vol. 33, No. 3, 2013, 1182–1189. http://dx.doi.org/10.1016/j.wasman.2013.01.038
12. Wang, Z.L., Jing, Z.Z., Shan, C.C., "Research on hydrothermal synthesis of sepiolite-based clay", *Non-Metallic Mines*, Vol. 34, No. 1, 2011, 6–10.
13. Jing, Z.Z., Matsuoka, N., Jin, F., "Municipal incineration bottom ash treatment using hydrothermal solidification", *Waste Manage*, Vol. 27, No. 2, 2007, 287–293. http://dx.doi.org/10.1016/j.wasman.2006.01.015
14. Jing, Z.Z., Jin, F., Hashida, T., "Influence of additions of coal fly ash and quartz on hydrothermal solidification of blast furnace slag", *Cement Concrete Res.*, Vol. 38, No. 7, 2008, 976–982. http://dx.doi.org/10.1016/j.cemconres.2008.01.017
15. Jing, Z.Z., Matsuoka, N., Jin, F., "Solidification of coal fly ash using hydrothermal processing method", *J. Mater. Sci.*, Vol. 41, No. 5, 2006, 1579–1584. http://dx.doi.org/10.1007/s10853-006-4648-6
16. Yu, P., Kirkpatrick, R.J., Poe, B., "Structure of calcium silicate hydrate (C-S-H): near-, mid- and far- infrared spectroscopy", *J. Am. Ceram. Soc.*, Vol. 82, No. 3, 1999, 742–748. http://dx.doi.org/10.1111/j.1151-2916.1999.tb01826.x
17. Sierra, E.J., Miller, S.A., Sakulich, A.R., "Pozzolanic activity of diatomaceous earth", *J. Am. Ceram. Soc.,* Vol. 93, No. 10, 2010, 3406–3410. http://dx.doi.org/10.1111/j.1551-2916.2010.03886.x
18. Shan, C., Jing, Z., Pan, L., "Hydrothermal solidification of municipal solid waste incineration fly ash", *Res. Chem. Intermed.,* Vol. 37, No. 2, 2011, 551–565. http://dx.doi.org/10.1007/s11164-011-0287-x
19. Jing, Z.Z., Jin, F.M., Yamasaki, N., Maeda, H., Ishida, E.H., "Potential utilization of riverbed sediments by hydrothermal solidification and its hardening mechanism", *J. Environ. Manage.* Vol. 90, No. 5, 2009, 1744–50. http://dx.doi.org/10.1016/j.jenvman.2008.11.013
20. Xu, J.Z., Zhou, Y.L., Tang, R.X., "Study on the solidification of heavy metals by fly ash based geopolymers", *J. Build. Mater.*, Vol. 9, No. 3, 2006, 341–346.

Synthesis and Mechanism of a Novel Organosilicone Used as a Selective Plugging Agent

BING HOU[1], QINGYANG LI[1,*] and YAN LUO[2]

[1]*State Key Laboratory of Petroleum Resources and Prospecting, China University of Petroleum, Beijing, 102249, China*

[2]*Department of Sustainable Bioproducts, Mississippi State University, Mississippi State, MS 39762, United States*

ABSTRACT: A novel selective blocking agent called PLA-21 was prepared by acrylamide (AM), Acrylic Acid (AA), diallyldimethylammonium chloride (DMDAAC) and 2-acrylamido-2-methyl-1-propanesulfonic acid (AMPS) in aqueous solution with organosilicon(WD-70) as cross-linking agent. The optimal synthesis conditions were discussed detailedly. The experimental results showed that its water plugging rate was higher than 95% and plugging rate of oil was less than 10%, which demonstrated excellent selective plugging ability. Meanwhile, cores with different permeability can be blocked effectively. Compared with some common selective blocking agents, it was found that the PLA-21 satisfied engineering demand better and it was an effective selective blocking agent for oil filed application. FTIR and EDS show PLA-21 was synthesized successfully and it contains anion group, cationic groups, nonionic groups and silicon. SEM was used to research and analyze the mechanism of selective plugging. It indicates that PLA-21 can expand sharply in water and shirk in oil, which making it good selective blocking efficiency.

INTRODUCTION

At present, the techniques of chemical water plugging are applied extensively for old wells in the process of water flooding. There are many chemical agents employed for water plugging and novel agents are developed continuously [1–4]. Depending on the plugging effect, chemical blocking agents can be divided into non-selective and selective water plugging agent. With the ever-increasing demand of cleaner production and environmental protection, selective water blocking agents become more and more popular and large quantities of water plugging agents are prepared and have been common used in oil field, such as oil-based cement, organosilicane resin, phenolic resin, foamy plugging agents and so on [5–8]. However, all of them exhibited have the shortages, such as less-than-ideal selectivity, high cost, and so on, which greatly limit their application. So, it is pressing and inevitable to develop a novel selective blocking agent with excellent selectivity, low cost and wide raw material sources [9–11].

Based on the existing deficiencies of conventional chemical blocking agents, molecules structure of new blocking agent was designed and optimized. A novel silicone based selective blocking agent named PLA-21 was synthesized by cross-linking polymerization of anionic, cationic and nonionic monomers through oxidation-reduction initiator system. The PLA-21 is three-dimension network spatial with excellent expansibility in water and good shrinkability in oil, which caused it higher water swelling ability and outstanding selectivity.

MATERIALS AND METHODS

Materials

Acrylic Acid (AA), acrylamide (AM), ammonium persulfate ($(NH_4)_2S_2O_8$), sodium sulfite (Na_2SO_3) were of chemical pure. Diallyldimethylammonium chloride (DMDAAC), organosilicone (WD-70) and 2-acrylamido-2-methyl-1-propanesulfonic acid (AMPS) were of industrial grade. HPAM (M = 5 million, industrial grade) was got from DaQing Oilfield of China. CAN-1, synthesized with AM (acryl amide), AA (AA) and AN (acrylonitrile), was obtained from Shenli Oilfield of China. JH-AP, copolymer of AA and DMDAAC,

*Author to whom correspondence should be addressed.
E-mail: houbing9802@163.com; Tel/Fax: +86-351-7018813; Postal address: No. 92 road, Taiyuan, Shanxi, China, 030006

1544-8053/15/03 149-08
© 2015 DEStech Publications, Inc.
doi:10.12783/issn.1544-8053/12/3/5

was provided by JiangHan Oilfield of China. Organosilicone was used as cross-linking agent. Ammonium persulfate and sodium sulfite were used as initiator. All the chemicals and materials above were used directly without any purification.

Methods

Synthesis and Characterization

First, a three-necked flask with 40 ml water was put into a thermostatic water bath. Under the protection of nitrogen, a certain amount of AM, AA, DMDAAC, AMPS and WD-70 were added into the three-necked flask orderly and mixed sufficiently. After that, ammonium and sodium sulfite persulfate were added in turn when the temperature of water reached 50~55°C. Some hours later, polymerization finished and a transparent viscoelastic substance was obtained. Lastly, the transparent viscoelastic substance was dried and granulated with different partical size. The whole synthetic process was controlled under the temperature of 60°C.

IR spectra were recorded with Nicolet iS50 FTIR spectrometers (KBr pellets) to analyze the functional groups of the product. The scanning electron microscope pictures were obtained with Quanta 250 SEM to study the surface structure and energy dispersive spectrometer (EDS) was used to analyze the relative element content of PLA-21.

Calculation of Swelling Degree

First, PLA-21 was dried in a beaker at 105°C. Then, a certain amount of PLA-21 was added into water for 24 h until it was saturated. Then, the PLA-21 was weighed after it was screened through mesh size of 12. The swelling degree of PLA-21 was calculated as the following equation at the temperature of 25°C:

$$Q = \frac{m_2 - m_1}{m_2} \tag{1}$$

where Q represents swelling degree, m_1 is the weight of original PLA-21 and m_2 is saturated PLA-21 which cannot pass though the mesh size of 12, respectively.

Plugging Rate of PLA-21

The device for core flooding experiment (Figure 1) was used to evaluate the plugging ability. The device is shown in Figure 1.

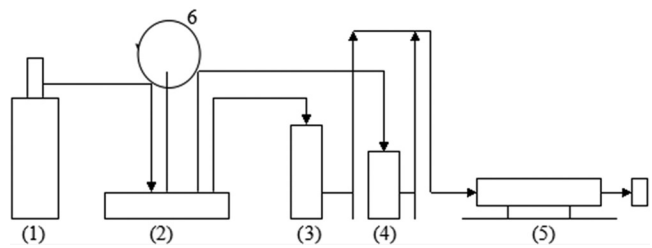

Figure 1. *Flowchart of core flooding experiment. (1) nitrogen cylinder; (2) six-way valve; (3) water cistern; (4) pressure accumulator; (5) core holders; and (6) manometer.*

First, the glue solution of plugging agent was poured into the pressure container and the pressure vessel head was screwed. Then, the device was assembled as Figure 1. The valve of nitrogen cylinder was opened after the water temperature rose up to 25°C and the volume of squeezed out water was recorded. After 1PV plugging agent was squeezed out, the valves at both ends of the core were closed. Then, the pressure was released and the well was shut. The volume of squeezed out plugging agent, the entry pressure and entry time of plugging agent were recorded. The well was opened again after the plugging agent was solidified. The change of pressure, which represented the relative strength and the cross-links of the gel system, was record when the volume of squeezed out plugging agent over 20 PV.

The permeability of cores was calculated before and after PLA-21 was added respectively. The darcy-weisbach formula was used to calculate the permeability.

$$K = \frac{Q\mu L}{10A\Delta P} \tag{2}$$

Where K is the permeability of the core, %; Q is the flow rate through the core at a certain differential pressure, ml/s; A is the cross sectional area of the core, cm^3; L is the length of the core, cm; μ is the viscosity of the fluid through the core, mPa·s; ΔP is the differential pressure of fluid before and after it passed though the core, MPa; K is the permeability coefficient of the core, D (μm^2).

The plugging ratio for core was expressed as following:

$$\eta = \frac{K_1 - K_2}{K_1} \times 100\% \tag{3}$$

Where η is the plugging rate, %; K_1 is the permeability of core before profile control, %; K_2 is the permeability of core after profile control, %.

RESULTS AND DISCUSSION

Synthesis

The single factor experiments were made to determine the most dosage of each monomer after orthogonal experiments had been made to ensure the probable addition of each monomer. The synthesis was in the distilled water with the volume of 40 ml. As swelling times was the most important parameter for blocking agent, so the optimal synthesis condition was determined according to the swelling times of synthetic product.

Effect of Dosage of AM on the Swelling Times

The optimal dosage of AM for PLA-21 was studied firstly. Table 1 illustrates the effect of AM on the swelling times. The reaction temperature, reaction time, initiator of $(NH_4)_2S_2O_8$ and Na_2SO_3 were 50°C, 6 h, 0.1 g and 0.05 g, respectively. As the increasing of AM from 1 g to 7 g, the swelling times increase from 4.7 times to 11.7 times. That is because AM is beneficial to synthesize plugging agent with certain molecular weight to absorb water.. However, too much AM may hinder other hydrophilic monomers from polymerization and crosslink excessively, which decreases the swelling degree. So, after that, the swelling times maintain and then drop [12]. Taking the cost of production into consideration, the best addition of AM is 7 g.

Effect of Dosage of AA on Swelling Times

The addition of AA was changed from 1.0 g to 11.0 g after the best dosage of AM was determined. The effect of AA on the swelling times is shown in Table 2. The reaction temperature, reaction time, initiator of $(NH_4)_2S_2O_8$ and Na_2SO_3 were 50°C, 6 h, 0.1 g and 0.05 g, respectively. As shown in Table 2, the swelling times increases with increasing AA from 1 g to 6 g and decreases with increasing of AA thereafter. So, 6 g AA here is the optimal choice. Because the water absorption of carboxylate radical in AA is stronger than that of amino group in AM. So, with the increase of AA, the water absorption of plugging agent become stronger. However, with much more AA is added, it may homopolymerize and synthesize straight-chain compounds, which destroy the three-dimensional network structure [13].

Table 1. Effect of Dosage of AM on Swelling Times.

AM (g)	AA (g)	AMPS (g)	DMDAAC (g)	WD-70 (g)	H_2O (ml)	Swelling Times
1.0	4.0	2.0	1.5	0.5	40.0	**4.7**
3.0	4.0	2.0	1.5	0.5	40.0	**5.6**
5.0	4.0	2.0	1.5	0.5	40.0	**6.9**
7.0	4.0	2.0	1.5	0.5	40.0	**11.7**
9.0	4.0	2.0	1.5	0.5	40.0	**11.8**
11.0	4.0	2.0	1.5	0.5	40.0	**9.2**

Table 2. Effect of Dosage of AA on Swelling Times.

AM (g)	AA (g)	AMPS (g)	DMDAAC (g)	WD-70 (g)	H_2O (ml)	Swelling Times
7.0	1.0	2.0	1.5	0.5	40.0	**8.6**
7.0	3.0	2.0	1.5	0.5	40.0	**9.0**
7.0	6.0	2.0	1.5	0.5	40.0	**16.9**
7.0	9.0	2.0	1.5	0.5	40.0	**12.9**
7.0	11.0	2.0	1.5	0.5	40.0	**10.5**

Effect of dosage of AMPS on swelling times

After the optimal addition of AM and AA was determined, experiments was made to determine the optimum dosage of AMPS. Table 3 illustrates the effect of AMPS on the swelling times. The reaction temperature, reaction time, initiator of $(NH_4)_2S_2O_8$ and Na_2SO_3 were 50°C, 6 h, 0.1 g and 0.05 g, respectively. AMPS has good water absorption for the reason that it contains hydrophilic amino group and sulfonic group So, with the dosage of AMPS increases from 1 g to 3 g, the swelling times of blocking agent increase from 15.7 times to 18.4 times. After that, the swelling times decrease with further more AMPS for the reason that the steric-hinerance effect of quaternary carbon and sulfonic group become obvious. So, 3 g here is best for synthesizing blocking agent.

Effect of Dosage of DMDAAC on Swelling Times

After the optimal addition of AM, AA and AMPS

Table 3. Effect of Dosage of AMPS on Swelling Times.

AM (g)	AA (g)	AMPS (g)	DMDAAC (g)	WD-70 (g)	H_2O (ml)	Swelling Times
7.0	6.0	1.0	1.5	0.5	40.0	**15.7**
7.0	6.0	2.0	1.5	0.5	40.0	**16.9**
7.0	6.0	3.0	1.5	0.5	40.0	**18.4**
7.0	6.0	4.0	1.5	0.5	40.0	**14.0**
7.0	6.0	5.0	1.5	0.5	40.0	**11.3**

was determined, experiments was made to find the optimum dosage of DMDDAC. Table 4 below shows the effect of AMPS on swelling times. With the dosage of DMDDAC increases from 1.0 g to 3.0 g, the swelling times increases firstly and decreases rapidly when the dosage exceeds 1.5 g. The reason is that quaternary ammonium cationic groups of DMDAAC have good hydrophilcity, which means a small number of DMDAAC can help to absorb more water. Meanwhile, the stereo-hindrance effect of quaternary ammonium cationic groups is obvious [14–15]. So, superabundant DMDAAC may hinder the polymerization between monomers.

Effect of Dosage of WD-70 on Swelling Times

Experiments were made to find the optimum dosage of WD-70 after the optimal addition of AM, AA, AMPS and DMDAAC were determined. Table 5 below shows the effect of WD-70 on the swelling times. The maximal swelling times appear when 0.1g WD-70 is added. According to Flory's inflation theory, apposite WD-70 is so important to strengthen an elastomer with three-dimensional network structure. However, higher dosage of cross-linking agent occupies the space of network structure for excessive crosslinking [16]. That's why the swelling capacity decreases sharply when the dosage exceeds 0.1 g. So, 0.1 g WD-70 here is appropriate for PLA-21.

Effect of Temperature and Time on Swelling Times

Experiments were made to find the optimum temperature and time after the optimal addition of all monomers was determined. The result is shown in Table 6. When the reaction time was set at 6 h, the swelling times of synthetic product increased with the rise in temperature and reduced after the temperature was over 50°C. At the low temperature, it is hard for free radicals to collide each other, which cause short-chain branch and low crosslinking degree, further influencing the swelling degree. At the high temperature, homopolymerization and thermal cross-linking become active, which cause low grafting and low swelling degree. So, the reaction temperature was set at 50°C.

When the reaction temperature was set at 50°C, relative experiments were done to optimize the reaction time. From Table 6, it is clearly to see that the best reaction time was 8 h. When the time is not long enough, the polymerization reaction cannot finish fully to form the best network structure. However, when the reaction time is too long, the product will crosslink excessively and the space of the plugging agent will be compressed, further reducing the swelling degree.

Effect of Initiators on Swelling Times

The optimal addition of initiators was determined finally when the other conditions mentioned above were set at the best value, respectively. The dosage of oxidizing agent and reductant was determined orderly and the results are shown in Table 7. When the dosage of initiator is not enough, the active centre will reduce, which cause low reaction speed and incomplete reaction. However, high dosage of initiator means more active centre, which increase the ratio of chain termination and excessive crosslinking. So, the optimal addition of oxidizing agent and reductant is 0.2 g and 0.075 g, respectively.

Table 5. Effect of Dosage of WD-70 on Swelling Times.

AM (g)	AA (g)	AMPS (g)	DMDAAC (g)	WD-70 (g)	H_2O (ml)	Swelling Times
7.0	6.0	3.0	1.5	0	40.0	**14.8**
7.0	6.0	3.0	1.5	0.1	40.0	**44.6**
7.0	6.0	3.0	1.5	0.2	40.0	**25.8**
7.0	6.0	3.0	1.5	0.3	40.0	**24.6**
7.0	6.0	3.0	1.5	0.5	40.0	**18.4**
7.0	6.0	3.0	1.5	0.7	40.0	**16.1**

Table 4. Effect of Dosage of DMDAAC on Swelling Times.

AM (g)	AA (g)	AMPS (g)	DMDAAC (g)	WD-70 (g)	H_2O (ml)	Swelling Times
7.0	6.0	3.0	1.0	0.5	40.0	**12.2**
7.0	6.0	3.0	1.5	0.5	40.0	**18.4**
7.0	6.0	3.0	2.0	0.5	40.0	**14.9**
7.0	6.0	3.0	2.5	0.5	40.0	**9.5**
7.0	6.0	3.0	3.0	0.5	40.0	**6.1**

Table 3. Effect of Temperature and Time on Swelling Times.

Temperature (°C)	Time (h)	Swelling Times	Temperature (°C)	Time (h)	Swelling Times
42		**30.4**		4	**23.1**
50		**44.8**		6	**45.2**
64	6	**38.6**	50	8	**73.0**
77		**36.2**		10	**49.9**
88		**35.9**		12	**36.9**

Table 7. Effect of Addition of Initiators on Swelling Time.

$(NH_4)_2S_2O_8$ (g)	Na_2SO_3 (g)	Swelling Times	$(NH_4)_2S_2O_8$ (g)	Na_2SO_3 (g)	Swelling Times
0.05		**88.4**		0.05	**163.8**
0.10		**92.1**		0.075	**167.8**
0.15	0.025	**100.5**	0.20	0.10	**159.9**
0.20		**109.6**		0.15	**154.1**
0.25		**98.3**		0.20	**132.0**

Plugging Effect of PLA-21

Blocking Efficiency of PLA-21 with Different Size

PLA-21 was grinded into particles with different size to plug cores with different permeability. Under the temperature of 25°C, plugging agent with the concentration of 0.1% was squeezed into the cores with the shape of $\varphi 25 \times 60$ mm. The displacing medium was sodium chloride solution with the concentration of 1,000 mg/L and the plugging the plugging time is 16 h. The results were shown in Table 8.

It is indicated in Table 8 that the PLA-21 with the particle size from 30 μm to 120 μm is effective to plug the cores with the air permeability from 0.9 μm^2 to 15 μm^2. The plugging rate of all the tested cores is higher than 95%. By analogy, it is efficient to choose PLA-21 with larger size to plug the cores with higher permeability. Though, the core with lower permeability can be easier plugged and the permeability reduces nearly to zero, the Breakthrough pressure gradient reduces and the plugging rate also drop with the enlargement of the permeability. That is because big PLA-21 can block big pores but may hardly plugging small pores. So, it is significant to add a proportion of small PLA-21when block the rock with big permeability.

Selectivity Comparison of the Different Plugging Agents on Oil and Water

Three kinds of commonly used commercial blocking agents, HPAM, CAN-1 and JH-AP, were used for plugging effect comparison to detect the selective plugging effect of PLA-21. Plugging effect of each blocking agent on oil and water was tested with kerosene and 2% saline used for the displacing medium. Plugging agents with same volume and concentration were squeezed into cores at the temperature of 25°C. Results shown in Table 9.

Table 8. Plugging Effect of PLA-21 with Different Size on Cores with Different Permeability.

K_g (μm^2)	Φ (μm)	P_1 (MPa)	K_1 (μm^2)	ΔP (MPa/m)	P_2 (MPa)	K_2 (μm^2)	η (%)
0.901	30	0.46	0.291	16.1	1.02	0.00027	**99.9**
3.852	60	0.30	1.276	4.3	0.91	0.02247	**98.2**
14.987	90	0.01	6.660	1.24	0.21	0.225	**96.6**
15.011	120	0.20	6.986	0.90	0.04	0.323	**95.4**

Table 9. Plugging Effect of Several Plugging Agents on Oil and Water.

Plugging Agent	K_{w1} (μm^2)	K_{w2} (μm^2)	η_w (%)	K_{o1} (μm^2)	K_{o2} (μm^2)	η_o (%)
PLA-21	0.675	0.0014	**99.8**	0.587	0.531	**9.5**
HPAM	0.558	0.0318	**94.3**	0.486	0.433	**10.9**
CAN-1	0.491	0.0162	**96.7**	0.452	0.301	**33.4**
JH-AP	0.607	0.0255	**95.8**	0.569	0.448	**21.2**

Table 3 shows that the water plugging rate of PLA-21 is above 95% and the oil plugging rate is less than 10%, behaving good selectivity. Though the plugging experiments are tested using the cores with the similar permeability, both water plugging effect and selectivity of PLA-21 are better than HPAM, CAN-1 and JH-AP , which shows good plugging and selectivity.

Characterization and Mechanism Analysis

FTIR Analysis and EDS

IR picture was used to analyze whether the PLA-21 had been synthesized successful. EDS was used to test the relative content of silicone.

FTIR peaks at 798.71 cm^{-1} and 1113.08 cm^{-1} represent the bending vibration and stretching vibration of Si–O–Si, respectively. The peaks of 1697.97cm^{-1} and 3212.52 cm^{-1} represent the C=O and N–H, respectively, which indicates the existence of amido. The band of 958.45 cm^{-1} represents quaternary ammonium. The band of 1716.25 cm^{-1} shows the vibration absorption of C=O in the acid. The peaks of 1037.05, 1174.05and 1216.24 demonstrate the existence of $-SO_3^{2-}$. The phenomenon shown above demonstrates that the PLA-21 was synthesized successful and it contains anion group, cationic group and non-ionic group.

Both elemental analysis and IR spectra indicate that PLA-21 contain silicon, it is because vinyl organosilicone is used as one of the monomers. Though, the relative content of silicone is very little, it plays a significant role. On one hand, silicon-containing group can react with the hydroxyl groups of rock surfaces,

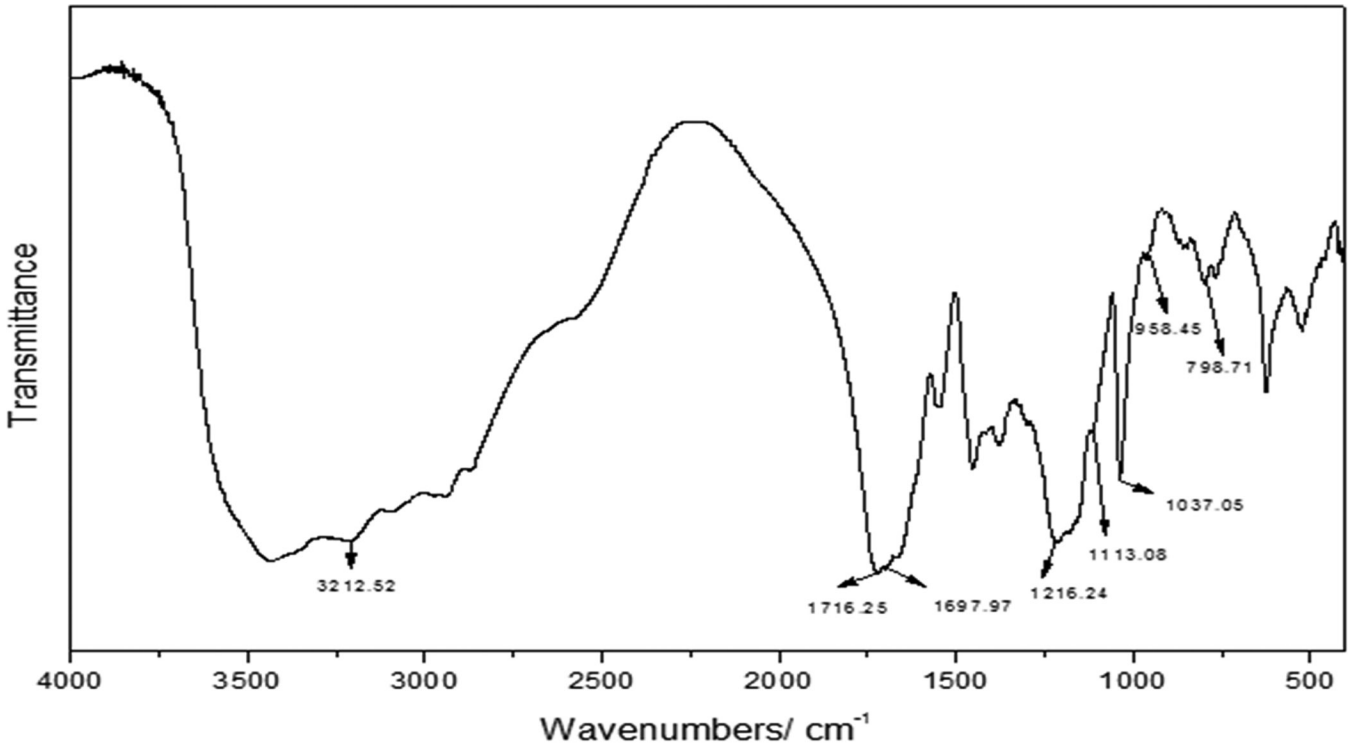

Figure 2. *IR spectra of PLA-21.*

changing oleophilic rock into the hydrophilic rock. On the other hand, the silicon-containing group can react with water and generate insoluble silanol, which block the pores of the reservoir. Meanwhile, it cannot produce insoluble substance in the oil reservoir for the reason that there is no water there. Also, it has the ability of forming and strengthening the grid structure of PLA-21. So, organosilicone can help to blocking water efficiently.

Observation with SEM

Four pieces of dried PLA-21 with the similar volume were prepared. One was used for comparison. Two of

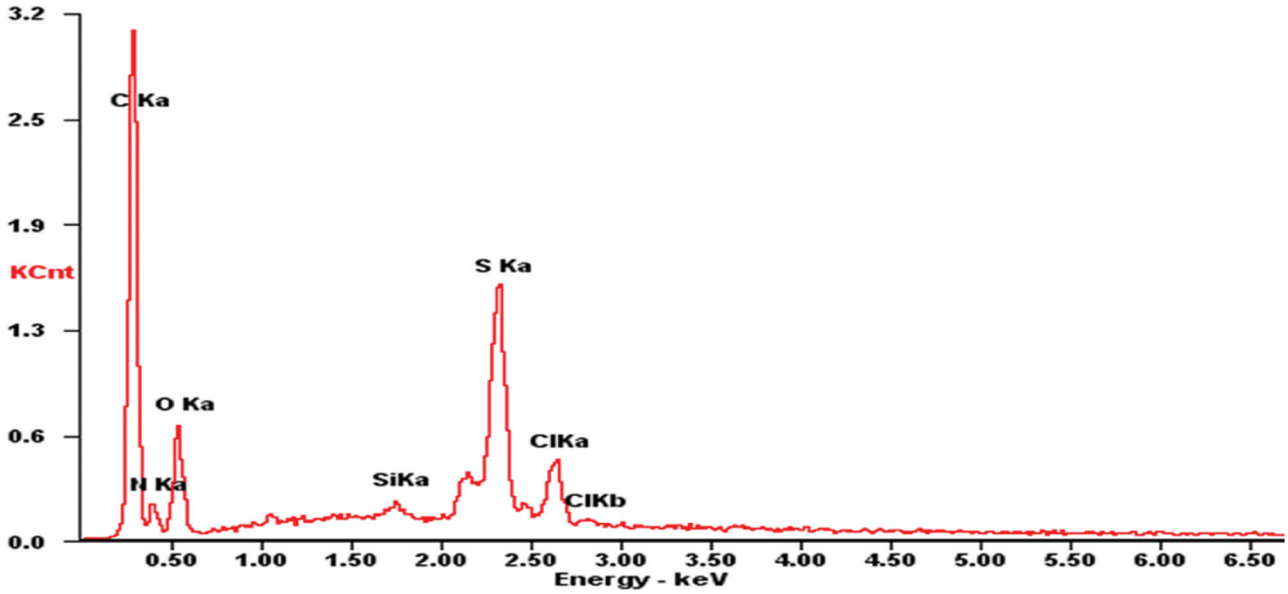

Figure 3. *EDS spectra of PLA-21.*

Table 10. Relative Element Contents of PLA-21.

Element	Wt%	At%
CK	64.02	72.47
NK	11.25	10.92
OK	14.58	12.39
SiK	00.41	00.20
SK	07.30	03.09
ClK	02.44	00.94
Matrix	Correction	ZAF

them were soaked in water and kerosene separately for 24 h. The last one was soaked in water for 24 h and then soaked in kerosene for more 24 h. The four pieces of PLA-21 were observed with SEM under environmental scanning mode. The pictures are shown as follows.

It is show in Figure 5, PLA-21 has good expansibility in water and it present regular space truss structures. It is because PLA-21 has solvation effect when it was put into water, which causes the ionic concentration inside and outside PLA-21 different, further producing osmotic pressure. PLA-21 inflated due to the osmotic pressure. Meanwhile, water can be absorbed by charged groups and hydrogen bond. So, water in the reservoir was locked effective by its sealing property and high affinity for water.

Normally, the PLA-21 will be dissolved in water and pump in to the reservoir. So, it is necessary to survey the change of the dissolved PLA-21 in oil layer. Figure 6 shows the picture of PLA-21 soaked in kerosene for 24h. It obviously show that the PLA-21 soaked in kerosene for 24h nearly have no difference with PLA-21 without any treatment (Figure 4), which indicates that the oil nearly had no effect on PLA-21. When swelling PLA-21 was surrounded with oil, the swelling equilibrium was destroyed. The swelling PLA-21 was dehydrated and shrink duo to the reverse osmosis. Figure 7 shows that the spatial structure of swelling PLA-21 is destroyed and it almost shirks to its original shape. On one hand, the PLA-21 in oil layer shrinks into small size and can be reverse discharged easily. On the other hand, there are hardly any functional groups that can absorb the oil. So, PLA-21 had just little plugging rate of oil.

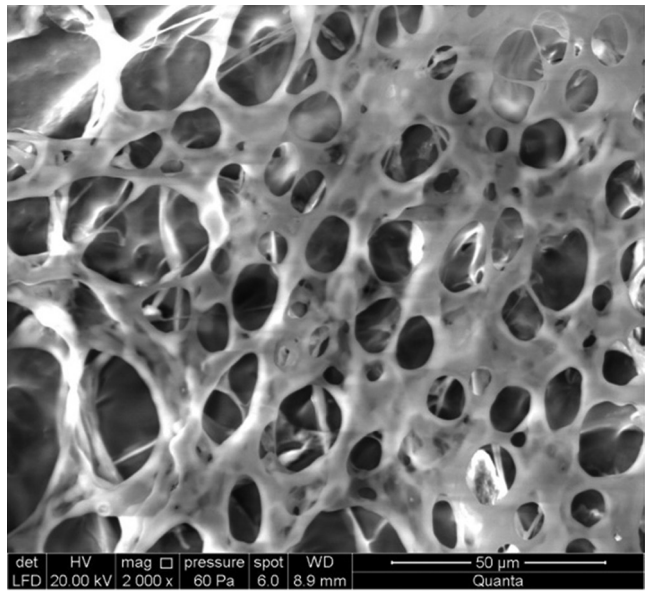

Figure 5. *Soaked in water (× 2000).*

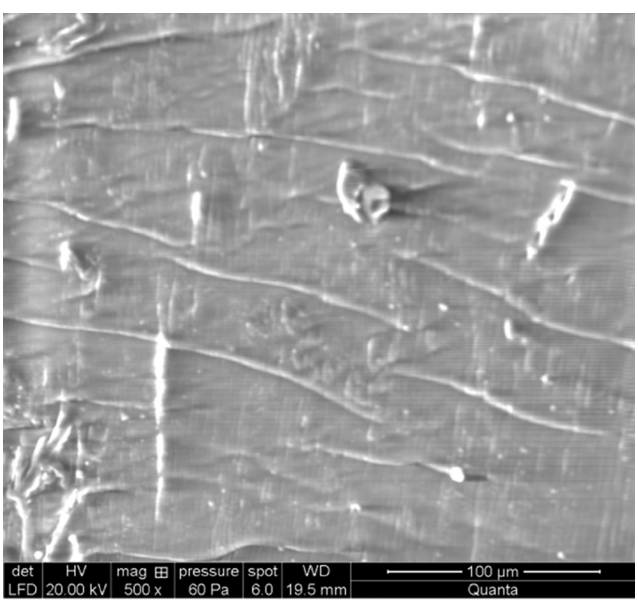

Figure 4. *PLA-21 (× 500).*

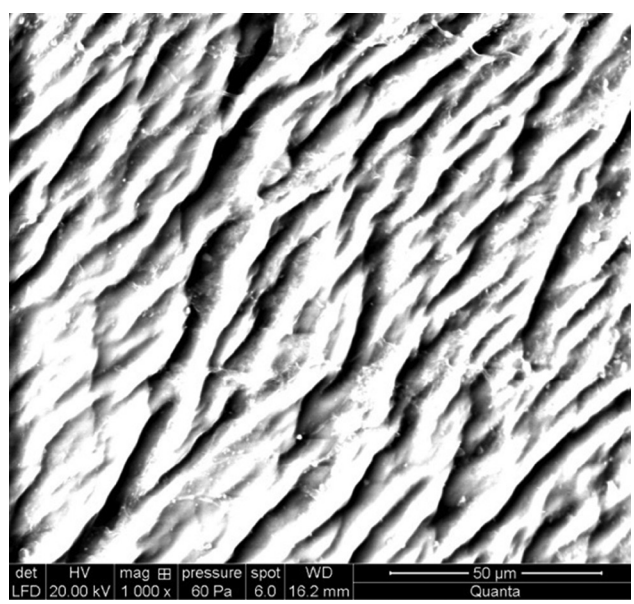

Figure 6. *Soaked in kerosene (× 1000).*

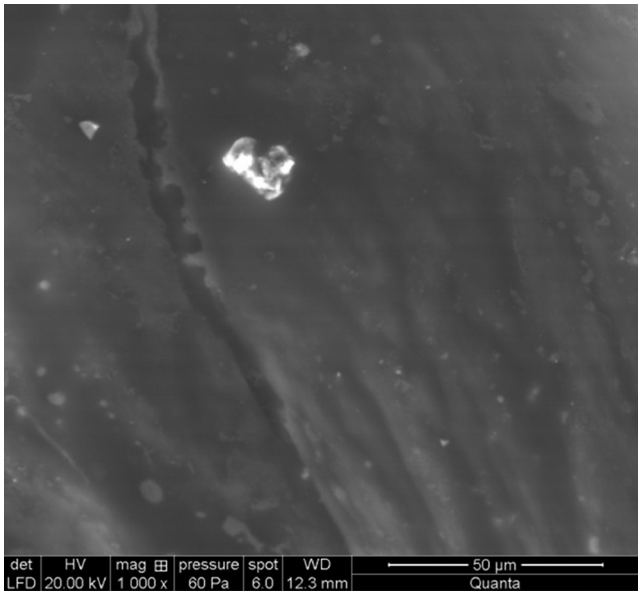

Figure 7. *Soaked in kerosene after soaked in water (× 1000).*

CONCLUSIONS

1. The technology of synthesis PLA-21 is very simple, the raw materials are available and cheap, and the reaction condition is mild. Also, the in site construction technology is easily operable.
2. PLA-21 shows good plugging ability for water and the plugging rate is always higher than 95%. Meanwhile, it just brings little damage to oil layer, which is always lower than 10%.
3. Its good selective plugging ability depends on that it expend severely in water and shirk in oil. So, PLA-21 is an efficient, accessible, affordable plugging agent for oilfield application.

NOMENCLATURE

K_{W_1} = water permeability before plugging
K_{W_2} = water permeability after plugging
η_W = water plugging rate
K_{O_1} = oil permeability before plugging
K_{O_2} = oil permeability after plugging
η_O = oil plugging rate
K_g = air permeability of core
Φ = particle size of selective plugging agent
V = squeezing volume of plugging agent
P_1 = squeezing pressure
K_1 = water phase permeability before plugging
P_2 = flowback pressure
K_2 = water phase permeability after plugging
η = water plugging rate

ACKNOWLEDEMENTS

The Authors are grateful for the Projects Support by NSFC (No.51204195, No.51490650 and No.51234006), Beijing Youth Elite Project (No. YETP0672).

REFERENCES

1. G. A. Al-Muntasheri, I. A. Hussein, and E. D. Nasr. *J. Pet. Sci. Eng 55*, 56 (2007). http://dx.doi.org/10.1016/j.petrol.2006.04.004
2. A. Kishita, S. Takahashi, H. Kamimura, *et al.*, *J. Jpn. Petrol. Inst 46*(5), 215 (2003). http://dx.doi.org/10.1627/jpi.46.215
3. C. A. Grattoni, H. H. Al-Sharji, and C. Yang. *J Colloid Interf Sci., 240*, 601(2001). http://dx.doi.org/10.1006/jcis.2001.7633
4. G. L. Lei, L.L. Li, and H.A. Nasr-EI-Din. *SPE Reserv Eval Eng 14*(1), 120(2011).
5. E.D. Nasr, and K.C.Taylor. *J. Pet. Sci. Eng. 48*, 141(2005). http://dx.doi.org/10.1016/j.petrol.2005.06.010
6. F. R. Wassmuth, K. Green, and I. Hodgins. *SPE 89403* (2004).
7. S. Durmaz, and O. Okay. *Polymer. 41*(36), 3693 (2000). http://dx.doi.org/10.1016/S0032-3861(99)00558-3
8. B. Hou, S. X. Xie, M. Chen, *et al. J. Residuals Sci.&Tech 9*, 95 (2012).
9. J.W. Yan, J.G. Li, and H.W. Liu. Oil Drilling & Production Technology 3, 50(2006).
10. Q. Yan, Y.F. Wang, W. Zhen, *et al. J. Can. Pet. Tec 48*, 51(2009).
11. S. Kokubo, K. Nishida, A. Hayashi, *et al. J. Jpn. Petrol. Inst 51*(5), 309 (2008). http://dx.doi.org/10.1627/jpi.51.309
12. S. Yasusato, O. Takahisa. *J Appl Polym Sci 82*, 1437(2001). http://dx.doi.org/10.1002/app.1981
13. L.J. Fetters, D.J. Lohse, D. Richter, *et al. Macromolecules 27*, 4639(1994). http://dx.doi.org/10.1021/ma00095a001
14. A. Gloria, F. Causa, T. Russo, *et al. Biomacromolecules 13*, 3510(2012). http://dx.doi.org/10.1021/bm300818y
15. M. Nichifor, M.C. Stanciu, B.C. Simionescu. *Polym 82*, 965(2010)
16. G.H. Sayeda, F.M. Ghuibab, M.I. Abdoub, *et al. Colloids Surf. A: Physicochem. Eng. Aspects 393*. 96 (2012). http://dx.doi.org/10.1016/j.colsurfa.2011.11.006

Recovery of Aluminum Residue from Incineration of Cans in Municipal Solid Waste

YANJUN HU[1,*] and M.C.M. BAKKER[2]

[1]*Zhejiang University of Technology, Institute of Energy and Power Engineering, Chaowang Road 18#, 310014, Hangzhou, China*

[2]*Delft University of Technology, Resources and Recycling group , P.O. Box 5048, 2628 CN, Delft, The Netherlands*

ABSTRACT: The interest to investigate to which degree aluminum residue from cans may be recovered from MSWI bottom ash. To this end an assessment was made of the cans residue size distribution in bottom ash and its potential for recovery. This study indicates that nonferrous concentrates from Amsterdam bottom ash contain interesting amounts of aluminum cans residue (0.055% of the ash). About 61.7% of the input of aluminum cans are ended after combustion in the 6–20 mm ash fraction. Also it is shown that a combination of dry and wet separation can improve aluminum residue recovery with respect to the single dry process.

INTRODUCTION

WITH the increasing growth of incineration of household waste, more and more aluminum residue ends up in MSWI bottom ash. The aluminum alloys that are presently lost in bottom ash treatment plants may form the largest single loss in the whole aluminum cycle [1–3]. According to some estimates, approximately 1.52 million tons of aluminum alloy with a high pure aluminum content is used annually for packaging cans in Europe [4]. However, on average only 43% of all cans consumed in Europe is recycled and the rest is ended up in different waste streams. The present increase in recycled aluminum is a positive trend, as secondary aluminum requires only 2.8 kWh/kg of the metal produced whereas primary aluminum production takes 45 kWh/kg [5]. It is therefore of advantage to industry to maximize the amount of recycled metal, both to achieve energy-saving and to reduce the EU dependence on primary resources. Increasing the use of recycled aluminum is also quite important from an ecological standpoint since producing aluminum by recycling creates only about 4% of the CO_2 emissions in comparison with primary production [5]. In addition, the recovery of aluminum from bottom ash reduces the problems of swelling and expansion that aluminum particles cause when bottom ash is reused in concrete production [6–7]. It is noted that some 75% of the bottom ash consists of minerals for which concrete may form a high-end outlet.

In recent years the recovery of aluminum from MSWI bottom ash is common practice in several European countries [8–10]. For instance, France, Netherlands and Italy are the experienced practitioners in separating non-ferrous metal scraps from waste incineration ashes. Though aluminum cans may also be oxidized to add to energy production during incineration, it proves much better to recover them from the bottom ash for recycling purposes. Characterization of treated bottom ashes and the recovered aluminium scraps from a Dutch MSW incinerator showed the bottom ash contained approximately 1.5% of aluminium [9]. XRF analyses of the aluminium particles from different size fractions of bottom ash showed that smaller particles generally have a different alloy composition than larger particles, and therefore must originate from different aluminium products. In particular, the more strongly alloyed aluminium of cans is suspected to report to the coarser aluminium particles fraction in the bottom ashes [11–12]. An innovative investigation into the behavior of different types of aluminum packaging materials in a full-scale waste to energy plant during standard operation reported that about 80% of cans could be recovered through an advanced treatment of the bottom ash [8]. The main issues in the valorization of the aluminum residues are the concentration, the mass distribution over the particle size ranges, and the effectiveness of available sorting technologies.

For aluminum recovery there are two distinct

*Author to whom correspondence should be addressed.
Tel. +86 +571 88320492, Email address: huyanjun@zjut.edu.cn

1544-8053/15/03 157-07
© 2015 DEStech Publications, Inc.
doi:10.12783/issn.1544-8053/12/3/6

types of bottom ash treatment method in the Amsterdam MSW incineration plant AEB in the Netherlands [13–14]. One is an operational system of dry physical separation for particles below 40 mm. The other is a combined system of dry and wet physical separation processes. The dry separation process is designed to recover the coarse aluminum and other nonferrous metal scraps larger than 6 mm. The drawback is that only a small part of metals in the ash can be recovered while the fine fraction is not treated at all. Some separation facilities also process the fine fraction using eddy current or density separation, but due to the high moisture content of the fine ash fraction the separation performance is relatively poor combination of dry and wet separation has been used in recent years to recover non-ferrous concentrates. It successfully improved the recovery rate of fine aluminum particles, i.e. below 6 mm. However, few investigations focused on the assessment regarding cans residue distribution in different size fractions of bottom ash and its potential for recovery.

The current work investigates the particle size ranges of aluminum cans residue and the concentration and distribution in Amsterdam MSWI bottom ash. A comparison is made between the recovery efficiencies of the cans residues using both an existing dry physical separation process and a combined dry and wet separation process. In addition, co-combustion tests of complete beer cans and synthetic household waste in a lab-scale stoker furnace were conducted to assess the aluminum residue partitioning and its recyclable contents from the bottom ash.

EXPERIMENTAL

Al Scraps in AEB Bottom Ash

A large amount of raw bottom ash with less than 10% moisture content was collected in the Amsterdam AEB MSW incineration plant. To assure the sample would be representative, 25 sub-samples were taken from different points and from different depths in the bottom ash heap to a total of 200 kg. The raw bottom ash samples were separated into different size fractions, where the procedure is shown in Figure 1(a) and (b). The resulting fractions were classified into four groups of products: > 40 mm (Product A) and 0–40 mm non-ferrous (NF) metals (Product B) from the dry process, non-ferrous metals (Product C) and treated bottom ash (Product D) from the wet process. Products A, B, C, and D were further treated to identify the aluminum scraps, as shown in Figure 1(c). Non-ferrous metal products were recovered from different bottom ash sub-samples, mainly by using dry and wet eddy current separation (ECS) systems. The operating principle of standard ECS is based on eddy currents which induce a secondary magnetic field around the non-ferrous metal scraps and generate a combined driving and repelling force which ejects the non-ferrous metal items from the bottom ash fractions. The high frequency ECS and wet backward ECS were employed to separate NF from dry bottom ash and wet bottom ash (the moisture content was preferably 10–15%), respectively [10–11]. Unlike a standard ECS, the rotor of a wet ECS rotates against the direction of the conveyor belt [11]. The NF particles are disengaged from the belt of a wet ECS and collected in front of the separator, while the non-metal and ferrous particles remain on the belt and are released below the separator.

Identification of Aluminum Cans and Metallic Aluminum

Identification of aluminum cans was carried out on the recovered aluminum scraps by means of chemical methods, XRF, and electron microprobe analysis. For the chemical tests three kinds of chemical liquid were used to determine the main alloying composition of each cans scrap with. They contained respectively 65% nitric acid, 30% sodium hydroxide solution, and 25% ammonia. A part of the aluminum scrap surface was polished and cleaned to remove corrosion, after which a few droplets of the chemical could be applied. The presence of the targeted alloying metal was detected visually from a change in color. For each alloying metal a different chemical liquid was used. XRF analysis was used to confirm and the chemical detection test and specify the alloy. The details of this procedure are described in an earlier publication [9]. Aluminum cans composition differs in some distinct ways from other Al alloys. They have a high Mn, Fe and Cu contents compared to casting alloys and wrought alloys, as presented in Table 1. The composition of the aluminum cans scraps recovered from MSWI bottom ash proved not identical with that of the input Al cans alloys. Therefore a global criterion for identifying Al cans was constructed as presented in Table 1.

Metal loss is a crucial factor in the recycling of incinerated Al cans scrap, and is a function of many parameters, such as the type of alloy and combustion conditions. The oxidation degree of Al may result in a major loss of metallic Al, which is why the measure-

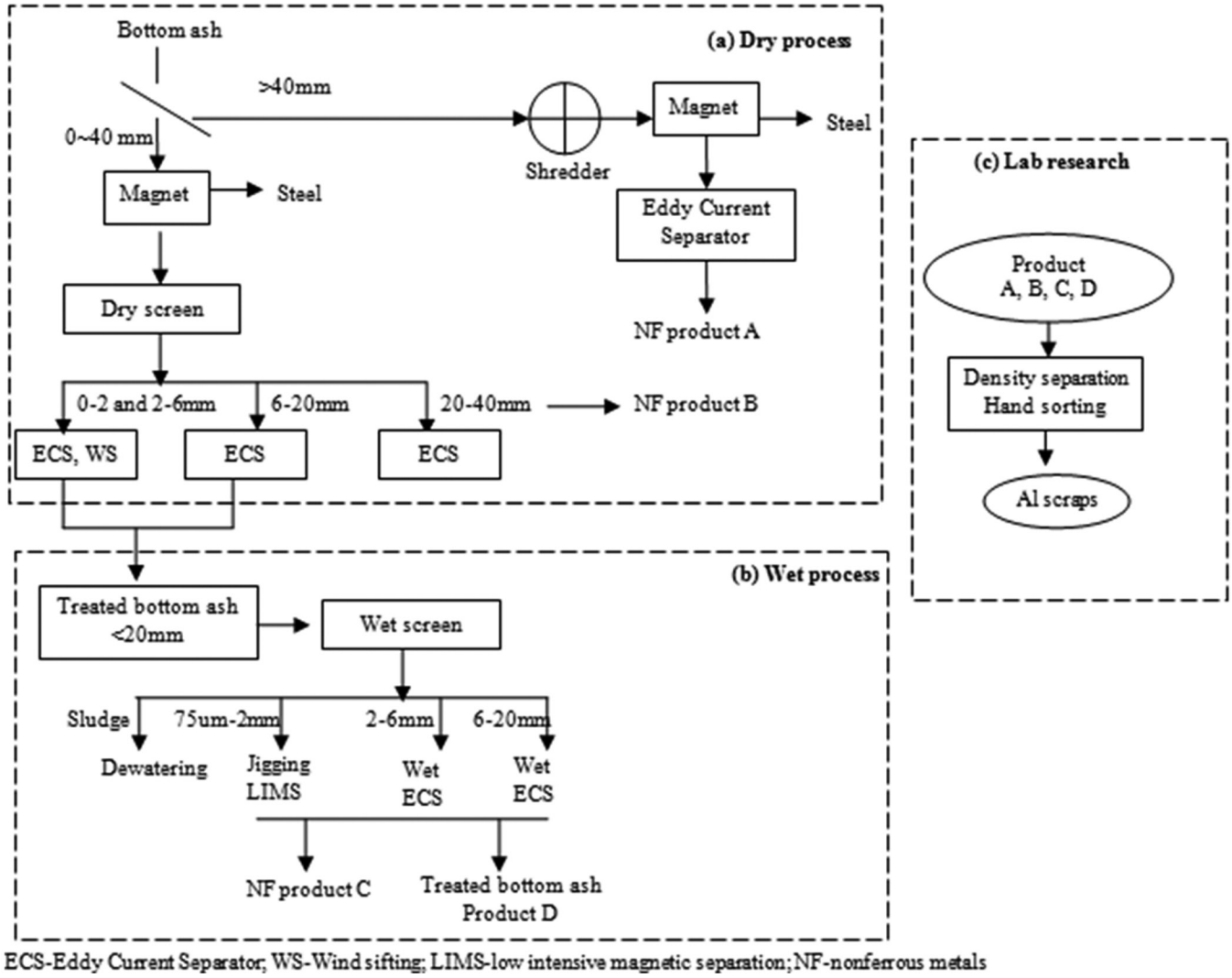

Figure 1. *Procedures for bottom ash treatment by combined dry and wet separation.*

ment of metallic Al content was carried out using a hydrogen generation test with sodium hydroxide solutions.

Laboratory Stoker Furnace Tests

Identification and study of the recovery rates of combusted cans required another research approach for which a laboratory scale stoker furnace was used. Co-combustion tests were conducted with base household waste and known amounts of aluminum cans as the only source of metallic aluminum input waste. The mass of the cans was accounted for 0.5% of the total input base waste. The aluminum can in these tests had a volume of 330 ml. First the bottle cap was removed and only the cans body was crumbled for combustion. The synthetic samples of base household waste were made using a mixture of representative household waste materials, such as organics, paper, sand, textile, ceramics, glass, wood, leather, ferrous, plastics and building material. These components were assembled from typical household waste sources in Western Europe [15]. More details of the combustion apparatus and the input base waste samples may be found in the literature [16]. The operational parameters of the incineration tests are shown in Table 2. Each test was duplicated once in view of operational errors and material variations between samples.

Table 1. Criterion for Identifying Al Cans.

	Al (%)	Cu (%)	Fe (%)	Mn (%)
Built Criterion	90–98	0.05–0.50	Max 1	0.6–1.6
Aluminum Can Standard	95–98	0.05–0.25	Max 0.8	0.8–1.4

The bottom ash from the stoker furnace was quenched and a magnetic separation was carried out

Table 2. Operational Parameters of Combustion Tests.

Test Series	Average	S-dev
Bed Temperature, °C (at the bottom)	850	10
Bed Temperature, °C (at the top)	800	15
Air flow (m^3/h)	10/12	0
Air ratio excess	1.2	0.01
Combustion time (minutes)	55	5
Flue gas, °C	620	25

to remove the ferrous metals. The ash samples were dried to bring the moisture level below 5%, after which they were sieved into four size fractions: 2 mm, 2–6 mm, 6–20 mm, and +20 mm. The experimental procedure for analyzing and recovering the cans residues is shown in Figure 1. ECS separation and hand sorting was employed to recover the aluminum scraps from the larger fraction above 2 mm. These scraps were evaluated for weight, size distribution, and recovery rate. The metallic aluminum contents in each size fraction were derived from the hydrogen generated in a sodium hydroxide solution (the so-called lime test). The chemical reaction that controls the hydrogen production is given in Equation (1) [17].

$$2Al + 2OH^- + 2H_2O \rightarrow 2AlO_2^- + 3H_2 \qquad (1)$$

RESULTS AND DISCUSSIONS

Cans Residue Concentrations

Figures 3, 4 and 5 present the aluminum cans residues concentrations over the different size fractions of products A and B from the dry process and Products C and D from the wet process. It proved that the recovered nonferrous concentrates from Amsterdam bottom ash contain an economically interesting amount of aluminum can residues. Based on the metallic aluminum content, 95% of the recovered residues could be recycled.

By extrapolating the concentration of aluminum from the incinerated cans to the different size fractions of the bottom ash we obtain Figure 6. The total content of metallic aluminum from cans is 0.055% of the raw bottom ash. About 65.3% of the recovered cans residues ended up in the 6–20 mm bottom ash fraction for which efficient recovery technologies are available. On the other hand, less than 5% ended up in the fine –2 mm fraction for which the conventional recovery technologies are far less effective. Nevertheless, promising advancements are made recently which can to improve the recovery of fine metals from bottom ash by means of sensor-supported eddy current separation [18]. Referring to the current separation process

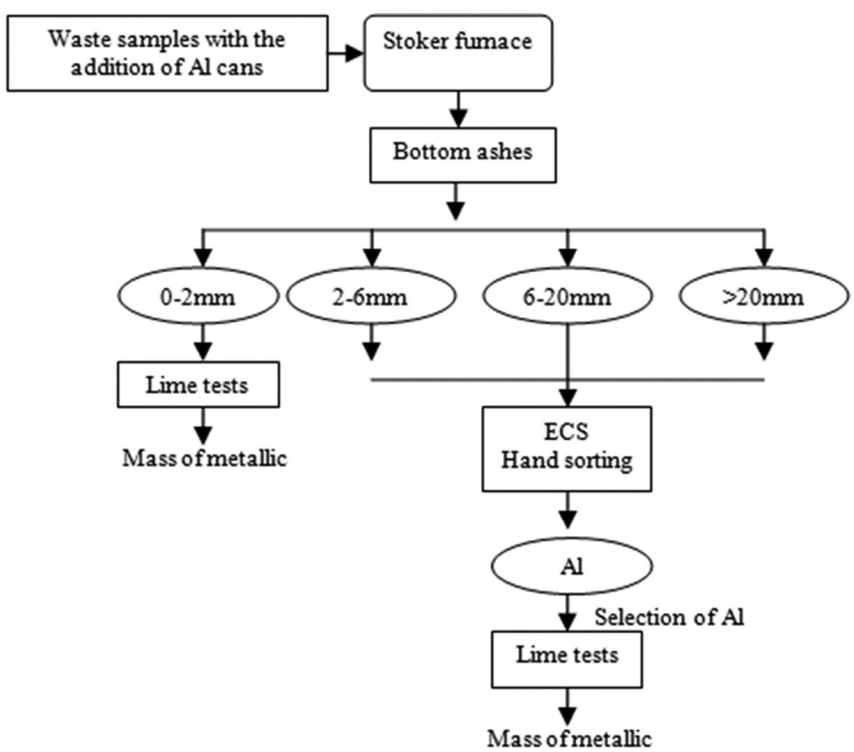

Figure 2. Procedure for recovering combusted aluminum can scraps.

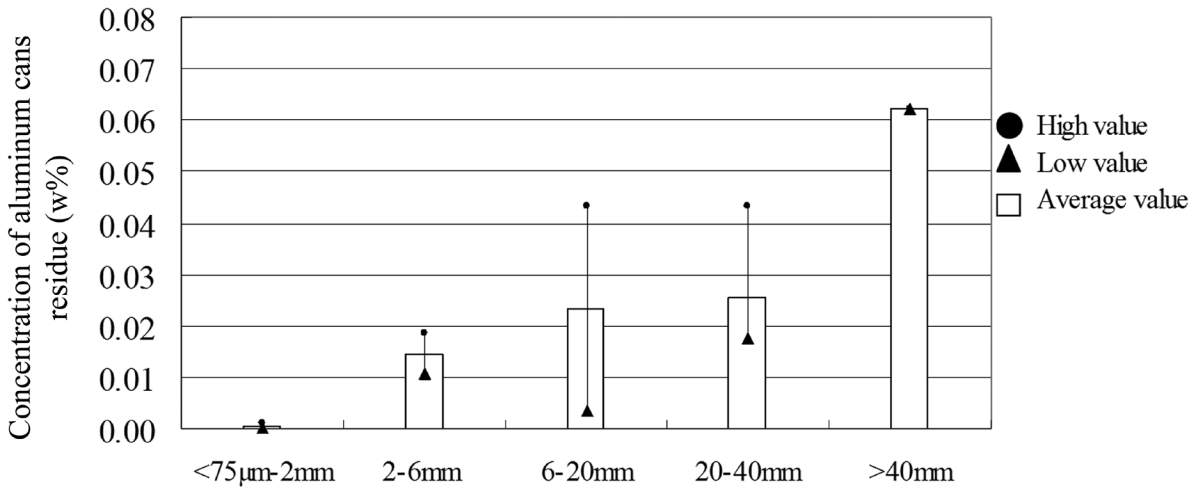

Figure 3. *Concentrations of Al cans residue in product A and B.*

of nonferrous metals in the Netherlands, the recovered aluminum can residues could well contribute to the general high recyclability of aluminum from bottom ash.

Recovery Efficiency of Al Cans Residues

The average recovery efficiency of aluminum cans residues using the single dry process or the combined process of dry and wet are compared in Figure 7. The recovery efficiency per fraction and product, which are averaged in Figure 7, was calculated as the ratio of the mass of the recovered aluminum cans from a fraction and the total mass of aluminum cans residues in the product (A-D). The dry process shows a lower recovery in the < 20 mm fractions than the combined process. The combined process can recover more metals, improving the recovery from 7.8% to 75.5% in the 2–6 mm fraction, and from 32.6% to 90.8% in the 6–20 mm fraction. In conclusion, the combined process dry and wet shows a promising improvement in aluminum recovery for the < 20 mm bottom ash fractions.

Partitioning of Incinerated Aluminum Cans

The particle size distribution of aluminum cans is a crucial parameter in the recovery process. Figure 8 presents the average partitioning of the incinerated aluminum cans in four size ranges. It proved that about 95% of the input cans is recyclable from the bottom ash and 61.7% of them concentrates in the 6–20 mm fraction. This result also confirms earlier research in that the more strongly alloyed aluminium of cans reports to the coarser aluminium fractions in the bottom ashes [12]. It is also consistent with the results obtained from the measurement of cans residues in the Amsterdam bottom ash in this study.

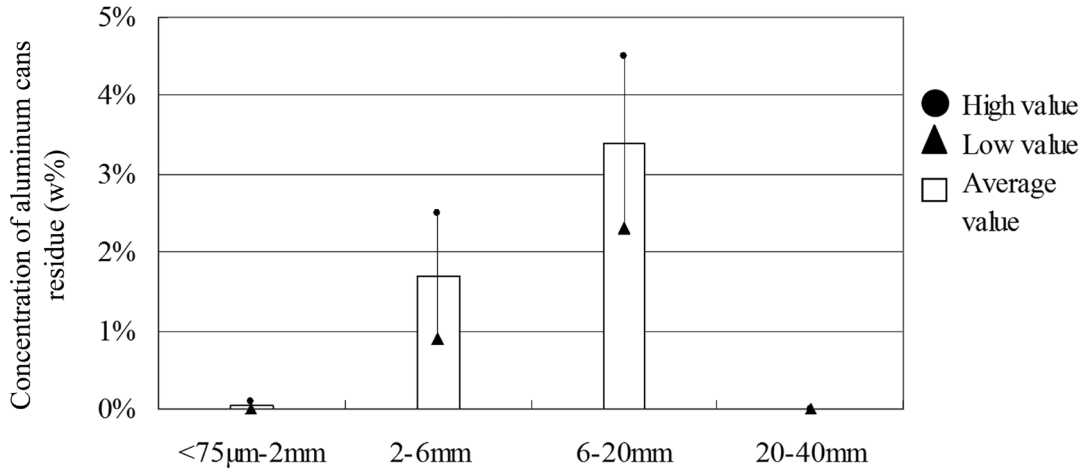

Figure 4. *Concentrations of Al cans residue in product C.*

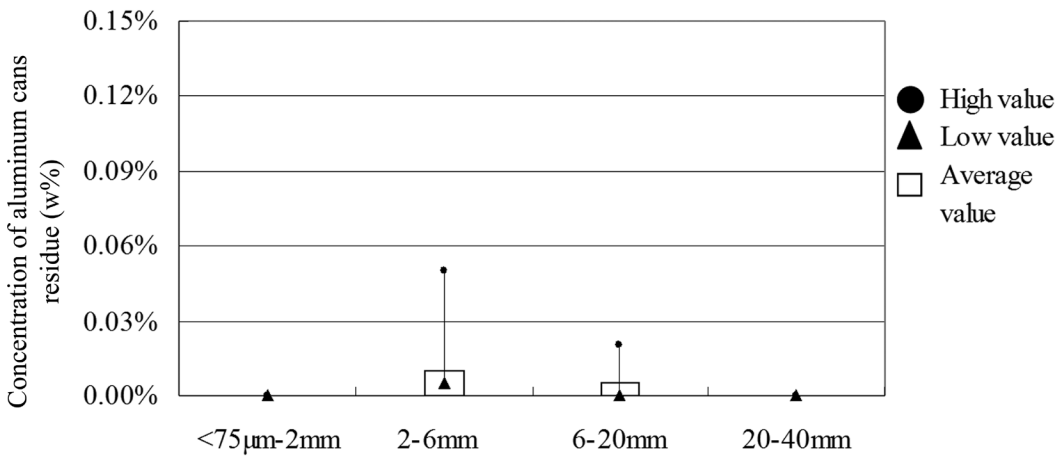

Figure 5. *Concentrations of Al cans residue in product D.*

Aluminum Can Residue Production

Based on the results in this work, the maximum content of aluminum cans in the different size fractions of MSWI bottom ash may be computed as follows:

$$C_{SF} = M_{INP} \times P_{AC} \times M_{CR} \times M_{SF} \times M_{IO} \qquad (2)$$

Here, C_{SF} is the content of the aluminum residues in the different size fractions where the subscript 'SF' denotes size fraction < 2 mm. 2–6 mm, or > 6 mm M_{INP} is the concentration of end of life aluminum cans in the input household waste, and P_{AC} = 0.95 is the concentration of metallic aluminum in a can. The maximum content is related to the latter concentration as:

$$\begin{aligned} C_{<2\,\mathrm{mm}} &= (0.2-0.7)\cdot P_{AC} \\ C_{2-6\,\mathrm{mm}} &= (4.1-6.1)\cdot P_{AC} \\ C_{>6\,\mathrm{mm}} &= (7.1-9.3)\cdot P_{AC} \end{aligned} \qquad (3)$$

Further in Equation (2) M_{CR} is the mass percentage of can residues after incineration, hereby referring to the data presented in Figure 8, M_{SF} is the total bottom ash mass divided by the ash mass per size fraction, (M_{SF} = 2.8–3.3 for < 2 mm 5–6.7 for 2–6 mm and 2.8–3.3 for > 6 mm), and M_{IO} is the total mass of the input household waste divided by total mass of the dry bottom ash (M_{IO} = 3.8–4.3).

CONCLUSIONS

It proves there are strong economic and environmental driving forces for strongly reducing the loss of aluminum such as those from cans in treated MSWI bottom ash. Based on the laboratory analyses, bottom ash generated from the Amsterdam MSWI plant contains about 0.055% of aluminum cans residue. This residue is mainly concentrated in the coarse bottom ash of which 65.3% in the 6–20 mm fraction is e amenable for efficient recycling. The combined dry and

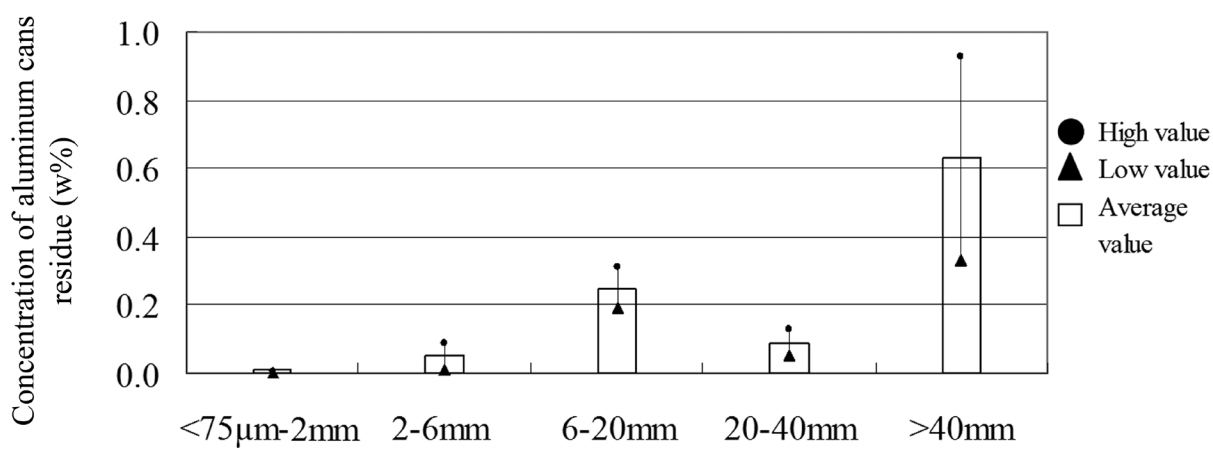

Figure 6. *Extrapolated concentrations of aluminum cans residue in size fractions of the bottom ash.*

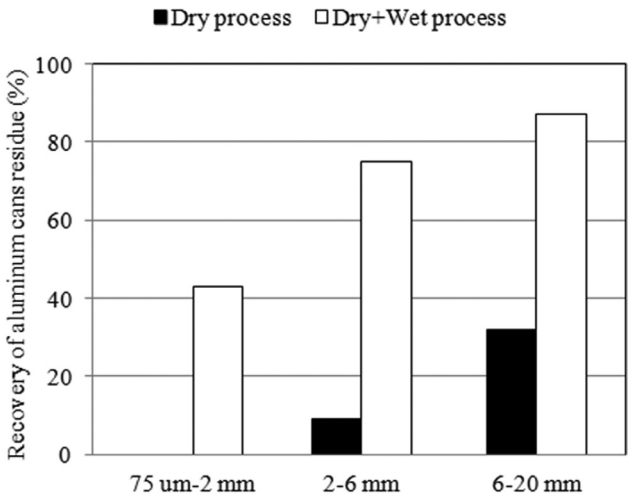

Figure 7. *Comparison of recovery efficiencies of aluminum residues in the dry and combined process.*

wet separation process displayed higher recovery efficiency for aluminum residues in the –20 mm fractions in comparison with the single dry process. In fact, the recovery efficiency of aluminum improved from 7.8% to 75.5%, in the 2–6 mm fraction, and from 32.6% to 90.8% in the 6–20 mm fraction. Controlled laboratory furnace tests using base synthetic household waste with cans as the only source of aluminum produced metallic aluminum recovery rates of 95% while 61.7% of the input aluminum ended up in the 6–20 mm bottom ash fraction. Based on the total of obtained data regarding concentration distributions of aluminum cans residues in bottom ashes from the Amsterdam plant and the lab-scale furnace, a formula is proposed that extrapolates the aluminum can residue concentration to the different size fractions of the bottom ash. This allows one to predict the amount of recyclable cans aluminum in the bottom ash of a real-scale incinerator.

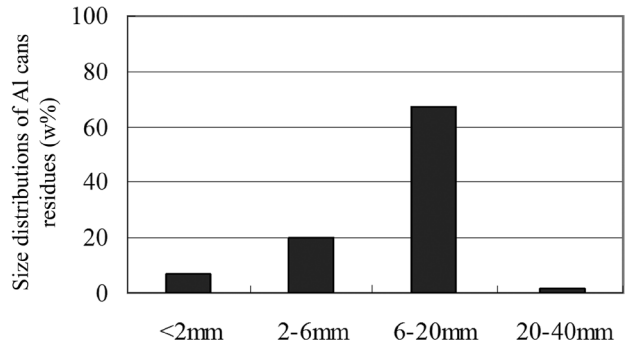

Figure 8. *Partitioning of the incinerated Al cans.*

REFERENCES

1. RIVM (Dutch National Institute for Public Health and the Environment), 2006. www.rivm.nl, sheet C14.6.
2. Grosso, M., Biganzoli, L., Rigamonti, L., A quantitative estimate of potential recovery from incineration bottom ashes. *Res. Conservat. Recycl., 55*, 2011, pp. 1178–1184. http://dx.doi.org/10.1016/j.resconrec.2011.08.001
3. Soler, L., Macansas, M., Casado, J., Aluminum and aluminum alloys as source of hydrogen for fuel cell applications. *J. Power Sources, 169*, 2007, pp. 144–149. http://dx.doi.org/10.1016/j.jpowsour.2007.01.080
4. International Aluminum Institute, 2011. http://www.world. aluminum.org [accessed on April, 2011].
5. Das, S.K., *Designing aluminum alloys for a recycle-friendly World. Material Science Forum*, Trans Tech Publications, Switzerland, 519-521, 2006, pp. 1239–1244.
6. Vegas, I., Ibanez, J. A., San Jose, J. T., Construction demolition wastes, Waelz slag and MSWI bottom ash: A comparative technical analysis as material for road construction [J]. *Waste Manage. Res., 28*(3), 2008, pp. 565–574. http://dx.doi.org/10.1016/j.wasman.2007.01.016
7. Muller, U., Rubner, K., The microstructure of concrete made with municipal waste incinerator bottom ash as an aggregate component. *Cem. Concr. Res. 36*, 2006, pp. 1434–1443. http://dx.doi.org/10.1016/j.cemconres.2006.03.023
8. Biganzoli, L., Gorla, L., Nessi, S., Grosso, M., Volatilisation and oxidation of aluminium scraps fed into incineration furnaces, *Waste Manage. Res., 32*, 2012, pp. 2266–2272. http://dx.doi.org/10.1016/j.wasman.2012.06.003
9. Hu, Y., Rem, P., Aluminum alloys in municipal solid waste incineration bottom ash. *Waste Manage. Res., 27*(3), 2009, pp. 251–257. http://dx.doi.org/10.1177/0734242X08095564
10. Settimo, F., Bevilacqua, P., Rem, P., Eddy current separation of fine non-ferrous particles from bulk streams. *Phys. Sep. Sci. Eng. 13*, 2004, pp. 15–23. http://dx.doi.org/10.1080/00207390410001710726
11. Rem, P.C., Zhang, S., Forssberg, E., de Jong, T.P.R., The investigation of separability of particles smaller than 5 mm by eddy-current separation technology—Part II: Novel design concepts. *Mag. Electr. Sep. 10*, 1999, pp. 85–105.
12. Rem, P. C., van Houwelingen, J., Future Aluminum Packaging Recycling Percentage. Delft report: TAGK01.01, 2001.
13. Muchova, L., Rem, P., Pilot plant for wet physical separation of MSWI bottom ash. *Conference proceeding MMME, 2006*, pp. 12.
14. Muchova, L., Rem, P., 2007. Wet or dry separation. Waste Management World,
15. Eurostat, Waste generated and treated in Europe, 2003,
16. Hu, Y., Bakker, M.C.M., de Heij, P.G., Recovery and distribution of incinerated aluminium packaging waste, *Waste Manage. 31*, 2011, pp. 2422–2430. http://dx.doi.org/10.1016/j.wasman.2011.07.021
17. Aubert, J., Husson, B., Vaquier, A., Metallic aluminum in MSWI fly ash: quantification and influence on the properties of cement-based products. *Waste Manage. 24*(6), 2004, pp. 589–596. http://dx.doi.org/10.1016/j.wasman.2004.01.005
18. A. Rahman, M.C.M. Bakker, Sensor-based control in eddy current separation of incinerator bottom ash, *Waste Manage. 33*, 2013, pp. 1418–1424. http://dx.doi.org/10.1016/j.wasman.2013.02.013

Evaluation of Physico-Chemical Pretreatment Methods for Landfill Leachate Prior to Sewer Discharge

M. POVEDA[1,*], Q. YUAN[1], S. LOZECZNIK[2] and J. OLESZKIEWICZ[1]
[1]*University of Manitoba, Department of Civil Engineering, Winnipeg, Canada MB R3T 5V6*
[2]*KGS Group, Environmental Engineering, Winnipeg, Canada MB R3T 5P4*

ABSTRACT: Leachate from Brady Road Resources Management Facility (Manitoba, Canada) was evaluated to determine the most effective pre-treatment method to reduce the high concentrations of COD (1900 mg/L) and ammonia (640 mg/L) present. Four pre-treatment options were studied: (a) air stripping (b) chemical coagulation (c) electro-coagulation and (d) advanced oxidation with sodium ferrate. Each one of the procedures was evaluated under different conditions (pH, dose, contact time, etc.) to determine the operating conditions that best reduce the effluent COD and ammonia concentrations. Chemical coagulation exhibited the highest COD removal at 43% while in terms of ammonia removal, air stripping with 86% removal rate, was far superior to the other treatments. Electro-coagulation and advanced oxidation with sodium ferrate were found not suitable as pre-treatment options for this particular leachate, while combining air stripping and chemical coagulation removed approximately 50% COD and 85% ammonia, providing the highest removal percentages. Batch nitrification kinetics tests were used to assess the impact on nitrification performance of blending untreated and pre-treated leachate with municipal wastewater at varying percentages: 0.5%, 1%, 5% and 10% by volume. Pre-treatment was successful in allowing unhindered nitrification in the activated sludge bioreactor.

INTRODUCTION

BRADY Road Resource Management Facility (BRRMF) opened in 1973 and is Winnipeg's only active landfill. Leachate collected at the BRRMF is hauled daily by trucks across the city for treatment at the city's North End Water Pollution Control Center (NEWPCC) located 35 km away on the other side of the city. Following current city regulations, the leachate cannot be discharged in the sewer system due to possible negative effects on the sewer system and to the treatment plant of the area, South End Water Pollution Control Center (SEWPCC). However, hauling the leachate by trucks is potentially dangerous in case of a traffic accident and a spill. The city's SEWPCC, which handles a smaller flow and is converting to biological nutrient removal, seems like a good option for treating the leachate provided that this is first pre-treated to decrease COD and ammonia levels. It was suggested that pre-treating leachate onsite of the BRRMF would allow for direct discharge to the sewer connected to SEWPCC, thus avoiding problems of truck transport to the NEWPCC.

Landfill leachate is produced by the seeping of liquids through landfilled Municipal Solid Waste (MSW). Rain water or melted snow percolating into the waste, as well as the original water content or humidity of the waste itself and the degradation and compaction of the organic fraction, all contribute to the generation of leachate [1,2].

The quantity and the characteristics of leachate produced are site specific and closely related to the age of the disposal cell. Different stabilization stages have been determined to be predominant after the waste is disposed and covered, starting with an aerobic acidic phase. During the initial days, the oxygen trapped in the waste is consumed and CO_2 is produced as the main by-product. Leachate produced during this stage is mostly due to the compaction process releasing moisture in the waste.

Then a prolonged anaerobic phase begins where acidogenic and methanogenic decomposition takes place [2]. The biodegradable fraction of the waste is hydrolyzed by fermentative bacteria that produce extracellular enzymes to help break down and solubilize large

*Author to whom correspondence should be addressed. Tel.: (204) 232-6821; Fax: (204) 474 7513; Email address: povedaqm@myumanitoba.ca

1544-8053/15/03 165-11
© 2015 DEStech Publications, Inc.
doi:10.12783/issn.1544-8053/12/3/7

compounds. In the last phase, methane producing microorganisms, utilize the available substrate and convert it into the gaseous compounds, from fully reduced methane to fully oxidized carbon dioxide. At the beginning of this methanogenic phase the highest concentrations of 5 days Biochemical Oxygen Demand (BOD_5) and Chemical Oxygen Demand (COD) are usually found in the produced leachate. As the simpler organic compounds are degraded, BOD concentration would decrease and COD would represent the most refractory compounds that are left behind.

The relationship of BOD to COD can be used to estimate the biodegradable fraction or biodegradability of a specific sample. A ration greater or equal to 0.5 is considered to be easily treated by biological means, while a ratio of 0.3 or lower is considered not biodegradable and/or to possess toxic components, and a period of acclimation may be required for biodegradability [3].

The values presented in Table 1 are based on summary tables reported by [4] and [1]. The mentioned tables were based on over 40 investigations related to the characterization and treatment of leachate, covering research from 1975 to 2008. In Table 1, it is clearly shown the very high variation within each parameter of leachate.

Compared to typical municipal wastewater, the higher concentrations of these compounds would inhibit and render inoperative a traditional wastewater treatment plant, if no pre-treatment is employed.

During the early stages at sites with a high percentage of biodegradable refuse, the leachate will contain a high concentration of volatile fatty acids (VFA's). Biological treatment would be a better option for this type of leachate. On the later stages, the older leachate will present higher concentrations of refractory compounds like humic substances [1,4]. Physic-chemical treatment would be a better option for this type of leachate.

There are numerous methods, such as physico-chemical and biological, designed to treat wastewater with high levels of toxic contaminants. The selection of the treatment will mainly depend on the characteristics of the leachate and implementation and operation costs. Given the complex characteristics of leachate, a multi-barrier system consisting of both physico-chemical and biological treatment is usually considered the best approach [4,5]. Therefore, pre-treating the leachate onsite before it is discharged into the sewer system and mixed with the municipal wastewater would be beneficial for the subsequent biological treatment on the plant.

Table 1. Summary of Common Leachate Parameters.

Parameter	Range (Values in mg/L except pH)
pH	4.5–9.5
COD	100–150,000
TSS	15–5,000
BOD_5	5–55,000
TN	5–13,000
NH_3-N	10–13,000
TP	0.1–23

Physico-chemical treatment of leachate is the most common practice for the removal of recalcitrant and toxic pollutants, usually coupled as a pre-treatment or polishing step with biological treatment. Processes such as flotation, adsorption, precipitation, pH adjustment, filtration and oxidation are used as pretreatment before further biological degradation or as a final step to improve the final effluent characteristics [2,4]. The pretreatment options selected for this research were: air stripping which focus on the removal of ammonia, chemical coagulation and electro-coagulation which target the removal of colloidal particles in order to reduce the chemical oxygen demand (COD) and advanced oxidation with sodium ferrate to provide a complete degradation of organic contaminants.

Air stripping is a common procedure used to lower high concentrations of ammonia in landfill leachate, with reported ammonia removal rates of around 95% [6–8]. The procedure typically employs air to strip ammonia, odorous gases and other volatile compounds. The efficiency of the removal process is related to the initial concentration of the ammonia to be removed from the liquid (first order reaction) as well as the pH, turbulence, temperature and reactor configuration (available surface area). Depending on the pH of the solution, ammonia nitrogen may be present as ionized (NH_4^+) or un-ionized (NH_3) ammonia. In these terms, the pH of the media must be increased over the pK value of ammonia 9.25 (estimated from the acid ionization constant of ammonia in water) to favor the conversion of ammonia nitrogen into ammonia gas (NH_3). With leachate, the optimum pH for ammonia stripping has been estimated at around 11.0 [6,7,9,10].

Chemical coagulation is a commonly used technique to remove non-biodegradable organic compounds from landfill leachate [11–13]. The objective is to destabilize colloidal particles (around 0.01 to 1 μm in diameter) using a metal coagulant compound. Formed flocs are then removed by settling or filtration [3]. Aluminum

sulfate (alum), ferrous sulfate and ferric chloride are among the most commonly used chemical coagulants for leachate [4,12]. [11] found that iron salts produced better results than aluminum salts in terms of turbidity and COD removal in a stabilized leachate presenting a low BOD/COD of 0.05. A wide range of "optimum" pH values for chemical coagulation of leachate using iron salts have been proposed in the literature, based on the leachate's pH, alkalinity, temperature and organic matter content. This can be explained by the various hydrolyzed species that Fe^{3+} can form depending on the sample's pH (acidic conditions: poly-nuclear cations like $Fe_2(OH)_2^{4+}$, basic conditions: anions like $Fe(OH)_3$, [21]. For the current research, the findings of [1,10,21] were used as a guide, which indicate that an acidic pH would render the optimum results with leachate in terms of COD removal. The evaluation of ferric chloride as coagulant at a pH higher that 7 was outside the boundaries of the current research.

Electro-coagulation is a treatment process that involves the formation of the coagulant by electrolytic oxidation of a sacrificial electrode. The contaminants are destabilized and eventual aggregated into flocs. The flocs are then removed by precipitation and/or filtration. Compared to traditional chemical coagulation, electro-coagulation advantages include less sludge production and reduced cost associated with sludge transportation [14].

Due to the numerous parameters governing this technique (electrode material and contact area, type and amount of current, voltage, contact time, etc.) its application is not very common for the treatment of landfill leachate. A wide range COD removal rates (from 32% to 90%) are reported [14,15].

Advanced oxidation with ferrate (VI) salts has recently been studied for disinfection purposes in wastewater and water treatment [16,17]. Ferrate salts are very strong chemical oxidants. As they are being reduced, they produce ferric hydroxide which additionally serves as a coagulant agent [18,19]. Two main compounds usually used are sodium ferrate (Na_2FeO_4) and potassium ferrate (K_2FeO_4).

The main goal of this research was to assess the effectiveness of the selected physico-chemical methods for the pretreatment of landfill leachate from BRRMF (Manitoba, Canada) in terms of ammonia and COD removal. Additionally, the effect of the pre-treated leachate mixing with municipal wastewater at different percentage on the nitrification performance of a biological nutrient removal (BNR) system was also evaluated.

MATERIALS AND METHODS

Sample Collection and Leachate Characterization

Two samples were taken from BRRMF on August 2013 (300 L) and February 2014 (100 L), to evaluate the variation in leachate composition between summer and winter. Due to variation of the chemical composition of leachate within the landfill, a sample was collected from two leachate collection wells and mixed in 1:1 ratio to be representative. Based on the historical landfill leachate data, leachate was collected from one well that has highest BOD values, and from the other well that has the highest COD and ammonia concentrations among all the wells in the landfill. High Density Polyethylene (HDPE) carboys were used for collecting leachate, which were filled to the top to reduce headspace in the containers and maintain anaerobic conditions. The samples were stored at 4°C to limit biological degradation. The main characteristic of the sampled leachate are presented in Table 2.

The leachate parameters determined in this research are consistent with the ones of an "intermediate" leachate (around 5 to 10 years of age), according to the literature [1,2,4]. Even though the landfill is over 40 years old, the leachate used for this research comes from cells currently in operation, which would correspond to this age range. Additionally, as was mentioned before the quantity and the characteristics of the leachate are also directly related to the MSW and the conditions of the site. No heavy metal characterization was determined, as the heavy metals are considered outside the boundaries of this study.

Analytical Methods

Total COD, Total Nitrogen (TN) and Total Phosphorus (TP) were measured using HACH® digestion vials and represent total concentrations. BOD_5 and TSS

Table 2. Characteristics of Evaluated Leachate.

Parameter	Average Value (mg/L)
pH	7.2 ± 0.1
COD	1939 ± 108
TSS	336 ± 203
BOD_5	248 ± 20
DOC	450 ± 105
TN	759 ± 56
NH_3-N	646 ± 84
TP	6.7 ± 1.1

measurements were carried out following laboratory procedures according to the Standard Methods [20]. Dissolved organic carbon (DOC) analyses were performed using the Fusion Total Organic Carbon Analyzer (TELEDYNE TEKMAR). Soluble Ammonia (NH_3-N), was measured using an automatic flow injection analyser Quick Chem 8500, LACHAT Instruments.

Leachate Pretreatment

Air Stripping

Clear polyvinyl chloride (PVC) reactors (20 cm in diameter and 40 cm in height) with 4.0 L working volume were used. The reactors were filled to the 4 L mark with leachate and the air bubbled through the liquid introduced by two small diffusers near the bottom, connected to a small air pump. Mixing speed was set at 125 rpm. Two operational conditions were tested: (1) mixing with no air flow and (2) mixing with 1 L air/L/min while four pH conditions were evaluated: original pH of the sample (7.0), 10.0, 11.0 and 12.0. The tests were conducted for 48 hours, with samples taken at 2 hour intervals. The effect of temperature on ammonia removal is outside the boundaries of this research, so the reactors were operated at room temperature (21 ± 2°C).

Chemical Coagulation

Chemical coagulation was carried out using Ferric Chloride solution ($FeCl_3$). A set of preliminary tests were conducted without pH adjustment of the sample (approximate pH = 7.2) with different coagulant dosages to determine the optimal range. Based on the results, a range from 34 to 172 mg as Fe/L (corresponding to a range from 100 to 500 mg $FeCl_3$/L) was determined. Jar tests were conducted following Standard Practice for Coagulation-Flocculation Jar Test of Water procedure [21] to evaluate the coagulant doses at different pH values: 7.0 (original pH of the sample), 6.0, 5.0 and 4.0.

Electro-coagulation

The electro-coagulation tests were conducted in a 1 L glass beaker. Two high purity Iron electrodes with an effective surface area of 45 cm^2 were used with a 2.0 cm distance in between. The following parameters were evaluated: (1) contact time of 5, 15 and 30 minutes, (2) pH values of 7.0 (original pH of the sample), 8.0 and 6.0, and (3) current density of 50, 100, 200 and 300 A/m^2. Current was supplied by a KEPCO DC power source (Model BOP 100-2D, 0 to ±100V, 0 to ±2A).

Advanced Oxidation with Sodium Ferrate

Sodium ferrate (Na_2FeO_4) was produced in the laboratory following a wet oxidation procedure where hypochlorite was used to oxidize an iron salt under a strong alkaline environment [22]. Due to the rapid degradation of this compound, the solution was prepared and used on the same day. Ferrate concentration was measured using a UV-Visible Spectrophotometer (Ultrospec 2100 pro, Biochrom Ltd.) at a wavelength of 510 nm.

Jar tests were conducted with the dosage from 50 to 200 mg Fe/L with 50 mg increments. Four pH conditions were tested: 7.4 (original pH of the sample), 6.0, 5.0 and 4.0. The additional measurement of dissolved organic carbon (DOC) was conducted to evaluate the effect of sodium ferrate on the decomposition of organic fraction of the leachate.

Combination of Pretreatment Options

Based on the removal percentages of the two parameters (COD and ammonia) obtained from previous tests, chemical coagulation and air stripping were selected as the two treatment options that provided the lowest effluent concentrations. These two options were combined under their optimal conditions to further evaluate the removal efficiency:

- *Combination 1*: Air stripping was employed as first treatment (48 h, air flow of 1 L/L·min, pH 11.0), followed by chemical coagulation with ferric chloride. During chemical coagulation two tests were conducted. In test one pH was adjusted 5.0 as it was the optimal pH condition. In test two, pH was not modified in order to evaluate the effectiveness of the coagulation at higher pH values after air stripping.
- *Combination 2*: Chemical coagulation was conducted first with pH adjustment to 5.0. Following 1 hour of settling, the effluent was transferred to the air stripping reactors and the aeration was carried out for 48 hours with and air flow of 1 L/L·min and a pH 11.0).

For all pH adjustments, a 25% w/w solution of sodium hydroxide (NaOH) or a 18% w/w hydrochloric acid (HCl) solution was used accordingly.

Pretreatment Effect on Nitrification Kinetics

A sequencing batch reactor (SBR) was setup to simulate a biological nutrient removal (BNR) system. Waste activated sludge (WAS) was taken from the West End Water Pollution Control Centre (WEWPCC) in Winnipeg to seed the reactors. The SBR had a 4 L working volume with a hydraulic retention time (HRT) of 12 hours and a solids retention time (SRT) of 10 days. The SBR was operated at 4 cycles per day. Each cycle consisted of an anaerobic period of 1.5 h and an aerobic period of 4 h. The temperature was maintained at 20 ± 1°C and Dissolved Oxygen (DO) concentration during the aerobic phase was maintained at 4 ± 0.5 mg O_2/L. The reactor was operated and monitored for over 30 days (3 times the SRT) before starting the kinetic testing to ensure stable conditions.

For the kinetic test, the biomass from the main reactor was divided into three 1 L beakers, one served as control while the other two served as testing reactors. The Control reactor was fed only wastewater, while each one of the two testing reactors was fed with a specific mixture percentage of wastewater and leachate (either untreated o pre-treated with the combination of air stripping and chemical coagulation). The leachate to wastewater mixing ratios, in percentage by volume, were: 0.5%, 1.0%, 5.0% and 10.0%. Two sets of Controls are reported in the discussion for untreated and for pre-treated tests. The reason is that one day the test was done for 0.5% and 1%, and a second day the tests were carried out for 5.0% and 10.0%.There were at least 7 days between each test to allow the recovery of the biomass.

RESULTS AND DISCUSSION

Phase I

Air Stripping

The overall ammonia removal rate was in the range of 24–95% after 48 hours—Table 3. The highest ammonia removal rate was achieved under the condition of pH value of 11 and 12 with no significant difference (2%). Considering the chemical cost associated with increasing pH (by adding NaOH for example), a pH of 11 was selected as the optimal pH condition for this treatment. This value is in accordance with results from [9,23]. One interesting observation was that for all the tests with pH adjustment aeration did not improve the ammonia removal efficiency significantly as was expected. On contrast, at pH 11 and 12, reactors without aeration showed slightly better ammonia removal rate. This suggested that pH is the key factor controlling the efficiency of ammonia removal and that the additional contact area provided by the air bubbles while moving through the leachate is not as important for ammonia removal, compared to the surface area of the liquid in the reactor. This is in concordance with results reported by [6]. At a pH higher than the pK value for ammonia in water (9.5), the majority of ammonia is in the free form (NH_3) and mechanical mixing is sufficient for assisting ammonia evaporate from leachate. This observation is important for the real practice as the cost associated with aeration can be expensive.

During this test, it was observed that a thick foam layer was formed over the leachate surface while airflow was applied. The foam layer usually overflowed the reactors during the first 30 minutes of the aeration process, then settled and formed a constant layer (5 to 20 cm) over the surface area. This foam layer dissipated after the air was turned off in less than one minute. Foaming could present serious operation and maintenance issues in a full size application.

The overall COD removal rate was quite low in the range of 0–7%. The results showed that at same pH condition, aeration resulted in slightly higher COD removal than the treatment without aeration. This can be explained by the concept that aeration facilities the removal of volatile of organic compound in the leachate.

Chemical Coagulation

For these tests different dosages of coagulant $FeCl_3$ (100–650 mg/L) as well as different pH values (4, 5, 6 and 7.1) were investigated. The highest COD removal rate of 43% was obtained at pH of 5.0 with $FeCl_3$ dosage of 500 mg/L (172 mg Fe/L). Tests carried out at a pH of 7.0 (leachate original pH) and at 6.0 produced a COD removal of around 10% in each case. When the pH is lowered past 5.0 to 4.0, COD removal decreases to 32%. It was, therefore, concluded that pH of 5.0 with 500 mg/L of $FeCl_3$ was the optimal condition for this pre-treatment option in terms of COD removal. These

Table 3. Ammonia Removal Rate at Different pH Conditions.

pH Value	7 (original)	10	11	12
Mixing, without aeration	24%	75%	93%	95%
Mixing with aeration	69%	81%	89%	89%

results are comparable to the ones reported by [24]. Because coagulation targets particulate and ammonia in the leachate is in the dissolved form, therefore, ammonia removal rates from all the tests were insignificant in the range from 1–4%. It was noticed that dosing $FeCl_3$ resulted excellent TSS removal rate (76–99%) in all the treatment condition. However, it also produced significant amount of sludge. This can be a drawback for the application of this technology.

Electro-coagulation

The highest removal results were provided by a current density (CD) of 300 A/m^2 and the longest contact time (CT) of 30 min without any pH modification. Under these conditions, COD removal reached 18%. The results for ammonia removal were fair low (average of 2%).

Iron electrodes were used to produce the Ferric ions that acted as a coagulant. It was expected with the same amount of ferric ion produced under certain current density and time, the COD removal rate should be similar to the chemical coagulation. However, the results obtained from electro-coagulation were much lower than the chemical coagulation. At current density of 300 A/m^2 with 15 minutes, theoretically 261 mg/L of Fe^{3+} were produced. The test conducted under above condition with leachate pH adjustment to 6.0 the COD removal rate obtained was 1%; while using $FeCl_3$ as coagulant with the same operational condition, much higher COD removal rate of 10% was achieved. Compared to the COD removal results provided in related literature under comparable conditions (32%, [14] and 90%, [15], and to the values obtained for chemical coagulation, the removal rates obtained from our test were much lower than expected.

These results confirm the complex nature of the treatment process and the numerous parameters that interact. A different electrode configuration (larger contact area, smaller gap between electrodes, larger number of electrode pairs) or different electrode materials could provide more positive results.

One of the most common problems associated with this process, is the formation of a scum layer on the electrodes, especially on the anode. The additional layer increases the resistance of the system which in turn demands more voltage to complete the circuit, resulting in higher electrical power consumption. The scum layer was observed during the experiments, but due to the relative short duration of the tests, no significant changes in resistance were measured.

Sodium Ferrate

Ferrate (VI) has been reported as a powerful oxidant and a coagulant. The highest COD and ammonia removal rates obtained from this treatment were 20% and 16%, respectively. These values were obtained under the condition of a pH of 5.0 and a dose of 200 mg Fe/L, as seen in Figure 1. Under the same operational condition, using $FeCl_3$ (172 mg Fe/L) as coagulant provided a much higher COD removal rate of 43%, but a lower ammonia removal rate of 5.7% (see chemical coagulation).

In order to better understand the oxidation of COD by ferrate, DOC concentration was measured. That ferrate is very effective in removing DOC (approximately 64%); however it is not as effective as $FeCl_3$ in terms of removal of particulate COD presented in the leachate. With comparison to chemical coagulation, the higher ammonia removal rate (16% vs 5.7%) can be explained by the oxidization of ammonia by Ferrate (VI) which is different mechanism of ammonia removal from coagulation.

The laboratory procedure followed to prepare the sodium ferrate stock solution was delicate and time consuming. Additionally, the solution must be prepared and used on the same day, as the ferrate compounds are unstable and can degrade in a matter of hours. This indicates that for the application of this particular treatment option, on site generation of the chemical would be required, along with the related operational costs.

Pre-treatments Comparison

Table 4 summarized the optimum operation condition for each pretreatment option in terms of COD and ammonia removal, obtained from the various testing conditions that were applied to each pre-treatment option.

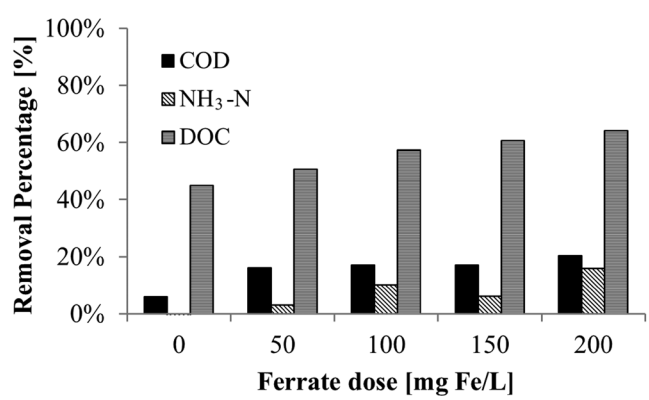

Figure 1. *Results of sodium ferrate pre-treatment at pH 5.0.*

Table 4. Optimum Conditions for the Evaluated Pre-treatment Options.

Parameters	Air Stripping	Chemical Coagulation	Electro-coagulation	Sodium ferrate
pH	11.0	5.0	7.0	5.0
Conditions	Air flow: 1 L air/(L·min)	$FeCl_3$ dose: 172 mg Fe/L	CT: 30 min CD: 300 A/m^2	Ferrate dose: 200 mg Fe/L

The optimum conditions for each pre-treatment option were evaluated one more time to corroborate the results. For this second round, BOD_5 was included to evaluate the pre-treatment options in terms of "biodegradability" improvement. Table 5 presents the removal efficiency values obtained under the optimum conditions of each treatment option. The highest COD removal was obtained with chemical coagulation, while for ammonia removal air stripping provided the best results in terms of ammonia removal.

Biodegradability Observations

BOD of the fresh leachate sample was measured at 248 mg/L from a onetime sample. However, this value is consistent with the average of 245 mg/L reported by the landfill laboratory reports. The BOD/COD ratio was used as a parameter to estimate "biodegradability" before and after each one of the pre-treatment methods—Table 6.

The untreated leachate presents a BOD/COD ratio of 0.12, which is considered as a low biodegradability. The four treatment options did not show any improvement in terms of increasing the BOD/COD ratio. Even more, for the last 2 treatment options the BOD/COD ratio decreased. Electro-coagulation and sodium ferrate had higher BOD removal compared to COD removal (40% BOD removal versus 18% COD removal for electro-coagulation, for example). This shows that the last two treatment options were more efficient targeting and degrading biodegradable compounds. This would indicate that these options would yield better results applied to leachate with a higher BOD concentration.

Combination of Selected Pretreatment

Air stripping and chemical coagulation were selected as the treatment options that produced the lowest COD and ammonia effluent concentrations. The results showed the order of treatments had no significant impact on the removal rate. i.e. air stripping followed by chemical coagulation obtain similar result of the chemical coagulation followed by air stripping. Both options provided COD and ammonia removal rate in the range of 45% to 50% and 83% to 85%, respectively. These results were also very close to the results obtained from each individual test at the optimum conditions. The capital cost and operation and maintenance of each scenario are considered outside the boundaries of this research.

Phase II

Effect of Pre-treated Leachate on Nitrification Kinetics

In this test, the performance of nitrification was evaluated in a SBR system fed with the mixture of wastewater with leachate with and without pre-treatment. The wastewater presented an average COD concentration of 278 mg/L (168 mg/L standard deviation) and an ammonia concentration of 32 mg/L (10 mg/L standard deviation). Each cycle consisted of an anaerobic period of 1.5 h and an aerobic period of 4 h.

Figure 2 present the results when untreated and pretreated leachate is mixed in with the wastewater at different percentages. Control represents the reactor with only wastewater as influent. Mixing leachate (either

Table 5. Removal Efficiency for the Analyzed Pre-treatment Options.

Parameters	Air Stripping	Chemical Coagulation	Electro-coagulation	Sodium ferrate
COD	18%	43%	18%	20%
TSS	0%	73%	70%	91%
BOD_5	5%	36%	40%	86%
DOC	1%	69%	8%	64%
NH_3-N	86%	6%	0%	16%
TP	22%	75%	74%	61%

Table 6. BOD/COD Ratios for Untreated and Treated Leachate.

Parameters	Untreated	Air Stripping	Chemical Coagulation	Electro-coagulation	Sodium ferrate
BOD/COD	0.12	0.10	0.10	0.08	0.02

pre-treated or untreated) with wastewater at 0.5% and 1.0% v/v does not produce any significant difference in the ammonia influent concentrations or the system response [Figure 2(a) and 2(c)]. However, when the mixing rate was increased to 5.0% and 10.0% v/v with untreated leachate [Figure 2(b)], it can be seen that the ammonia influent concentration increased 2 to 3 times the value of the control. Additionally, the system was not able to achieve full nitrification in one cycle (ammonia concentrations in the effluent are 3.6 mg/L and 20.4 mg/L, respectively). This is suspected to be due to the higher concentration of ammonia in the influent and not a problem with nitrification inhibition, as the rate of nitrification (shown for 5.0% and 10.0% as the slope of the curve) is similar to the rate presented by the control. A longer aeration period would be needed

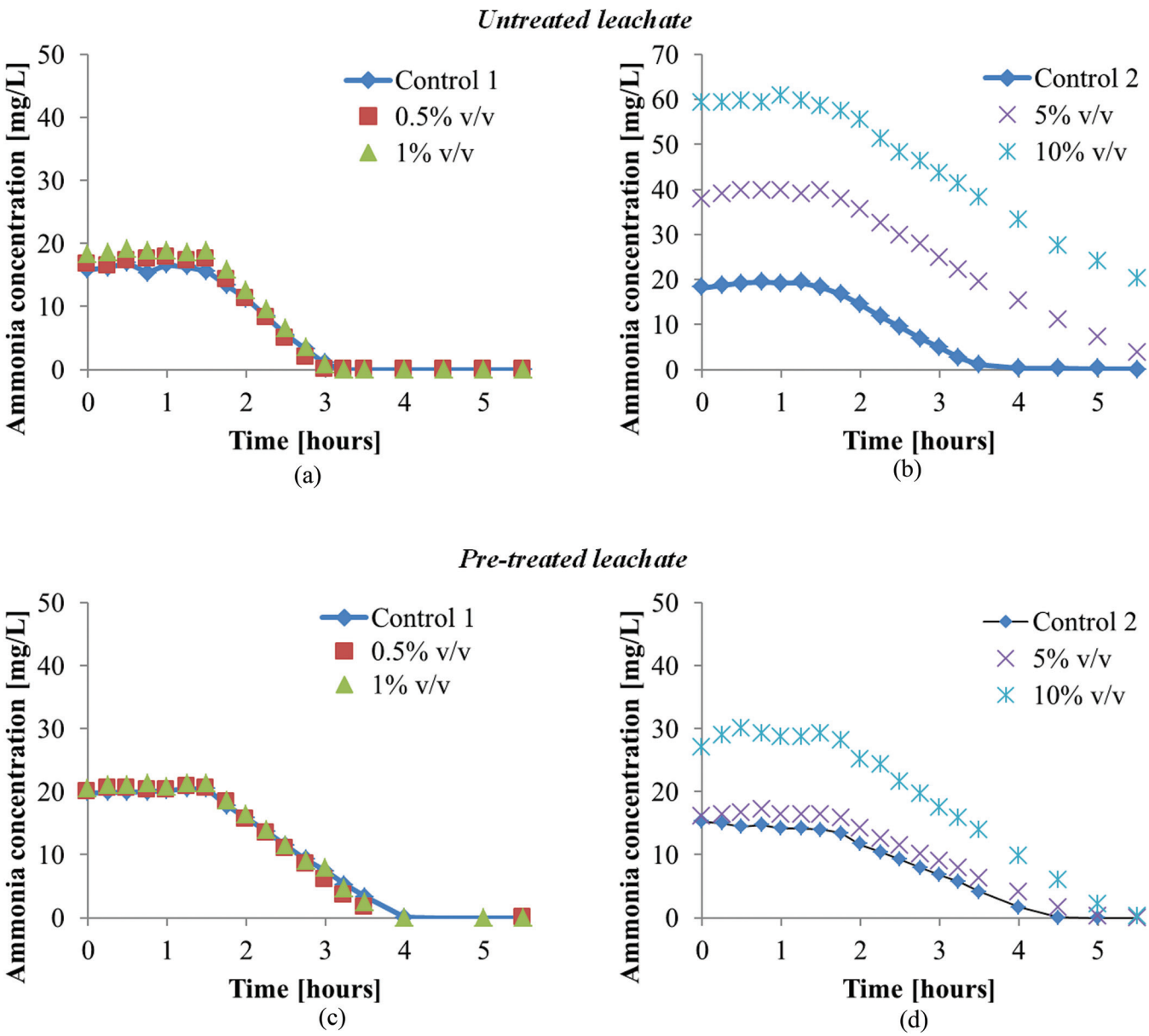

Figure 2. *Impact of untreated and pre-treated leachate on ammonia degradation at different proportion of added leachate.*

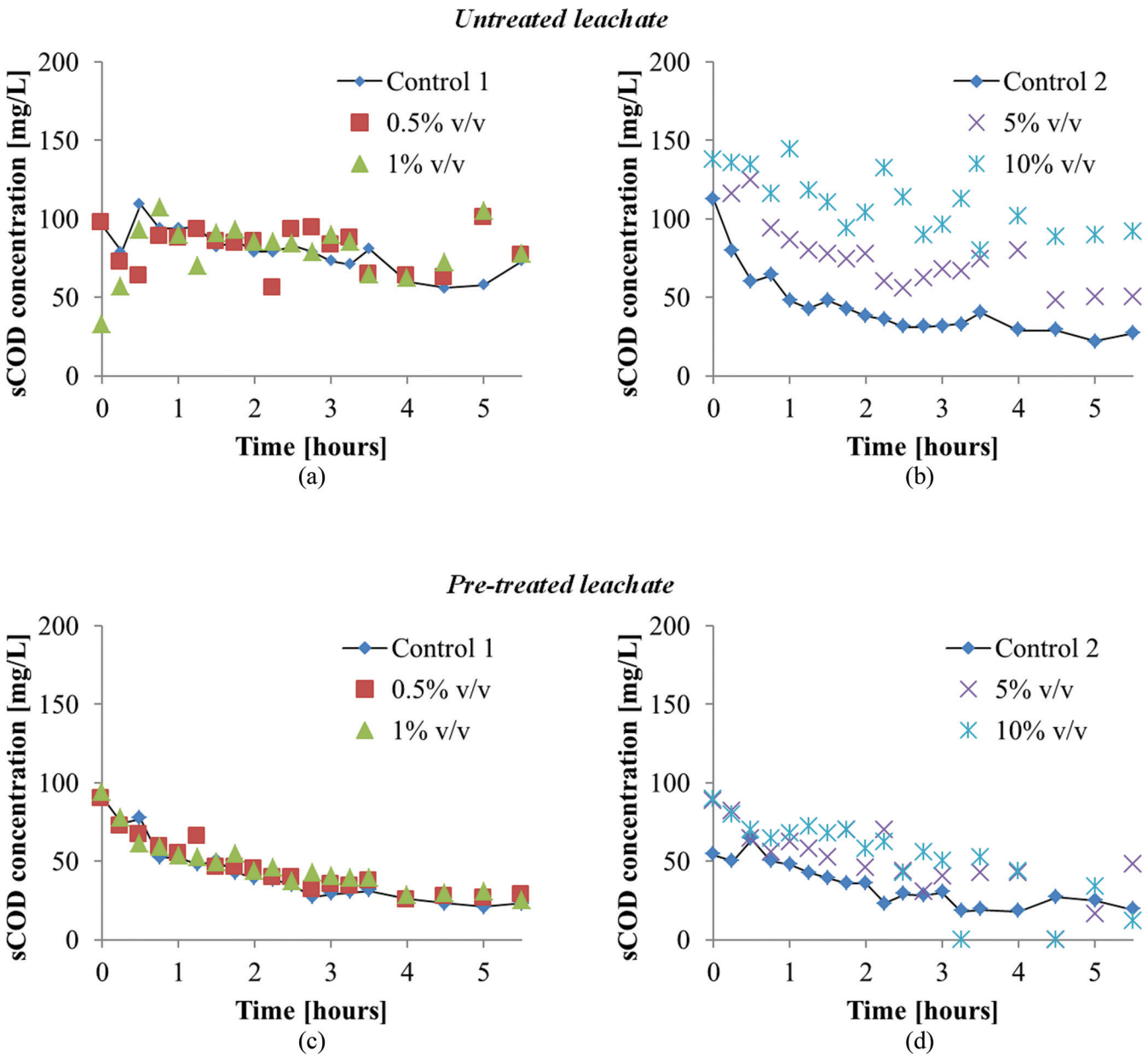

Figure 3. *Impact of untreated and pre-treated leachate on soluble COD degradation at different proportion of added leachate.*

for the full conversion of ammonia at these higher concentrations.

As shown in Figure 2(d), the pre-treatment of leachate lowered the ammonia in the influent, therefore, allowing full nitrification under the same operational condition. It was concluded that pre-treatment of leachate is necessary when the mixing ratio of leachate with wastewater is higher (5.0% to 10.0%), to assure the performance of nitrification at the wastewater treatment plant.

In terms of soluble COD removal, systems fed with the pre-treated leachate also provide a better removal than the ones with untreated leachate. The effluent sCOD concentration after the 5.5 hour operation with the pre-treated leachate in all cases was lower than 50 mg/L, which is very close to the control values [Figures 3(c) and 3(d)]. However, for the ones with untreated leachate, the sCOD in the effluent was in the range of 50 to 92 mg/L [Figures 3(a) and 3(b)].

The pre-treatment methods selected were previously proven to reduce soluble COD and ammonia concentrations on the leachate. Without the pre-treatment, mixing the leachate with the municipal wastewater increased the influent values of sCOD and ammonia to a point where removal by biological means was not achievable in the time provided by the BNR system.

CONCLUSIONS

- Four methods of leachate pre-treatment were evaluated to determine the most efficient procedure in terms of COD and ammonia removal: air stripping, chemical coagulation, electro-coagulation and oxidation with sodium ferrate. Chemical coagulation provided the overall best COD removal rate at 43%, while air stripping provided an ammonia removal rate of 86%, superior to the results from the other pre-treatments for this compound. Chemical coagulation reduces COD by destabilizing the electric charges of colloidal particles and removing said particles by precipitation, co-precipitation (sweeping effect) and/or filtration. On the other hand, air stripping relies on the desorption of ammonia from the liquid by providing the right conditions (pH, temperature, contact surface area, etc.) to favor the release of the gas.
- The idea behind electro-coagulation was to provide the same iron salts (as chemical coagulation) without the additional compounds to minimize sludge production and costs. However, the delicate set of parameters needed to optimize the treatment to a specific leachate was not favorable. In the case of advanced oxidation with sodium ferrate, the compound was theorized to degrade recalcitrant compounds thus lowering the COD and providing a more biodegradable leachate. The long and complicated procedure to prepare and dose the right amount of sodium ferrate made the pre-treatment not efficient for the objectives of this research.
- The optimum conditions for chemical coagulation (dosage of 172 mg Fe/L at a pH of 5.0) are comparable to the conditions reported by [13,24]. However, a lower COD removal rate was achieved in this experiment. In the case of air stripping, the conditions found in this research as optimum in terms of ammonia removal were similar to the ones reported by [8,9,23], except for the longer duration (48 hours) needed to achieve ammonia removal rates over 85%.
- Pre-treating leachate with a combination of air stripping and chemical coagulation was shown to effectively reduce ammonia (83–85% removal) and COD (45–50% removal) from the leachate. The order in which the methods were applied did not affect the overall efficiency of the combined treatment.
- For Phase II, the effect of untreated and pre-treated leachate blended with sewage was evaluated by the response of the biological nutrient removal SBR bench-scale system. Mixing the leachate with or without pre-treatment with municipal sewage at low concentrations (0.5–1.0% v/v) does not produce any significant difference in terms of soluble COD or ammonia influent concentrations, and therefore the response of the system is comparable to the response from the controls fed only wastewater.
- However, when the untreated leachate mix rate was increased (5.0% and 10.0% v/v) the ammonia influent concentration doubled or tripled, respectively. Soluble COD influent and effluent concentrations increased as well. Under these conditions the BNR system was not able to achieve full nitrification during one cycle. No nitrification inhibition is suspected as the rate of ammonia removal is similar to that of the controls. The pre-treatment of leachate lowered the ammonia in the influent, therefore, allowing again for full nitrification.
- It was concluded that pre-treatment of leachate is necessary when the mixing ratio of leachate with wastewater is higher (5.0% to 10.0%), to assure the performance of nitrification at the wastewater treatment plant.

REFERENCES

1. P. Kjeldsen, M. Barlaz, and A. Rooker, "Present and long-term composition of MSW landfill leachate: a review," *Crit. Rev. . . . ,* vol. 32, no. 4, pp. 297–336, 2002. http://dx.doi.org/10.1080/10643380290813462
2. T. A. Kurniawan, W.-H. Lo, and G. Y. S. Chan, "Physico-chemical treatments for removal of recalcitrant contaminants from landfill leachate." *J. Hazard. Mater.*, vol. 129, no. 1–3, pp. 80–100, Feb. 2006. http://dx.doi.org/10.1016/j.jhazmat.2005.08.010
3. G. Tchobanoglous, F. Burton, and D. Stensel, Eds., *Wastewater Engineering, Treatment and Reuse, Fourth*. New York: McGraw-Hill, 2004, p. 1819.
4. S. Renou, J. G. Givaudan, S. Poulain, F. Dirassouyan, and P. Moulin, "Landfill leachate treatment: Review and opportunity." *J. Hazard. Mater.*, vol. 150, no. 3, pp. 468–493, Feb. 2008. http://dx.doi.org/10.1016/j.jhazmat.2007.09.077
5. J. Wiszniowski, D. Robert, J. Surmacz-Gorska, K. Miksch, and J. V. Weber, "Landfill leachate treatment methods: A review," *Environ. Chem. Lett.*, vol. 4, no. 1, pp. 51–61, Mar. 2006. http://dx.doi.org/10.1007/s10311-005-0016-z
6. K. C. Cheung, L. M. Chu, and M. H. Wong, "Ammonia stripping as a pretreatment for landfill leachate," *Water. Air. Soil Pollut.*, vol. 94, no. 1–2, pp. 209–221, Feb. 1997. http://dx.doi.org/10.1007/BF02407103
7. C. Collivignarelli, G. Bertanza, M. Baldi, and F. Avezzu, "Ammonia stripping from MSW landfill leachate in bubble reactors: process modeling and optimization," *Waste Manag. Res.*, vol. 16, no. 5, pp. 455–466, Oct. 1998. http://dx.doi.org/10.1177/0734242X9801600508
8. M. Cotman and A. Z. Gotvajn, "Comparison of different physico-chemical methods for the removal of toxicants from landfill leachate." *J. Hazard. Mater.*, vol. 178, no. 1–3, pp. 298–305, Jun. 2010. http://dx.doi.org/10.1016/j.jhazmat.2010.01.078
9. J.-S. Guo, A. Abbas, Y.-P. Chen, Z.-P. Liu, F. Fang, and P. Chen, "Treatment of landfill leachate using a combined stripping, Fenton, SBR, and coagulation process." *J. Hazard. Mater.*, vol. 178, no. 1–3, pp. 699–705, Jun. 2010. http://dx.doi.org/10.1016/j.jhazmat.2010.01.144
10. T. Yilmaz, S. Apaydin, and A. Berktay, "Coagulation-Floccula-

tion and Air Stripping as a Pretreatment of Young Landfill Leachate," *Open Environ. Eng. J.*, vol. 3, pp. 42–48, 2010. http://dx.doi.org/10.2174/1874829501003010042

11. A. Amokrane, C. Comel, and J. Veron, "Landfill leachates pretreatment by coagulation-flocculation," *Water Res.*, vol. 31, no. 11, pp. 2775 – 2782, 1997. http://dx.doi.org/10.1016/S0043-1354(97)00147-4
12. A. Tatsi, A. Zouboulis, K. Matis, and P. Samaras, "Coagulation-flocculation pretreatment of sanitary landfill leachates." *Chemosphere*, vol. 53, no. 7, pp. 737–744, Nov. 2003. http://dx.doi.org/10.1016/S0045-6535(03)00513-7
13. E. Mara-ón, L. Castrillón, Y. Fernández-Nava, A. Fernández-Méndez, and A. Fernández-Sánchez, "Coagulation-flocculation as a pretreatment process at a landfill leachate nitrification-denitrification plant." *J. Hazard. Mater.*, vol. 156, no. 1–3, pp. 538–544, Aug. 2008. http://dx.doi.org/10.1016/j.jhazmat.2007.12.084
14. F. Ilhan, U. Kurt, O. Apaydin, and M. Gonullu, "Treatment of leachate by electrocoagulation using aluminum and iron electrodes," *J. Hazard. Mater.*, 2008. http://dx.doi.org/10.1016/j.jhazmat.2007.10.035
15. S. Veli, T. Öztürk, and A. Dimoglo, "Treatment of municipal solid wastes leachate by means of chemical-and electro-coagulation," *Sep. Purif. Technol.*, vol. 61, no. 1, pp. 82–88, 2008. http://dx.doi.org/10.1016/j.seppur.2007.09.026
16. J.-Q. Jiang, "Research progress in the use of ferrate(VI) for the environmental remediation," *J. Hazard. Mater.*, vol. 146, no. 3, pp. 617–623, Jul. 2007. http://dx.doi.org/10.1016/j.jhazmat.2007.04.075
17. Y. Lee, S. G. Zimmermann, A. T. Kieu, and U. Von Gunten, "Ferrate (Fe(VI)) application for Municipal wastewater treatment: a novel process for simultaneous micropollutant oxidation and phosphate removal." *Environ. Sci. Technol.*, vol. 43, no. 10, pp. 3831–8, May 2009. http://dx.doi.org/10.1021/es803588k
18. D. Tiwari, J.-K. Yang, and S.-M. Lee, "Aplications of Ferrate (VI) in the treatment of wastewaters," *Environ. Eng. Res.*, vol. 10, no. 6, pp. 269–282, 2005. http://dx.doi.org/10.4491/eer.2005.10.6.269
19. J.-Q. Jiang, A. Panagoulopoulos, M. Bauer, and P. Pearce, "The application of potassium ferrate for sewage treatment," *J. Environ. Manage.*, vol. 79, no. 2, pp. 215–220, Apr. 2006. http://dx.doi.org/10.1016/j.jenvman.2005.06.009
20. A. Eaton, E. Rice, and R. Baird, Eds., Standard Methods for the Examination of Water and Wastewater, 22nd ed. American Public Health Association (APHA), American Water Works Association (AWWA), Water Environment Federation (WEF), 2012, p. 1496.
21. ASTM Standard D2035, "Standard Practice for Coagulation-Flocculation Jar Test of Water," West Conshohocken, PA.: ASTM International, 2013.
22. J.-Q. Jiang and B. Lloyd, "Progress in the development and use of ferrate(VI) salt as an oxidant and coagulant for water and wastewater treatment," *Water Res.*, vol. 36, no. 6, pp. 1397–408, Mar. 2002. http://dx.doi.org/10.1016/S0043-1354(01)00358-X
23. A. R. Abood, J. Bao, Z. N. Abudi, D. Zheng, and C. Gao, "Pretreatment of nonbiodegradable landfill leachate by air stripping coupled with agitation as ammonia stripping and coagulation–flocculation processes," *Clean Technol. Environ. Policy*, vol. 15, no. 6, pp. 1069–1076, Jan. 2013. http://dx.doi.org/10.1007/s10098-012-0575-1
24. W. Li, T. Hua, Q. Zhou, S. Zhang, and F. Li, "Treatment of stabilized landfill leachate by the combined process of coagulation/flocculation and powder activated carbon adsorption," *Desalination*, vol. 264, no. 1–2, pp. 56–62, Dec. 2010. http://dx.doi.org/10.1016/j.desal.2010.07.004

Screening of Bioflocculant and Preliminary Application to Treatment of Tannery Wastewater

QINHUAN YANG[1], HONGMEI MING[2], XINGXIU ZHAO[2], JING ZHANG[2], WEI ZOU[2], CHANGQING ZHAO[2,*] and XIUQIONG GUAN[2]

[1]*College of Material and Chemical Engineering, Sichuan University of Science and Engineering, Zigong 643000, China*
[2]*College of Bioengineering, Sichuan University of Science and Engineering, Zigong 643000, China*

ABSTRACT: In this study, three strains of bacteria *Bacillus cereus* CZ1001, *B. subtilis* CZ1002, and *B. fusiformis* CZ1003 were inoculated into four different kinds of culture medium. After growth, the supernatants were collected and added to kaolin suspensions to determine whether these Bacillus strains produced flocs that could be filtered out. Efficient bacteria and media were then selected to produce bioflocculants which were subsequently extracted using pre-cooled ethanol. After freeze drying, the flocculants were used to treat tannery wastewater. Results showed cultures of *B. subtilis* CZ1002 growing in media No. 4, *B. cereus* CZ1001 growing in media No. 1, and *B. fusiformis* CZ1003 growing in media No. 1. All had better flocculation effects. Treatment of the tannery wastewater with the bioflocculants produced under three conditions revealed bioflocculant produced by *B. cereus* CZ1001 growing in media No. 1 was best for treatment of tannery wastewater. This work contributes to application of bioflocculants for removal of tannery wastewater.

INTRODUCTION

TANNERY wastewater contains complex components such as organic materials and nitrogen-containing compounds with a large amount of dark sewage. There are currently many physical, chemical, and microbial methods for treatment of tannery wastewater [1]. However, it is important to look for economical and effective methods to treat tannery wastewater. Recently, the method of using bioflocculant to treat tannery wastewater has become a new research direction. It is well known that bioflocculants produced by microbes under unique culture conditions consist of polymers possessing flocculation activity. Owing to their potential for easy treatment of secondary pollution and unique effects on the biodegradation of pollutants, researchers have been paying increasing attention to bioflocculants [2,3].

There to date have been several studies of treatment of tannery wastewater with bioflocculant. Zhang *et al.* treated tanning wastewater using bioflocculant produced from a kind of bacterium which was signed C-62 [4]. Li *et al.* isolated six species of bacteria producing bioflocculant and used one to treat leather effluent [5]. Chai *et al.* isolated two species of bacteria that produced bioflocculant and used them to treat tannery effluent [6]. Qin used microorganisms as flocculants to treat leather effluent and found they effectively removed the chemical oxygen demand (COD), suspended solids (SS), and Cr^{3+} from leather effluent [7]. Wang *et al.* selected four species of bacteria producing bioflocculants and found that the color, turbidity, and COD of the tannery wastewater were significantly reduced after using the composite bioflocculant [8]. Liu *et al.* summarized the mechanism and research status of bioflocculant during treatment of tannery wastewater [9]. Rajan *et al.* found that *Trichococcus flocculiformis* and *Pseudomonas fluorescens* isolated from polluted tannery soil had flocculation ability [10]. Serdar *et al.* found there was polysaccharide in bioflocculant used to treat tannery wastewater [11]. Despite these findings, the higher cost or lower flocculation efficiency have limited application of these organisms for industrial processes [12,13].

To improve treatment effects of the pollutants in tannery wastewater and to obtain new bioflocculants, it is necessary to find more and better bioflocculants. Previous experiments in our laboratory revealed that *Bacillus cereus* CZ1001, *B. subtilis* CZ1002, and *B. fusiformis* CZ1003 isolated from activated sludge from a tannery effectively removed COD, chrominance, and to-

*Author to whom correspondence should be addressed.
E-mail: zhaocq81@126.com

1544-8053/15/03 177-05
© 2015 DEStech Publications, Inc.
doi:10.12783/issn.1544-8053/12/3/8

tal nitrogen from tannery wastewater. Optimum culture media here were screened for the ability to produce bioflocculant from three strains. After extraction and freeze drying, the bioflocculants were used to treat COD, chrominance, and total nitrogen from tannery wastewater.

EXPERIMENTAL PROCEDURE

Materials

Yeast extract, peptone, and bovine serum albumin were biochemical grade and purchased from Beijing AoBoXing Leiverseen Biotech Co. Ltd (China). Wastewater was obtained from a tannery in Sichuan (China). All other reagents used in this study were research grade.

Bacteria Strains

B. cereus CZ1001, *B. subtilis* CZ1002, and *B. fusiformis* CZ1003 were isolated from activated tannery sludge and preserved in our laboratory. Before use, organisms were cultured in Luria broth containing tannery wastewater by gradually increasing the quantity of wastewater to domesticate strains.

Culture Media

To rapidly determine if the isolated strains had flocculation ability or not, the following four types of culture media known to enable bacteria to produce bioflocculants were used [14].

- *Media No. 1*: sucrose 30.0 g, $NaNO_3$ 2.0 g, KC1 0.5 g, K_2HPO_4 1.0 g, $MgSO_4$ 0.5 g, $FeSO_4$ 0.01 g and water 1 L. The pH of the media was not altered.
- *Media No. 2*: glucose 12.0 g, yeast extract 1.0 g, K_2HPO_4 1.0 g, KH_2PO_4 0.5 g, NaCl 0.2 g, $MgSO_4$ 0.2 g, $CaCl_2$ 0.1 g and water 1 L. The pH of the media was adjusted to 7.0
- *Media No. 3*: glucose 10 g, K_2HPO_4 2.0 g, KH_2PO_4 5.0 g, NaCl 0.1 g, $MgSO_4 \cdot 7H_2O$ 0.2 g, NH_4Cl 0.5 g and water 1 L. The pH of the media was not altered.
- Media No. 4: glucose 30.0 g, yeast extract 8.0 g, $K_2HPO_4 \cdot 3H_2O$ 2.0 g, $MgSO_4$ 0.25 g, sodium glutamate 10.0 g and water 1 L. The pH of the media was adjusted to 7.5.

Bacterial Culture

Bacterial strains including *B. cereus* CZ1001, *B. subtilis* CZ1002, and *B. fusiformis* CZ1003 were inoculated into the aforementioned media and then incubated for 48 h at 35°C while shaking at 180 rpm, after which the strains were inoculated into sterilized conical flasks containing 100 mL of the same media into which samples were inoculated. Next, flasks were cultured at 35°C while shaking at 180 rpm for 24 h.

Preliminarily Screening of Bioflocculant

Cultured cells were centrifuged at 8,000 rpm for 10 min at 4°C. Next, 2 mL of the supernatants were added to 100 mL of 4 g/L kaolin suspension. If flocculation occurred in the suspension it was assumed that the strain had the ability to produce bioflocculant when grown in the media being investigated [6].

Secondary Screening of Bioflocculant

Strains shown to produce bioflocculant upon preliminary screening were inoculated into the same media used in the initial screening and then incubated for 24 h at 35°C while shaking at 180 rpm after which cells were centrifuged at 8,000 rpm for 10 min at 4°C. Supernatants were subsequently investigated for their flocculation activity by measuring the flocculation rate using spectrophotometric method [8].

Preparation of Bioflocculant [15]

Strains found to produce bioflocculant upon secondary screening were cultured in corresponding media at 35°C for 24 h. Cells were then centrifuged at 8,000 rpm for 10 min at 4°C after which the supernatants were amended with absolute ethyl alcohol that had been pre-cooled to 4°C at 3 times the volume of the supernatants. The mixture was then incubated at 4°C for 6 h after which it was centrifuged at 10,000 rpm for 10 min. The precipitate was then collected and washed with distilled water after which it was centrifuged at 8,000 rpm for 10 min. Finally, the centrifuged precipitate was freeze-dried under a vacuum which yielded the bioflocculant.

Removal of COD from Tannery Wastewater with Bioflocculant

A total of 100 mL of filtered tannery wastewater with a chemical oxygen demand (COD) of 1082.2 mg/L was poured into conical flasks and amended with 0.2 g/L of the prepared bioflocculant after secondary screen-

ing. The flasks were then placed in the magnetic stirring device (SH-3A, Ziguang Instrument Co., Beijing, China) and stirred at 200 rpm for 2 min, followed by 40 rpm for 10 min at room temperature (25°C). Next, the samples were allowed to stand for 20 min, then filtered through filter paper and the COD of each sample was determined using a Water Quality Analyzer (SQ-UV04, Shangqing Technology Co. Ltd, China) which can detect the concentration of COD, total nitrogen and total phosphorus. In addition, the wastewater was subjected to stirring without exposure to the bioflocculant as a control. The removal rate of the COD was then calculated as follows:

$$F = (A_1 - A_2)/S \quad (1)$$

Where F is the removal rate of the COD in tannery wastewater; A_1 is the content of the COD for the control that was not treated by the bioflocculant; A_2 is the content of the COD in tannery wastewater that was treated by the bioflocculant; S is the content of the COD before reaction. The removal rates of the chrominance for the subsequent procedures were also determined using this formula.

Removal of Chrominance in Tannery Wastewater with Bioflocculant

A total of 50 mL of tannery wastewater containing 2410.8 mg/L of chrominance was poured into conical flasks and amended with 0.11 g/L of the prepared bioflocculant after secondary screening. The flasks were then magnetically stirred under the same conditions as for the COD treatment. After 20 min, the samples were filtered and the chrominance value in each sample was determined using a Water Quality Analyzer (SQ-UV04, Shangqing Technology Co. Ltd, China). In addition, wastewater that was stirred but untreated by bioflocculant was used as a control.

Removal of Total Nitrogen in Tannery Wastewater with Bioflocculant

A total of 50 mL of tannery wastewater containing 452.83 mg/L of total nitrogen was poured into conical flasks, after which 0.11 g/L of the prepared bioflocculant identified by secondary screening was added. After 20 min, the samples were filtered and the chrominance value in each sample was determined using a Water Quality Analyzer (SQ-UV04, Shangqing Technology Co. Ltd, China). In addition, wastewater that was stirred but untreated by bioflocculant was used as a control.

RESULTS AND DISCUSSION

Preliminarily Screening of Bioflocculant

Observation of the growth of the strains in four media revealed that *B. fusiformis* CZ1003 cultured in Media No. 3 did not grow well. Therefore, it was not selected for production of bioflocculant. Following centrifugation of supernatants of other culture broths, they were added to a kaolin suspension after which flocculation phenomenon in the suspension was observed (Table 1).

As shown in Table 1, flocculation occurred in the kaolin suspension amended with culture broths of *B. subtilis* CZ1002 growing in four types of media (No. 1 to 4), *B. cereus* CZ1001 growing only in media No. 1 and No. 2, and *B. fusiformis* CZ1003 growing only in media No. 1. Therefore, *B. subtilis* CZ1002 growing in four media (No. 1 to 4), *B. cereus* CZ1001 growing in media No. 1 and No. 2, and *B. fusiformis* CZ1003 growing in media No. 1 were preliminarily screened for bioflocculant production.

Secondary Screening of Bioflocculant

A high flocculation rate indicates that the activity of flocculation is high and there are many bioflocculants produced. As shown in Table 2, the culture broth of *B. subtilis* CZ1002 growing in media No. 2 had no flocculation activity, while that from media No. 1, No. 3 and No. 4 did have flocculation activity. However, the activity of flocculation in media No. 1 and No. 3 was somewhat low (14.34% and 19.59%, respectively). This may have occurred because that sodium glutamate in media No. 4 which was most different from other three media and the media's pH (7.5) which was obviously higher than other three media (6.8–7.0) were

Table 1. Flocculation of Kaolin Suspension Amended with Culture Broths of the Three Tested Strains Growing in Four Types of Media.

Media	*B. subtilis*	*B. cereus*	*B. fusiformis*
No. 1	+	+	+
No. 2	+	+	–
No. 3	+	–	did not grow well
No. 4	+	–	+

Note: "+" indicates that flocculation occurred in the kaolin suspension amended with culture. broths; "–" indicates that there was no flocculation in the kaolin suspension.

Table 2. Flocculation Rate for Culture Broths of Strains Growing in Different Media.

Media	*B. subtilis*	*B. cereus*	*B. fusiformis*
No. 1	14.34%	43.72%	44.28%
No. 2	—	6.62%	—
No. 3	19.59%	—	—
No. 4	40.83%	—	—

more suitable for *B. subtilis* CZ1002 to produce the bioflocculant to treat tannery wastewater.

According to previous experiments in our laboratory, saccharides and proteins in the bioflocculant produced by *B. cereus* CZ1001 played a role in flocculation and subsequent removal of pollutants from tannery wastewater, with saccharides exerting the main effects. The culture broth of *B. cereus* CZ1001 growing in media No. 1 and No. 2 showed flocculation, but the activity was only 6.62% in media No. 2. This may have occurred because components in media No. 1 such as sucrose and sodium nitrate were more suitable for *B. cereus* CZ1001 to produce bioflocculant that contained saccharides and proteins.

The culture broth of *B. fusiformis* CZ1003 only showed flocculation activity when it was grown in media No. 1.

Based on these findings, *B. subtilis* CZ1002 growing in media No. 4, *B. cereus* CZ1001 growing in media No. 1 and *B. fusiformis* CZ1003 growing in media No. 1 were selected for preparation of the bioflocculant.

Removal of COD from Tannery Wastewater by Bioflocculant

The bioflocculants produced by the strains identified upon secondary screening were prepared and used to treat COD from tannery wastewater with an initial COD value of 1082.2 mg/L. The removal effects are shown in Table 3.

As shown in Table 3, the removal of COD from tannery wastewater showed little difference after treatment by three bioflocculants, with removal rates ranging from 22.71% to 25.97%. Therefore, the bioflocculants produced by *B. cereus* CZ1001 growing in media No. 1, *B. subtilis* CZ1002 growing in media No. 4 and *B. fusiformis* CZ1003 growing in media No. 1 could be used for removal of COD from tannery wastewater.

Table 3. Removal of COD from Tannery Wastewater by Bioflocculants.

Strains and Media Producing Bioflocculant	COD (mg/L)	Removal Rate of COD (%)
B. cereus CZ1001 growing in media No. 1	801.2	25.97
B. fusiformis CZ1003 growing in media No. 1	836.4	22.71
B. subtilis CZ1002 growing in media No. 4	824.9	23.78

Table 4. Removal of Chrominance from Tannery Wastewater by Bioflocculants.

Strains and Media Producing Bioflocculant	Chrominance (mg/L)	Removal Rate of Chrominance (%)
B. cereus CZ1001 growing in media No. 1	699.85	70.97
B. fusiformis CZ1003 growing in media No. 1	1919.48	20.38
B. subtilis CZ1002 growing in media No. 4	2103.66	12.74

Removal of Chrominance from Tannery Wastewater with Bioflocculant

Removal of secondary screened bioflocculants on tannery wastewater containing 2410.8 mg/L of chrominance are shown in Table 4.

As shown in Table 4, the removal of chrominance from tannery wastewater differed greatly in response to treatment by the three bioflocculants. The effects of the bioflocculant produced by *B. cereus* CZ1001 growing in media No. 1 were significantly greater than those of the other bioflocculants, with a chrominance removal rate of 70.97%. Therefore, the bioflocculants produced by *B. cereus* CZ1001 growing in media No. 1 could be used to remove chrominance from tannery wastewater.

Removal of Total Nitrogen from Tannery Wastewater with Bioflocculant

The results of treatment of tannery wastewater containing 452.83 mg/L total nitrogen by secondary screened bioflocculants are shown in Table 5.

As shown in Table 5, the removal of total nitrogen

Table 5. Removal of Total Nitrogen from Tannery Wastewater by Bioflocculants.

Strains and Media Producing Bioflocculant	Total Nitrogen (mg/L)	Removal Rate of Total Nitrogen (%)
B. cereus CZ1001 growing in media No. 1	278.81	38.43
B. fusiformis CZ1003 growing in media No. 1	350.01	22.71
B. subtilis CZ1002 growing in media No. 4	330.13	27.10

from tannery wastewater did not differ significantly among bioflocculants. During treatment, the effects of bioflocculant produced by *B. cereus* CZ1001 growing in media No. 1 were slightly better than those of the other bioflucculants, with a removal rate of 38.43%. Therefore, bioflocculants produced by *B. cereus* CZ1001 growing in media No. 1, *B. subtilis* CZ1002 growing in media No. 4 and *B. fusiformis* CZ1003 growing in media No. 1 could be used to remove total nitrogen from tannery wastewater.

Overall, the removal rates for COD, chrominance and total nitrogen in tannery wastewater by bioflocculant treatment were relatively low (12.74–70.97%) when compared with other similar studies [7,8,10]. This was likely because few bioflocculants were used in the experiment and the conditions including production of the bioflocculants and treatment of wastewater were not optimized, even though suitable media were selected. However, future studies should be conducted to identify the specific reasons for these discrepancies and obtain new bioflocculants for treatment of tannery wastewater.

CONCLUSIONS

Overall, the results of this study indicate that bioflocculants produced by *Bacillus cereus* CZ1001 growing in media No. 1 had better ability to remove COD, chrominance and total nitrogen from tannery wastewater. The results presented herein will contribute to the removal of COD, chrominance and total nitrogen removal in tannery wastewater by bioflocculants.

ACKNOWLEDGEMENTS

This work was financially supported by Science & Technology Department of Sichuan Province (Item No. 2014JY0011), Department of Education of Sichuan Province (Item No. 14ZA0204, 15ZA0225), Science and Technology Bureau of Zigong city (2014H10).

REFERENCES

1. Yang Qinhuan, Zhao Changqing, Removal of total nitrogen from tannery wastewater by bioflocculant prepared by Bacillus cereus, *Journal of Pure and Applied Microbiology*, 2013, 7, 137–143.
2. Vijayalakshmi, S.P. and Raichur, A.M., The Utility of Bacillus Subtilis as Bioflocculant for Fine Coal. *Colloids and Surfaces B: Biointerfaces*, 2003, 29(4), 265–270. http://dx.doi.org/10.1016/S0927-7765(03)00005-5
3. Levy, N., Magdassi, S. and Bar-Or, Y., Physico-chemical aspects in flocculation of bentonite suspensions by a cyanobacterial bioflocculant. *Water Research*, 1992, 26(2), 239–254. http://dx.doi.org/10.1016/0043-1354(92)90225-S
4. Zhang Tong, Zhu Huailan, Lin Zhe. Progresses of microbial flocculant studies and application. *Chinese Journal of Applied & Environmental Biology*, 1996, 2(1): 95–105.
5. Li Zhiliang, Zhang Benlan, Pei Jian. Screening of flocculant-producing bacteria and their flocculating effects on some wastewaters. *Chinese Journal of Applied & Environmental Biology*, 1997, 3(1): 67–70.
6. Chai, X. L., Wang, M., Chen, J., *et al.*, Screening for characteristics of microbial flocculant. *Pollution Control Technology*, 2000, 13 (2), 68–70.
7. Qin, Y. M. Experimental study on the leather wastewater treatment by bioflocculant. *Industrial Water Treatment*, 2006, 26(9), 45–47.
8. Wang, J. X. and Li, Y. C., Selections of compounded microbial flocculant and its application in tannery waste water treatment. *China Leather*, 2009, 38(3), 27–32.
9. Liu Kesheng, Yang Shuangyue, Shi Shiqi, *et al.*, Research progress and application of flocculants in tannery effluent treatment. *Leather and Chemicals*, 2011, 28(3): 20–24.
10. Rajan M R, Nithya C. Isolation of bioflocculant producing microbes from tannery polluted soil. Ecology, Environment and Conservation Paper, 2006, 12(1): 175–178.
11. Serdar S, Faruk K, Orhan Y, *et al.* Flocculating performances of exopolysaccharides produced by a halophilic bacterial strain cultivated on agro-industrial waste. Bioresource Technology, 2011, 102(2): 1788–1794. http://dx.doi.org/10.1016/j.biortech.2010.09.020
12. Jin He, Zhen Quanwei, Qiu Ning, *et al.* Medium optimization for the production of a novel bioflocculant from Halomonas sp. V3a' using response surface methodology. Bioresource Technology, 2009, 100(23): 5922–5927. http://dx.doi.org/10.1016/j.biortech.2009.06.087
13. Wang Jianlong, Wan Wei. Optimization of fermentative hydrogen production process by response surface methodology. *International Journal of Hydrogen Energy*, 2008, 33(23): 6976–6984. http://dx.doi.org/10.1016/j.ijhydene.2008.08.051
14. Yao Jun, JiangMin, Sang Li, *et al.* The screening of a flocculant-producing Bacterium nx-2 and its characteristics. *Food and Fermentation Industries*, 2004, 30(4): 7–11.
15. Qian B G, Huang LQ, Feng B, *et al.* Study on the fermentation conditions and flocculating characters of bioflocculant production by bacillus subtilis. *Technology of Water Treatment,* 2011, 37(8): 26–30.

Temperature and Concentration Effects on Biodegradation Kinetics and Surface Properties of Phenol Degrading *Rhodotorula glutinis*

AYSUN VATANSEVER BOŞÇA[1] and SELİM L. SANİN[2,*]
[1]*Ministry of Environment and Urbanization, 06560, Ankara, Turkey*
[2]*Department of Environmental Engineering, Hacettepe University, 06800, Ankara, Turkey*

ABSTRACT: Biotoxicity and low temperature are among the challenges of biodegradation as well as microbial transport in *in-situ* bioremediation applications. This study investigates the effect of low temperature, high and low concentrations of phenol, on biodegradability and the surface properties of *Rhodotorula glutinis* which may be instrumental to develop control mechanisms in engineering applications. Results showed that *Rhodotorula glutinis* is able to grow at low phenol (< 0.5 g/L) and glucose (1.0 g/L) concentrations. Microbial growth rates of *Rhodotorula glutinis* is the highest at 25°C for phenol fed reactors. Temperature and type of carbon source affected the total amount of extracellular polymeric substances (EPS) and the relative amounts of EPS constituents. Phenol fed *Rhodotorula glutinis*, at 4°C, were found to be hydrophobic whereas *Rhodotorula glutinis* showed less hydrophobic characteristics at 25°C, regardless of the carbon source. Surface hydrophobicity of *Rhodotorula glutinis* is related to the distribution of carbohydrate and proteins in the EPS.

1. INTRODUCTION

IN-SITU bioremediation is declared as the most effective and economical treatment technology for the removal of anthropogenic pollutants. Effectiveness of the remediation is enhanced by increasing the number of native species involved in the process. Low temperatures (≤ 10°C) of groundwater and the type and concentration of the contaminant, in addition to nutrient scarcity are among the restrictions of the biodegradation process. Because of low environmental temperatures biodegradation rates slow down and removal of the organic contaminant require longer time.

Phenolic compounds are considered as priority pollutants since they are harmful to organisms even at low concentrations and many of them have been classified as hazardous pollutants because of their effect on human health [1]. Moreover, phenolic compounds in drinking water cause taste and odor problems at very low concentrations (~2 μg/L) and can form toxic polychlorinated phenols after chlorination [2].

Phenol is currently produced from fossil resources and an industrially versatile chemical [3] used in the synthesis of dyes, pharmaceuticals and picric acid. Phenol-methanal (formaldehyde) resins are the basis of the oldest plastics, and currently used to make low cost thermosetting plastics such as melamine and Bakelite, used in electrical equipment. These resins are also used extensively as bonding agents in manufacturing wood products such as plywood and MDF generated by the activities of petrochemical, coal conversion, pesticide, paint, solvent, pharmaceutical, wood processing (playwood and MDF), and pulp and paper industries. They are also widely used as construction materials for automobiles and appliances, epoxy resins [4] and adhesives, and polyamide for various applications [5,6].

Because of its versatile use in industry and its adverse effects on nature and human beings, phenol is frequently used as a model hazardous chemical for aromatic pollutants.

Phenol is introduced into the environment as a result of accidental releases or inefficient treatment of industrial wastes. Concentration above 50 mg/L of phenol is toxic to most of the microorganisms. Remediation of phenol in natural environments is achieved by both physicochemical and biological techniques [7]. Among these methods, biodegradation processes is preferred because they are cost effective and considered as environmentally friendly. Complete mineralization is also

*Author to whom correspondence should be addressed. Tel.: +90 312 297 78 00; Fax: +90 312 299 20 53; e-mail address: sanin@hacettepe.edu.tr

1544-8053/15/03 183-07
© 2015 DEStech Publications, Inc.
doi:10.12783/issn.1544-8053/12/3/9

possible by several microorganisms [8]. Thus, phenol metabolizing microorganisms are of major interest to the researchers and it has been known that some members of bacteria and yeast genera are resistant to phenol toxicity and utilize it as the sole carbon and energy source [9,10].

Most of the phenol removal studies in the literature are focused on bacterial biodegradation [1–12] and there is limited information on the phenol metabolization by the yeasts. Furthermore, little is known about the biodegradability of phenol by yeasts at colder temperatures [13,14] which is more significant for *in-situ* applications, compared to mesophilic temperatures [15]. Phenol is a well-known and used disinfectant therefore the species that can biodegrade phenol (especially at high concentrations) are limited since it inhibits the microbial growth [16].

The yeast strain *Rhodotorula glutinis*, used in this study, is an industrial strain and there is limited report on their capability to biodegrade phenolic compounds [17–18]. In previous researches phenol biodegradation was determined at relatively less toxic conditions (~200 mg/L) and kinetic parameters were not reported [19]. For the industrial uses of *R. glutinis* phenol is removed from the supernatant to eliminate its toxic effect [20]. This species is not known as a phenol degrading microorganism. Although, the knowledge on biodegradation of phenol at low temperatures by *Rhodotorula glutinis* is important for *in-situ* remediation of soils and groundwater, there is insufficient information on phenol biodegradation performance of *Rhodotorula glutinis* at these temperatures. To our knowledge in any of these studies biodegradation kinetics or different phenol concentrations are not investigated.

Moreover, there is no information on the subsequent changes of surface properties of *Rhodotorula glutinis* due to carbon source. Microbial surface properties are important parameters to control the transport of microorganisms in porous media. According to Sanin *et al.* [21] hydrophobic properties of EPS related to carbon source, toxic organic material may trigger EPS in higher quantities as a survival response. On the other hand relatively low carbon concentration may limit the EPS amount, even if its biodegradable. Kim (2009) [22] showed that specific and non-specific interactions occurring between the microorganisms and substratum determines the extent of deposition, rather than transport from the bulk to the collector surface. Therefore, controlled bacterial surface hydrophobicity can be an effective engineering tool in *in-situ* bioremediation applications.

In this study the effect of temperature, low (4°C) and moderate (25°C), and concentration on the degradation of phenol by *Rhodotorula glutinis* are investigated. A reactor containing glucose at 25°C is also used to determine the biodegradation rate of the yeast, for a non-toxic chemical. In addition, surface properties (EPS production and hydrophobicity) of *Rhodotorula glutinis* are examined and their contribution to *in-situ* bioremediation is discussed.

2. MATERIALS AND METHODS

2.1. Initial Sampling of Microorganisms

Rhodotorula glutinis culture is isolated from the soil contaminated with petrochemical compounds. For isolation of *Rhodotorula glutinis* 1.0 gram of soil was placed into 50 mL of sterilized distilled water and mixed on an orbital shaker. This solution was transferred into a reactor containing 0.1 g phenol and basic minerals. The transfer cycle is repeated 5 times with increasing phenol concentrations (0.1, 0.25, 0.5, 0.75 1.0 g of phenol). A sample was taken from the solution and grown on solid agar that contains phenol and basic minerals. Pure culture was obtained by repeated transfer of microorganisms on other agar plates and isolated single culture was conserved in slant agar tubes. Then, the microorganism specie was identified using VITEC® (bioMerieux, UK) and Analytical Profile Index, API® Strips as *Rhodotorula glutinis* and used in experiments.

2.2. Biodegradation Studies

The experiments were conducted in three sets, each set included four reactors with different carbon concentrations, given in Table 1. The first and the second set of reactors, which included phenol as the sole carbon souerce, were operated at 4°C and 25°C, respectively. The third set of reactors was operated at 25°C, using glucose as the sole carbon source at four different concentrations. The reactors which included glucose are used to determine maximum growth rate of *Rhodotorula glutinis* in the absence of substrate inhibition. The glucose concentrations used in these reactors was selected to have same amount of carbon atoms as in phenol reactors (i.e. 0.25 g/L phenol and 0.48 g/L glucose have same amount of carbon atoms).

The composition of growth media and the type and concentration of carbon source (phenol or glucose) is given in Table 1. The pH of the mineral medium was

Table 1. Composition of Carbon and Basal Mineral medium.

Phenol (g/L)	0.25	0.50	0.75	1.00
Glucose (g/L)	0.48	0.96	1.44	1.91
Carbon Equivalent in the reactors (g/L)	0.2	0.4	0.6	0.8
Constituent	**Composition per liter**			
K_2HPO_4	12.5 g			
KH_2PO_4	3.8 g			
$(NH_4)_2SO_4$	1.0 g			
$MgSO_4 \cdot 7H_2O$	0.1 g			
Trace element solution (per liter)	5.0 mL			
H_3BO_3	0.232 g			
$ZnSO_4 \cdot 7H_2O$	0.174 g			
$FeSO_4(NH_4)_2SO_4 \cdot 6H_2O$	0.116 g			
$CoSO_4 \cdot 7H_2O$	0.096 g			
$(NH_4)_6Mo_7O_{24} \cdot 4H_2O$	0.022 g			
$CuSO_4 \cdot 5H_2O$	8.0 mg			
$MnSO_4 \cdot 4H_2O$	8.0 mg			

7.2 ± 0.2 at 25°C. For each reactor, 600 mL of basal mineral medium was added into 1 L Erlenmeyer flasks and sterilized by autoclaving. The carbon source was added from stock solutions after sterilization by cold-sterilization (0.2 µm pore size syringe filter) in laminar flow chamber. Then, isolated and enriched *Rhodotorula glutinis* culture was transferred to the reactors which were incubated at the corresponding temperatures, mixed at a rate of 130 rpm on a rotary shaker. A C/N ratio of 1 is used during experiments.

The growth of the microorganisms were monitored by optical density (O.D.) measurements (@ 600 nm) using a spectrophotometer (DR Lange-CADAS 200). Deionized water was used as blank during the experiments. A control reactor without microbial inoculation is used as control reactor during each experimental setup. No significant change in phenol concentration is observed (< 3%) in control reactors. The growth rates in the reactors were modeled using Haldane kinetics [23]. Maximum specific growth rate (μ_{max}), K_s and K_i values of *Rhodotorula glutinis* are calculated using quadratic interpolation method. Each measurement is repeated three times and the averages are reported.

2.3. Determination of Phenol Concentration

Phenol concentrations in the reactors were determined in triplicate samples, by direct photometric method (Method 5530.D) of APHA, AWWA, WEF. 4-aminoantipyrene was used as the coloring agent and the absorbance was measured at 500 nm [24].

2.4. Extracellular Polymer and MLVSS Determination

Extracellular polymers (EPS) was extracted using a cation exchange resin (CER) which was fully developed by Durmaz and Sanin [25]. Briefly, MLVSS (Mixed Liquor Volatile Suspended Solids) value of each completely mixed reactor sample was measured. A dose of 100 gCER/gVSS was used for each sample based on the previous experience. Separately weighed cation exchange resins for each reactor were put into glass beakers and washed with a phosphate buffer saline (PBS) for about 2 hours, to prevent leaching from the CER and to eliminate subsequent interferences during chemical analysis. When washing was complete, CER was filtered using millipore filter and dried at room temperature until the next day. EPS was released to the medium as a result of cation removal from floc structure during stirring the samples with CER. After 5 hours mixing, the jars were left to settle down for about half an hour. Then the supernatants were centrifuged for 10 minutes and the centrates were used for carbohydrate and protein analyses. Carbohydrate content of EPS in the centrates of the samples were measured using Dubois method [26] where alginate is used as the standard. Protein content of polymers in each EPS extraction set were determined using folin-ciocalteu protein measurement method developed by Lowry [27]. Bovine Serum Albumin from Sigma (A-7906) was used as a standard for the preparation of the calibration curve. MLVSS measurements were conducted according to Standard Methods for the Examination of Water and Wastewater Method number 2540 [24].

2.5. Measurement of Hydrophobicity

Surface hydrophobicity of the microorganisms was measured according to the Microbial Attachment To Hydrocarbon (MATH) test that was developed by Rosenberg [21,28]. The MATH test exploits the tendency of various microorganisms possessing hydrophobic surface characteristics to adhere to liquid hydrocarbons (e.g. n-hexadecane, n-octane). In this research, n-hexadecane was used as the hydrocarbon phase.

3. RESULTS AND DISCUSSION

3.1. Growth of *Rhodotorula glutinis* at Different Temperature and Phenol Concentration

Rhodotorula glutinis was able to grow using differ-

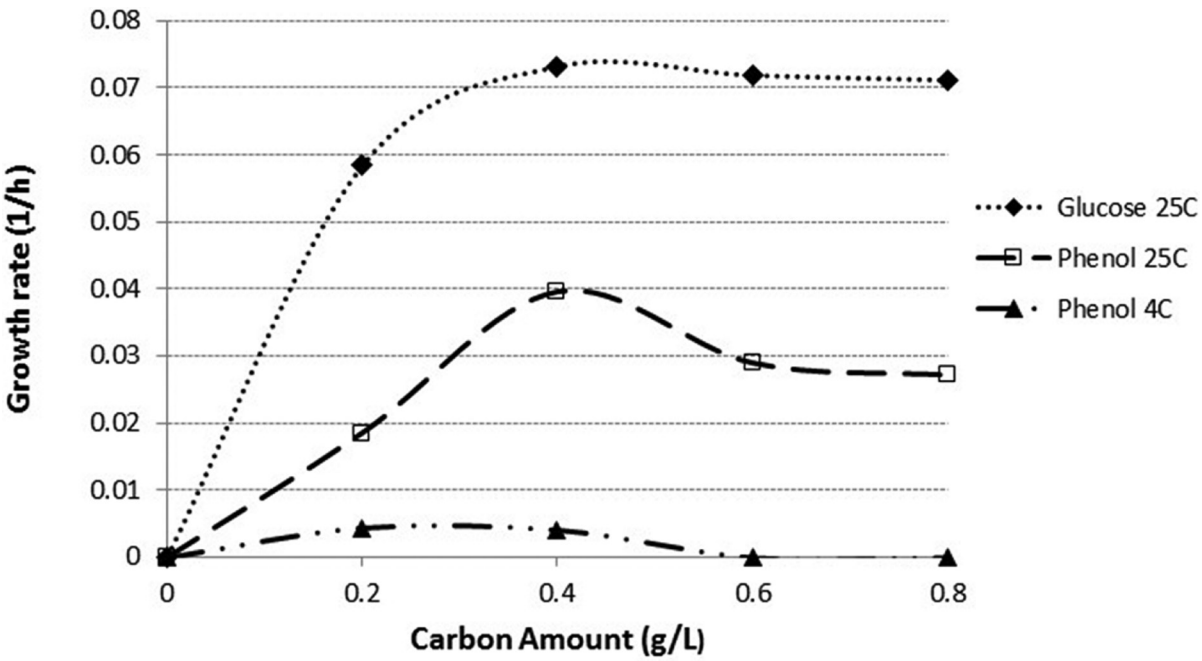

Figure 1. *Growth rates of Rhodotorula glutinis with respect to temperature and carbon source.*

ent concentrations of phenol as the sole carbon source, under mesophilic (25°C) conditions. Low temperature and high phenol concentration is a stress factor in biodegradation for *Rhodotorula glutinis*. High phenol concentrations (0.75 and 1.0 g/L) stopped the growth of the yeast at low temperature (at 4°C). Decreasing specific growth rates (μ) in the phenol containing reactors were calculated. The growth rates were five times lower then 25°C reactors in the reactors at 4°C, for 0.25 g/L concentrations of phenol. The growth rate reduction is much more significant for the rectors containing 0.5 g/L phenol, which may indicate an increasing toxicity effect of phenol with the increasing concentration. At 0.75 g/L and 1.0 g/L reactors no growth is observed at 4°C. Phenol degradation results show typical substrate inhibition phenomena especially at high phenol concentrations as well at low temperature. Although this is the first reporting of low temperature biodegradation study for *R. glutinis*, similar behavior are also reported for other yeast species in the literature [13–19].

Glucose concentrations used in this study are significantly lower than the studies which used *Rhodotorula glutinis* for industrial purposes (e.g. carotene production) [29] which may be considered as carbon deficit condition for the specie; when the type of carbon source for microbial growth is considered, specific growth rate calculated for glucose at 25°C is two folds faster than growth rates of phenol at the same temperature which is an expected result since glucose is an easily biodegradable compound, whereas phenol is not, Figure 1.

Results indicate that Haldane kinetics was capable of explaining biodegradation and growth kinetics. Haldane inhibition constants calculated as 0.0138 for 0.5 g/L phenol at 4°C . We did not observe significant inhibition at 0.25 g/L phenol concentration at 4°C. Apparent growth is not observed in the reactors containing

Table 2. Kinetic Parameters of Haldane Inhibition for Rhodotorula glutinis during Phenol Degredation.

Carbon Concentration (mg/L)	4°C				25°C			
	μ	μ_{max}	K_s	K_i	μ	μ_{max}	K_s	K_i
0.2	0.0043	0.0046	0.075	–	0.0213	0.033	0.219	–
0.4	0.004	0.0046	0.075	0.0138	0.0332	0.033	0.219	–
0.6	N.G.	N.G.	N.G.	N.G.	0.0187	0.033	0.219	0.615
0.8	N.G.	N.G.	N.G.	N.G.	0.0135	0.033	0.219	1.210

N.G. = No growth is observed.

Table 3. Phenol Removal Efficiencies of Rhodotorula glutinis at Different Temperature and Concentrations* (given as carbon amount).

Temperature	0.2 g/L	0.4 g/L	0.6 g/L	0.8 g/L
25°C	99%	99%	40%	20%
4°C	15%	10%	**	**

*At 25°C glucose removal efficiencies in all reactors were 100%.
**Could not be measured.

0.75 and 1.0 g/L phenol. At 25°C , no inhibitory effect is observed in 0.25 and 0.5 g/L phenol concentrations. Inhibitory effect is observed for 0.75 g/L (K_i = 0.615 g/L) and 1.0 g/L (K_i = 1.2102 g/L) phenol concentrations. Haldane kinetics results are given in Table 2.

3.2. Biodegradation of Phenol by *Rhodotorula glutinis*

The residual phenol concentrations in the reactors were measured when stationary phase is observed. Calculated removal efficiencies of phenol are given in Table 3. *Rhodotorula glutinis* is capable of biodegrading low phenol concentrations (< 0.5 g/L) at all temperatures. Although phenol is removed in all reactors at 25°C, removal efficiencies were low at high concentration reactors, 40% and 20% for 0.75 and 1.0 g/L reactors, respectively. At 4°C reactors maximum removal rate was 15%. No removal is observed in 0.75 and 1.0 g/L reactors at 4°C reactors, which also supports the unchanged O.D. measurements in these reactors. According to the phenol treatment efficiency results, low temperature is an important limitation for phenol biodegradation, since biodegradation rates are directly related to the temperature of the environment.

3.3. Production and Composition of Extracellular Polymeric Substances (EPS)

Since the amount of EPS and their properties may significantly affect the transport of xenobiotic degrading organisms in porous media, EPS produced by *Rhodotorula glutinis*, under different conditions, were examined.

Rhodotorula glutinis is widely used to produce extracellular polysaccharides [30]. The EPS composition of *R. glutinis* consists of almost entirely with neutral sugars, when fed with glucose. In our study the use of phenol, as carbon source, seem to effect the composition of the EPS produced by *R. glutinis*. The change on the chemical structure of extracted EPS in terms of the amounts of carbohydrate and protein components as well as total EPS quantities are summarized in Table 4. Results show that the quality and quantity of EPS changed significantly when the reactors were operated under different temperatures, carbon sources and concentrations. The amount of proteins was greater than carbohydrates in EPS composition, at all studied phenol concentrations at 4°C whereas no carbohydrate type of polymers were obtained for phenol fed reactors at 25°C except for 0.5 g/L phenol concentration. On the other hand, carbohydrates were the dominant constituent of EPS for the glucose fed reactors above 0.25 g/L glucose concentration. It seems that 0.25 g/L glucose is a starvation initiating concentration for *R. glutinis*, and an increase in the protein content in the EPS composition, as a stress response, is observed. According to literature, almost all EPS composition is composed of carbohydrates in the *R. glutinis* cultivating reactors which used easily biodegradable carbon source (i.e. glucose). In our reactors (@ 25°C), as the glucose concentration increases from 0.25 to 1 g/L, carbohydrate percent of EPS increases 25% to 98 %. Therefore, 1 g/L glucose concentration can be considered as a critical concentration for EPS composition of *R. glutinis*.

Total amount of EPS increased with the increase in carbon concentrations in all reactors, which may indicate the importance of amount of carbon source,

Table 4. Effect of Temperature and Carbon Source Concentration on the Production and Composition of EPS.

Carbon Source and Temperature	Carbon Concentrations Equivalent to 0.25; 0.5; 0.75 and 1.0 g/L Phenol											
	0.2			0.4			0.6			0.8		
	Carbohydrate (mg/g)	Protein (mg/g)	Total EPS	Carbohydrate (mg/g)	Protein (mg/g)	Total EPS	Carbohydrate (mg/g)	Protein (mg/g)	Total EPS	Carbohydrate (mg/g)	Protein (mg/g)	Total EPS
Phenol (4°C)	25.1	153.4	178.5	47.3	77.1	124.4	57.4	197.8	255.2	99.9	430.9	530.8
Phenol (25°C)	nd	1.7	1.7	5.1	5.9	11	nd	97.3	97.3	nd	200	200
Glucose (25°C)	0.9	2.7	3.6	2.7	2.0	4.7	4.9	1.5	6.4	22.8	0.4	23.2

nd: not detected.

independent of carbon type, in EPS production. *Rhodotorula glutinis* fed with phenol, tend to produce significantly greater amounts of EPS at 4°C compared to 25°C which is compatible with the smaller growth rates obtained at 4°C compared to 25°C. In other words, at difficult survival conditions *Rhodotorula glutinis* produce high amount of EPS instead of proliferation. Similarly, smallest amount of EPS was extracted from glucose fed reactors, which showed highest growth rates, less stress conditions and growing microbial population. The EPS composition of glucose fed reactors contain higher carbohydrate concentrations. These observation may indicate that non-toxic carbon source is instrumental in the production of EPS carbohydrates.

3.4. Effects on Hydrophobicity

Relative hydrophobicities measured by MATH test depending on temperature and carbon concentration in the reactors are demonstrated in Figure 2. Our results indicate that growth temperature may have an effect on hydrophobicity of phenol degrading microorganisms. Low hydrophobicity was detected for phenol fed reactors at 25°C. It is evident from the data that the surface of microorganisms was more hydrophobic (60%) when phenol was degraded at 4°C.

As to the effect of carbon source, the reactors that contain glucose having a hydrophobicity value of around 20%, were found to be more hydrophobic than the ones fed with phenol at 25°C. In some of previous researches

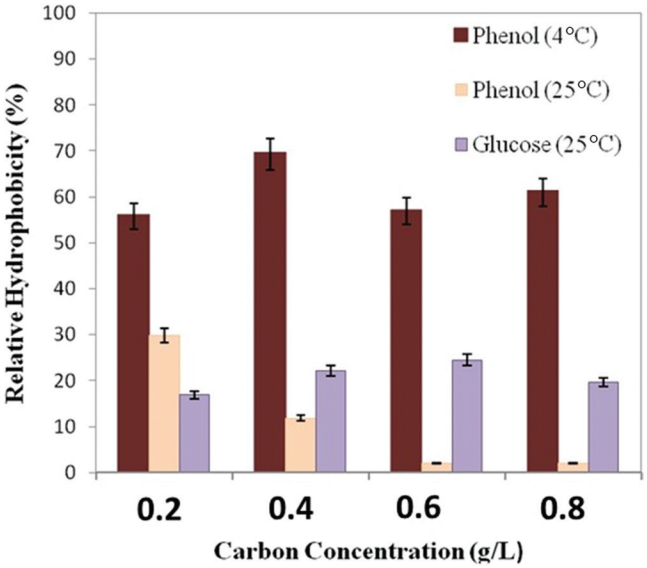

Figure 2. *Relative hydrophobicity values with respect to temperature and carbon source concentration.*

it was proposed that the proportions of EPS components (proteins/carbohydrates and/or proteins/(carbohydrates + DNA)) were more important than the quantities of individual EPS components in controlling hydrophobicity [31,30]. When the hydrophobicity data is evaluated considering the relative amounts of carbohydrates and proteins to each other, it is seen that there is a positive relationship between proteins and hydrophobicity for phenol at 4°C. Similarly, microorganisms in glucose fed reactors having more carbohydrates than proteins (except for 0.25 g/L), showed low hydrophobicity.

4. CONCLUSIONS

Rhodotorula glutinis is capable of biodegrading phenol at mesophilic temperatures (20–25°C), which makes these species useful for bioremediation applications. On the other hand, removal efficiencies of high phenol concentrations decreases at low temperatures.

According to the results of the study, biodegradation of phenol by *Rhodotorula glutinis* requires longer time at low temperature (4°C) which may indicate stress response compared to room temperature (25°C). The microorganisms exhibit seven times faster maximum phenol utilization rates at 25°C and maximum specific growth rate is doubled when glucose was used as carbon source instead of phenol at 25°C. The amount of extracted total EPS was very high for phenol reactors at 4°C which can be explained as a response of microorganisms to difficult survival conditions. As the temperature increased to 25°C and carbon source shifted to glucose, the amount of EPS decreased parallel to the increase in growth rates. EPS production increases with the increasing initial carbon concentrations in the reactors. Besides total amount of EPS, relative amounts of EPS components also showed differences. Proteins were dominant in the composition of EPS of phenol reactors, independent of temperature, while carbohydrates were dominant in glucose fed reactors.

Rhodotorula glutinis fed with phenol at 4°C had hydrophobic surfaces with relative surface hydrophobicity values changing between 55–70%. However, at a room temperature (25°C), which may mean better survival conditions, the surfaces turned to be less hydrophobic (5–30%).

Our results indicate *Rhodotorula glutinis* is capable of degrading phenol, can be used for controlled transport in natural environment and can be instrumental for long term bioremediation applications.

5. REFERENCES

1. Parr AJ, Bolwell GP., 2000 Phenols in the plant and in man. The potential for possible nutritional enhancement of the diet by modifying the phenols content or profile, *Journal of the Science of Food And Agriculture, 80*: 985–1012. http://dx.doi.org/10.1002/(SICI)1097-0010(20000515)80:7<985::AID-JSFA572>3.0.CO;2-7
2. Onodera S., 2010. Formation Mechanism and Chemical Safety of Nonintentional Chemical Substances Present in Chlorinated Drinking Water and Wastewater,Yakugaku Zasshi. *Journal of the Pharmaceutical Society of Japan, 130*:1157–1174. http://dx.doi.org/10.1248/yakushi.130.1157
3. Weber, M., Weber, M., Phenols. in: Pilato, L. (Ed.), *Phenolic resins: A Century of Progress*, Springer, 2010. http://dx.doi.org/10.1007/978-3-642-04714-5_2
4. Tejado, A, Pena, C, Labidi, J. Echeverria, JM, Mondragon, I., 2007. Physico-chemical characterization of lignins from different sources for use in phenol-formaldehyde resin synthesis, *Bioresource Technology, 9*(8), 1655–1663. http://dx.doi.org/10.1016/j.biortech.2006.05.042
5. Niwa, S., Eswaramoorthy, M., Nair, J A., Raj, A., Itoh, N., Shoji, H., Namba, T., Mizukami, F., 2002. One-step conversion of benzene to phenol with a palladium membrane, *Science, 295*:5552, 105–107. http://dx.doi.org/10.1126/science.1066527
6. Cordova-Rosa SM, Dams RI, Cordova-Rosa EV, Radetski MR, Corrêa AXR, Radetski CM., 2009. Remediation of phenol-contaminated soil by a bacterial consortium and *Acinetobacter calcoaceticus* isolated from an industrial wastewater treatment plant. *Journal of Hazardous Materials 2009*;164:61–66. http://dx.doi.org/10.1016/j.jhazmat.2008.07.120
7. Busca, G., Berardinelli, S., Resini, C., Arrighi, L., 2008. Technologies for the removal of phenol from fluid streams: A short review of recent developments, *Journal of Hazardous Materials, 160*:2-3, 265–288.
8. Juang SJ, Tsai SY. 2006. Growth kinetics of Pseudomonas putida in the biodegradation of single and mixed phenol and sodium salicylate. *Biochem Eng J*, 133–140. http://dx.doi.org/10.1016/j.bej.2006.05.025
9. Sanin, SL, Yilmaz, G, 2006. Effect of change in carbon source on the dewaterability of xenobiotic degrading mixed culture, *Journal of Residuals Science & Technology, 3*:211–216.
10. Hoodaj MI, Tahmourespour A, Eskandary S. 2013. Effect of Environmental Conditions on Phenol Biodegradation by Newly Isolated Bacterium (Alcaligenes sp. ATHE8) from Coke Processing Wastewater, *Journal of Residuals Science & Technology, 10*:127–131.
11. Feitkenhauer H, Schnicke S, Müller R, Markl H. 2001. Determination of the kinetic parameters of the phenol-degrading thermophile *Bacillus themoleovorans* sp. A2. *Appl Microbiol Biotechnol, 57*:744–750. http://dx.doi.org/10.1007/s002530100823
12. Liu YJ, Zhang AN, Wang XC. 2009. Biodegradation of phenol by using free and immobilized cells of Acinetobacter sp. XA05 and *Sphingomonas* sp. FG03. *Biochem Eng J., 44*:187–192. http://dx.doi.org/10.1016/j.bej.2008.12.001
13. Margesin, R., Fonteyne, PA., Redl, B., 2005. Low-temperature biodegradation of high amounts of phenol by Rhodococcus spp. and *Basidiomycetous* yeasts, *Research in Microbiology, 156*:68–75. http://dx.doi.org/10.1016/j.resmic.2004.08.002
14. Bergauer, P; Fonteyne, PA; Nolard, N; Schinner, F, Margesin, R. 2005. Biodegradation of phenol and phenol-related compounds by psychrophilic and cold-tolerant alpine yeasts, *Chemosphere 59*: 909–918. http://dx.doi.org/10.1016/j.chemosphere.2004.11.011
15. Margesin, R, Moertelmaier, C, Mair, J., 2013. Low-temperature biodegradation of petroleum hydrocarbons (n-alkanes, phenol, anthracene, pyrene) by four Actinobacterial strains, *International Biodeterioration & Biodegradation 84*:185–191. http://dx.doi.org/10.1016/j.ibiod.2012.05.004
16. Tsai, SC; Tsai, LD; Li, YK., 2005. An isolated Candida albicans TL3 capable of degrading phenol at large concentration, *Bioscience Biotechnology and Biochemistry 69*:2358–2367. http://dx.doi.org/10.1271/bbb.69.2358
17. Walker N., 1973. Metabolism of chlorophenols by *Rhodotorula glutinis*. *Soil Biol Biochem 5*:525–530. http://dx.doi.org/10.1016/0038-0717(73)90042-4
18. Katayama-Hirayama K, Tobita K, Hirayama K., 1991. Degradation of phenol by yeast *Rhodotorula*. *J Gen Appl Microbiol 37*:147–156. http://dx.doi.org/10.2323/jgam.37.147
19. Katayama-Hirayama K, Tobita K, Hirayama K., 1994. Biodegradation of phenol and Monochlorophenol by yeast *Rhodotorula glutinis*. *Wat Sci Tech, 30*:59–66.
20. Lian, JN, Chen, SL, Zhou, SA, Wang, ZH, O'Fallon, J, Li, CZ, Garcia-Perez, M., 2010. Separation, hydrolysis and fermentation of pyrolytic sugars to produce ethanol and lipids, *Bioresource Technology, 101*(24), 9688–9699. http://dx.doi.org/10.1016/j.biortech.2010.07.071
21. Sanin, SL; Sanin, FD; Bryers, JD (2003) Effect of starvation on the adhesive properties of xenobiotic degrading bacteria, *Process Biochemistry, 38*(6), 909–914. http://dx.doi.org/10.1016/S0032-9592(02)00173-5
22. Kim, Hyunjung N.; Walker, Sharon L. (2009) Escherichia coli transport in porous media: Influence of cell strain, solution chemistry, and temperature, *Colloids And Surfaces B-Biointerfaces,71*(1), 160–167. http://dx.doi.org/10.1016/j.colsurfb.2009.02.002
23. Briggs, G. E., and Haldane, J. B. (1925) A Note on the Kinetics of Enzyme Action, *Biochem J* 19, 338–339.
24. American Public Health Association, APHA . Standard Methods for the Examination of Water and Wastewater. 20th ed., American Water Work Association, Water Environment Federation, Washington, D.C. 1989.
25. Durmaz B, Sanin FD. 2000. Effect of carbon to nitrogen ratio on the composition of microbial extracellular polymers in activated sludge. *Wat Sci Rech, 44*:221–229.
26. Dubois M, Gilles KA, Hamilton JK, Rebers PA, Smith F., 1956. Colorimetric Method for the Determination of Sugar and Related Substances. *Anal Chem, 28*:350–356. http://dx.doi.org/10.1021/ac60111a017
27. Lowry OH, Rosebrough NJ, Farr AL, Randall RJ., 1951. Protein Measurement with Folin Fenol Reagent. *J Biol Chem, 193*:265–275.
28. Rosenberg M, Gutnick D, Rosenberg E., 1980. Adherence of bacteria to hydrocarbons: a simple method for measuring cell surface hydrophobicity. *FEMS Microbial Lett, 9*:29–33. http://dx.doi.org/10.1111/j.1574-6968.1980.tb05599.x
29. Xue FY, Miao JX, Zhang, X, Luo H, Tan TW., 2008. Studies on lipid production by Rhodotorula glutinis fermentation using monosodium glutamate wastewater as culture medium, *Bioresource Technology, 99*:5923–5927. http://dx.doi.org/10.1016/j.biortech.2007.04.046
30. Liao BQ, Allen DG, Droppo IG, Leppard GG, Liss SN., 2001. Surface properties of sludge and their role in bioflocculation and settleability. *Wat Res, 35*:339–350. http://dx.doi.org/10.1016/S0043-1354(00)00277-3
31. Cho, DH; Chae, HJ; Kim, EY., 2001. Synthesis and characterization of a novel extracellular polysaccharide by *Rhodotorula glutinis*, *Applied Biochemistry and Biotechnology, 95*:183–193. http://dx.doi.org/10.1385/ABAB:95:3:183

GUIDE TO AUTHORS

1. Manuscripts shall be sent electronically to the Editor-in-Chief, Dr. P. Brent Duncan at pduncan@unt.edu using Microsoft Word in an IBM/PC format. If electronic submission is not possible, three paper copies of double-spaced manuscripts may be sent to Dr. P. Brent Duncan, (Editor of the *Journal of Residuals Science & Technology,* University of North Texas, Biology Building, Rm 210, 1510 Chestnut St., Denton, TX 76203-5017) (Tel: 940-565-4350). Manuscripts should normally be limited to the space equivalent of 6,000 words. The editormay waive this requirement in special occasions. As a guideline, each page of a double-spaced manuscript contains about 300 words. Include on the title page the names, affiliations, and addresses of all the authors, and identify one author as the corresponding author. Because communication between the editor and the authors will be electronic, the email address of the corresponding author is required. Papers under review, accepted for publication, or published elsewhere in journals are normally not accepted for publication in the *Journal of Residuals Science & Technology*. Papers published as proceedings of conferences are welcomed.
2. Article titles should be brief, followed by the author's name(s), affiliation, address, country, and postal code (zip) of author(s). Indicate to whom correspondence and proofs should be sent, including telephone and fax numbers and e-mail address.
3. Include a 100-word or less abstract and at least six keywords.
4. If electronic art files are not supplied, submit three copies of camera-ready drawings and glossy photographs. Drawings should be uniformly sized, if possible, planned for 50% reduction. Art that is sent electronically should be saved in either a .tif or .JPEG files for superior reproduction. All illustrations of any kind must be numbered and mentioned in the text. Captions for illustrations should all be typed on a separate sheet(s) and should be understandable without reference to the text.
5. DEStech uses a numbered reference system consisting of two elements: a numbered list of all references and (in the text itself) numbers in brackets that correspond to the list. At the end of your article, please supply a numbered list of all references (books, journals, web sites etc.). References on the list should be in the form given below. In the text write the number in brackets corresponding to the reference on the list. Place the number in brackets inside the final period of the sentence cited by the reference. Here is an example [2].

   Journal: 1. Halpin, J. C., "article title", *J. Cellular Plastics,* Vol. 3, No. 2, 1997, pp. 432–435.

   Book: 2. Kececioglu, D. B. and F.-B. Sun. 2002. *Burn-In Testing: Its Quantification and Optimization,* Lancaster, PA: DEStech Publications, Inc.
6. Tables. Number consecutively and insert closest to where firstmentioned in text or type on a numbered, separate page. Please use Arabic numerals and supply a heading. Column headings should be explanatory and carry units. (See example at right.)
7. Units & Abbreviations. Metric units are preferred. English units or other equivalents should appear in parentheses if necessary.
8. Symbols. A list of symbols used and their meanings should be included.

Table 5. Comparison of state-of-the-art matrix resins with VPSP/BMI copolymers.

Resin System	Core Temp. (DSC peak)	T_E	Char Yield, %
Epoxy (MY720)	235	250	30
Bismaleimide (H795)	282	>400	48
VPSP/Bismaleimide copolymer			
C379: H795 = 1.9	245	>400	50
C379: H795 = 1.4	285	>400	53

9. Page proofs. Authors will receive page proofs by E-mail. Proof pages will be in a .PDF file, which can be read by Acrobat Reader. Corrections on proof pages should be limited to the correction of errors. Authors should print out pages that require corrections and mark the corrections on the printed pages. Pages with corrections should be returned by FAX (717-509-6100) or mail to the publisher (DEStech Publications, Inc., 439 North Duke Street, Lancaster, PA 17602, USA). If authors cannot handle proofs in a .PDF file format, please notify the Editor, Dr. P. Brent Duncan at pduncan@unt.edu.
10. Index terms.With proof pages authors will receive a form for listing key words that will appear in the index. Please fill out this form with index terms and return it.
11. Copyright Information. All original journal articles are copyrighted in the name of DEStech Publications, Inc. All original articles accepted for publication must be accompanied by a signed copyright transfer agreement available from the journal editor. Previously copyrighted material used in an article can be published with the *written* permission of the copyright holder (see #14 below).
12. Headings. Your article should be structured with unnumbered headings. Normally two headings are used as follows:

    Main Subhead: DESIGN OF A MICROWAVE INSTALLATION Secondary Subhead: Principle of the Design Method

    If further subordination is required, please limit to no more than one (*Third Subhead*).
13. Equations. Number equations with Arabic numbers enclosed in parentheses at the right-hand margin. Type superscripts and subscripts clearly above or below the baseline, or mark them with a caret. Be sure that all symbols, letters, and numbers are distinguishable (e.g., "oh" or zero, one or lowercase "el," "vee" or Greek nu).
14. Permissions. The author of a paper is responsible for obtaining releases for the use of copyrighted figures, tables, or excerpts longer than 200 words used in his/her paper. Copyright releases are permissions to reprint previously copyrighted material. Releases must be obtained from the copyright holder, which is usually a publisher. Forms for copyright release will be sent by the editor to authors on request.

General: The *Journal of Residuals Science & Technology* and DEStech Publications, Inc. are not responsible for the views expressed by individual contributors in articles published in the journal.